SYNTHESIS, CHARACTERIZATION AND ENERGETIC PERFORMANCE OF METAL BORIDE COMPOUNDS FOR INSENSITIVE ENERGETIC MATERIALS

by

Michael L. Whittaker

A thesis submitted to the faculty of
The University of Utah
in partial fulfillment of the requirements for the degree of

Master of Science

Department of Materials Science and Engineering

University of Utah

May 2012

The University of Utah Graduate School

STATEMENT OF THESIS APPROVAL

The thesis of **Michael L. Whittaker**

has been approved by the following supervisory committee members:

Raymond A. Cutler	, Chair	**03/09/2012** Date Approved
Anil V. Virkar	, Member	**03/09/2012** Date Approved
Gerald B. Stringfellow	, Member	**03/09/2012** Date Approved

and by **Feng Liu** , Chair of

the Department of **Materials Science and Engineering**

and by Charles A. Wight, Dean of The Graduate School.

ABSTRACT

Six metal boride compounds (AlB_2, MgB_2, $Al_{0.5}Mg_{0.5}B_2$, AlB_{12}, $AlMgB_{14}$ and SiB_6) with particle sizes between 10-20 μm were synthesized for insensitive energetic fuel additives from stoichiometric physical mixtures of elemental powders by high temperature solid state reaction. B_4C was also investigated as a lower cost source of boron in AlB_2 synthesis and showed promise as a boron substitute.

Thermal analysis confirmed that the formation of boride compounds from physical mixtures decreased sensitivity to low temperature oxidation over the aluminum standard. Both Al+2B and AlB_2 were much less sensitive to moisture degradation than aluminum in high humidity (10-100% relative humidity) and high temperature (20-80°C) environments. AlB_2 was determined to be safe to store for extended periods of time in cool, dry environments. Impact, friction and shock sensitivity testing indicated that AlB_2 and MgB_2 were less sensitive than aluminum. The activation energies for the oxidation of Al, B, Al+2B and AlB_2 were determined through an isothermal, isoconversional method in N_2-20%O_2 and O_2 at one atmosphere. An activation energy of 413 ± 20 kJ/mol was calculated for AlB_2 in O_2.

The incorporation of magnesium and/or aluminum with boron increased its oxidation rate and overall conversion through the formation of metal-borate crystals ($2Al_2O_3 \cdot B_2O_3$ and $3MgO \cdot B_2O_3$) which removed liquid B_2O_3 from the surface of oxidizing particles. Aluminum also increased the oxidation efficiency of B_4C by a similar

mechanism. AlB_2, MgB_2 and $Al_{0.5}Mg_{0.5}B_2$ oxidized to greater than 85% of their theoretical values while exhibiting decreased sensitivity to low temperature oxidation, making them top candidates for further energetic testing.

Cylinder expansion testing of $AlMgB_{14}$ showed little reaction of the boride material within seven volume expansions, corresponding to poor energetic performance. Detonation calorimetry of AlB_2 and Al + 2B using proprietary energetic mixtures in an argon atmosphere showed that AlB_2 reacted almost completely while Al + 2B did not. Future work should focus on testing the diboride materials and synthesizing and testing similar materials made from B_4C.

Dedicated to my family,

and the Flying Spaghetti Monster

TABLE OF CONTENTS

ACKNOWLEDGEMENTS

First and foremost I would like to thank Dr. Raymond Cutler, who has been a teacher, boss, advisor and role model. He challenged me to live up to my potential, and taught me not what to think, but how. Dr. Paul Anderson provided part of the funding for this work. I am indebted to Dr. Anil Virkar and Dr. Gerald Stringfellow, not only for advising me through the thesis process, but for inspiring me to learn as much as they have learned in order to make a real difference in the world, as they have. I could not have produced Chapter 5, possibly the most significant portion of this thesis, without the help of Dr. Hong Yong Sohn. This thesis would not have been on time or in print without the help of Ashley Quimby, who keeps me focused and punctual with a smile on her face. Marc Finders offered advice and encouragement on many weekends and late nights. Lyle Miller helped collect TGA data and allowed me to temporarily take over part of his characterization lab. Finally, thanks to the faculty, staff, and students of the Materials Science department, who keep me on my toes and challenge me every day.

1. INTRODUCTION

1.1 Background

Energetic materials are generally characterized as materials that contain a significant amount of chemical energy that can be released quickly.[1] Metals are commonly used fuels and fuel additives in binary energetic systems (a combination of fuel and oxidizer) due to their relatively high heats of combustion and fast reaction kinetics.[1] Boron is a promising energetic fuel because of its high volumetric and gravimetric heats of combustion,[2-6] but unlike metals the slow oxidation kinetics of boron limit its ability to perform adequately in most energetic systems.[2-8]

The poor performance of boron can be attributed to the unique relationship between boron and its oxides. Elemental amorphous boron melts at a temperature of 2077°C and boils at 3867°C.[9] Because boron does not readily liquefy, the combustion of boron particles proceeds as a heterogeneous reaction controlled by diffusion of an oxidizing species from the surroundings to the boron particle surface.[3, 5-6] Furthermore, the most favorable oxide of boron at typical reaction temperatures, B_2O_3, melts at 450°C but does not boil until 2067°C.[9] The molten, vitreous B_2O_3 layer that exists across a large temperature range (1617°C)[10] retards the combustion process, either by limiting oxygen diffusion inward or boron diffusion outward.[2-3, 5-6] Because energetic applications for boron generally require particles 1-50 μm in size, the thermal behavior and oxidation kinetics of particles in this size range are of particular importance.

The combustion of boron in a gaseous atmosphere leads to a well-characterized two-stage combustion,[5-6] in which the first stage corresponds to the vaporization of the oxide layer on the surface of the particle and the second stage corresponds to the burning of the 'clean' boron particle. The time required for completion of the first stage is known as the 'ignition delay' and the second stage is known as the 'burning time.' Included in the ignition delay is the time required to form an oxide layer initially, which at high temperatures is a few microseconds[3] but at lower temperatures can be in the millisecond range.[5-6] At higher pressures only one stage of combustion is observed,[12] corresponding to burning of the boron particle without a significant oxide layer or in conjunction with a thin oxide layer. Higher pressures and temperatures have been shown to reduce the ignition delay and burning time of boron particles.[2-3, 5-6, 8]

Various coatings on the surface of boron particles have been used to assist their combustion as well. LiF has been used as a chemical additive to reduce the ignition delay time of boron particles,[2, 8,13-14] corresponding to the removal of B_2O_3 by the reaction[3]

$$B_2O_{3(l)} + LiF_{(l)} \rightarrow LiBO_{2_{(l,g)}} + BOF_{(g)} \qquad (1.1)$$

However, the use of LiF is no longer desired due to its toxicity and the toxicity of its combustion products. Other methods of reducing boron particle combustion time have also been used, such as metal mixtures (mechanical alloys) and metal coatings.

The oxidation behavior of most metal fuel particles is much different from that of boron.[15-18] Two common fuels are aluminum and magnesium. These metals melt at

660°C and 649°C, respectively, while their oxides (Al_2O_3 and MgO) remain solid until 2054°C and 2832°C.[9] The combustion of these materials in air involves a molten particle developing a brittle solid oxide layer that cracks and spalls under the stress of the thermally expanding core,[19] in contrast with the viscous liquid oxide layer of boron.

Metal coatings on boron particles have been investigated.[2, 20] Thin magnesium coatings on boron particles have been shown to decrease the ignition delay of boron particles, but coatings with increasing thickness begin to increase the first stage combustion time.[21] Exothermic magnesium oxidation increases particle temperature, which aids the combustion of boron by increasing the kinetics of oxidation, but as the metal coating becomes increasingly thick, diffusion of oxygen to the metal surface becomes limited and particle combustion slows. Similar models have been proposed for aluminum and titanium.[22-24] Copper oxide (CuO) has been used as a catalyst in Al-B systems with submicron boron, where CuO catalyzes aluminum oxidation, raising the temperature sufficiently to allow rapid boron oxidation.[24] Flower et al.[25] investigated mechanically alloyed boron-aluminum mixtures and noted an increase in heat release in combustion calorimetry.

Synthesis of metal-boron compounds has been investigated as an alternative to elemental metal or boron fuels. Some of these compounds, including AlB_2, AlB_{12}, MgB_2 and LiB_2 were tested by Hsia,[8] who found that many metal borides exhibit better combustion characteristics than elemental boron. Mota et al.[26] made explosive mixtures with AlB_2 but it was unclear whether performance was enhanced. Despite generally promising results, little follow-up work has been done on metal borides as energetics.

Investigations into the energetic properties of $AlMgB_{14}$ were proposed by Ceramatec, Inc., after it was initially studied as a ceramic armor material (Appendix C). The Army showed interest in this material for use in insensitive munitions due to the presence of three common energetic elements in the same compound. It was hypothesized that the formation of the metal-boron compound would reduce the sensitivity of a fine powder to low temperature oxidation and accidental discharge by electrostatic shock, friction, or impact while maintaining high energetic performance. This compound was compared to some of the boride compounds previously examined (AlB_2, AlB_{12} etc.) as well as untested boride compounds of promising energetic elements.

1.2 Material Selection

Many energetic elements exist. Table 1.1 summarizes basic physical properties and relative cost of various energetic elements that were potential candidates for use in energetic formulations. By screening the elements based on physical properties, thermochemical properties, and cost, the best candidate elements for insensitive energetics were selected. Any large-scale application of new energetic materials would require the raw materials to be inexpensive. Aluminum, iron, magnesium and silicon were the cheapest elements available at the time of writing. Boron is one of the most expensive, with costs ranging from \$100/kg to \$300/kg.[a]

Compared to aluminum (\$22/kg[b]) and magnesium (\$30/kg[c]), elemental boron is prohibitively expensive. One alternative to boron is boron carbide (B_4C), which would

a. SB Boron (Bellwood, IL) Grades I, II, III and H. C. Starck (Germany) amorphous B.
b. Valimet (Stockton, CA) Grade H-30.
c. Hart Metals (Tamaqua, Pa) atomized Mg.

Table 1.1

Energetic Element Physical Characteristics and Cost

Metal	Atomic Weight (g/mol)	Theoretical Density (g/cc)	Crystal Structure	Melting Temperature (°C)	Relative Cost
Al	26.98	2.70	Cubic	660	Low
B	10.81	2.34	Rhombohedral	2077	High
Co	58.93	8.90	Hexagonal	1768	Medium
Fe	55.85	7.87	Cubic	1495	Low
Li	6.94	0.53	Cubic	181	Medium
Mg	24.31	1.74	Hexagonal	649	Low
Ni	58.69	8.90	Cubic	1455	Medium
Si	28.09	2.42	Cubic	1412	Low
Ti	47.87	4.54	Hexagonal	1666	Medium
Zr	91.24	6.51	Hexagonal	1852	High

provide a less expensive source of boron ($20/kg-$40/kg), as it is already produced in large quantities for a number of industrial applications. B_4C was investigated alongside boron in this thesis to determine whether B_4C is a realistic alternative. Regardless of how B_4C performs, a drastic improvement in energetic performance over the current baseline material (aluminum) by any boride mixture or compound can also justify the use of a more expensive material. Many considerations must be weighed.

On a thermodynamic basis, the potential of an energetic material can be gauged by its standard enthalpy (or heat) of combustion, $\Delta H°c$. It is found by measuring the heat released upon oxidation, such as in the reaction

$$B_{(s)} + \frac{3}{4} O_{2(g)} \rightarrow \frac{1}{2} B_2 O_{3(s)} \tag{1.2}$$

where the ΔH^o_c is given by

$$\Delta H^\circ_c = \frac{1}{2}\Delta H^\circ_{f,B_2O_3} - \left(\Delta H^\circ_{f,B} + \frac{3}{4}\Delta H^\circ_{f,O_2}\right) \quad (1.3)$$

where $\Delta H_f°$ for boron and oxygen, as elements in their standard state, is defined to be zero. Heats of combustion are usually reported on a molar basis, but in an energetic system it is more meaningful to compare materials on a mass or volume basis because the design of an energetic system calls for a specific mass or volume. The heats of combustion of the elements in Table 1.1 are reported, along with heat capacities, in Table 1.2. Boron, lithium, silicon, aluminum and magnesium have the highest heats of combustion per gram. Cobalt, boron, aluminum, zirconium, silicon and titanium are the highest on a volume basis. With high heats of formation and relatively low heat capacities (important to limit the energy absorbed by the materials upon heating), it is clear that boron, aluminum and silicon are thermodynamically favorable elemental fuels. Compounds of these elements are of particular interest for energetic applications.

Boron-metal compounds may provide an advantage over elemental fuels by decreasing the sensitivity of the energetic powders. Sensitivity of a powder is related to

Table 1.2

Thermodynamic Comparison of Energetic Elements

Metal	ΔH_c (kJ/mol)	ΔH_c (kJ/g)	ΔH_c (kJ/cc)	C_p (J/mol K)
Al	-847.0	-31.4	-84.7	31.8
B	-618.5	-57.2	-135.5	25.0
Co	-902.3	-15.3	-136.3	36.9
Li	-302.2	-43.5	-23.2	28.9
Mg	-608.9	-25.1	-43.6	32.6
Ni	-235.0	-4.0	-35.6	33.0
Si	-905.1	-32.2	-75.1	26.3
Ti	-750.0	-15.7	-71.1	32.5
Zr	-1091.0	-12.0	-77.9	31.1

its reactivity with surrounding material(s) and atmosphere, thermal characteristics and electrostatic behavior. An insensitive material can withstand rapid fluctuations in temperature, electrostatic charge or oxidizing environments without initiating a reaction. However, these materials must also be comparable in heat release to standard elemental fuels when activated deliberately.

Table 1.3 gives physical characteristics and cost of some boride compounds of interest. Table 1.4 shows the heats of combustion and heat capacities for the borides from Table 1.3 except for SiB_6, for which no thermodynamic data were found. Similar to the elemental fuels, heats of formation compared on a mass and volume basis give a preliminary indicator of potential energetic performance. AlB_{12}, B_4C, AlB_2, MgB_2 and $Al_{0.5}Mg_{0.5}B_2$ have the highest heats of combustion on a gravimetric basis.

CoB, CoB_2, AlB_{12}, B_4C and AlB_2 have the highest heats of combustion on a volume basis. The toxicity of cobalt limits its feasibility for use in energetic applications. Therefore, AlB_{12}, AlB_2 and B_4C are the top boride compound candidates from a thermodynamic standpoint. In addition to thermodynamics considerations, the crystal structure of fuel additives at the atomic level may play a critical role in material selection.

All crystalline boron is either rhombohedral or tetragonal, with large numbers of atoms ($12 \leq Z \leq 315$) making up a single unit cell. The high melting point comes as a result of the covalent bonding between atoms. One such structure contains four boron icosahedra connected by a central boron atom as shown in Figure 1.1.[27] Amorphous boron is comprised of the same icosahedral structure but lacks long range order.[27] Many boride compounds are composed of the same type of icosahedra as shown in Figure 1.2 where $MgAlB_{14}$ has the same orthorhombic crystal structure as MgB_{12} or AlB_{12}.

Table 1.3

Physical Properties and Relative Cost of Selected Boride Compounds

Compound	Molecular Weight (g/mol)	Theoretical Density (g/cc)	Crystal Structure	Decomposition/Melting Temperature (°C)	Relative Cost
AlB_2	48.6	3.17	Hexagonal	1400	High
AlB_{12}	156.7	2.58	Tetragonal	2150	High
B_4C	55.3	2.52	Rhombohedral	2470	Low
CoB	69.7	6.77	Orthorhomcic	1460	High
Co_2B	128.7	8.06	Tetragonal	1280	High
MgB_2	45.9	2.63	Hexagonal	1545	High
$Mg_{.5}Al_{.5}B_2$	47.3	2.9	Hexagonal	---	High
$AlMgB_{14}$	190.5	2.75	Orthorhombic	---	High
SiB_6	93.0	2.17	Cubic	---	High
TiB_2	69.5	4.52	Hexagonal	3225	Medium
ZrB_2	112.8	6.10	Hexagonal	3245	Medium
ZrB_{12}	221.0	3.63	Cubic	2250	High

Table 1.4

Thermodynamic Comparison of Selected Boride Compounds

Compound	$\Delta H_{f\ 1000\ K}^{o}$ (kJ/mol)	$\Delta H_{c,\ 1000\ K}$ (kJ/mol)	$\Delta H_{c,\ 1000K}$ (kJ/g)	$\Delta H_{c,\ 1000K}$ (kJ/cc)	$C_{p,\ 1000K}$ (J/mol K)
AlB_2	-165.2	-1919	-39.5	-125.1	78.2
AlB_{12}	-289.0	-7980	-50.9	-131.4	317.8
B_4C	- 73.1	-2796	-50.6	-127.5	114.3
CoB	- 96.2	-1425	-20.4	-138.3	56.5
Co_2B	-128.7	-2295	-17.8	-143.7	89.3
MgB_2	-106.6	-1739	-37.9	- 99.6	71.7
$Mg_{.5}Al_{.5}B_2$	-135.9	-1829	-38.7	-112.2	---
$AlMgB_{14}$	-395.6	-5390	-28.3	- 77.8	---
TiB	-162.0	-1207	-20.6	- 93.8	51.9
TiB_2	-326.7	-1660	-23.9	-108.0	77.1
ZrB_2	-325.4	-2003	-17.7	-108.3	72.0

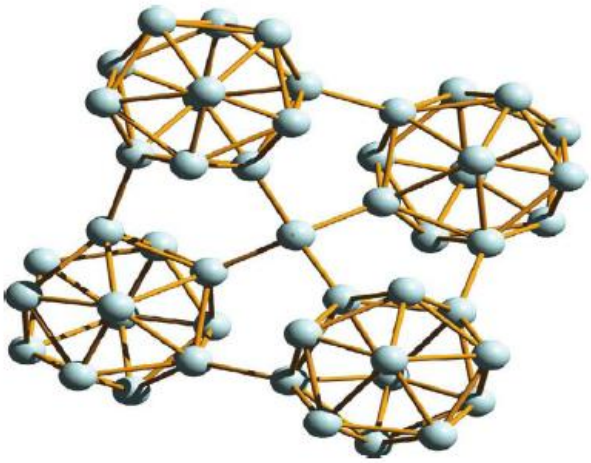

Figure 1.1. Structure of tetragonal boron composed of four icosahedra bonded by boron.[27] Boron has a high melting point due to the strong covalent bonding between atoms.

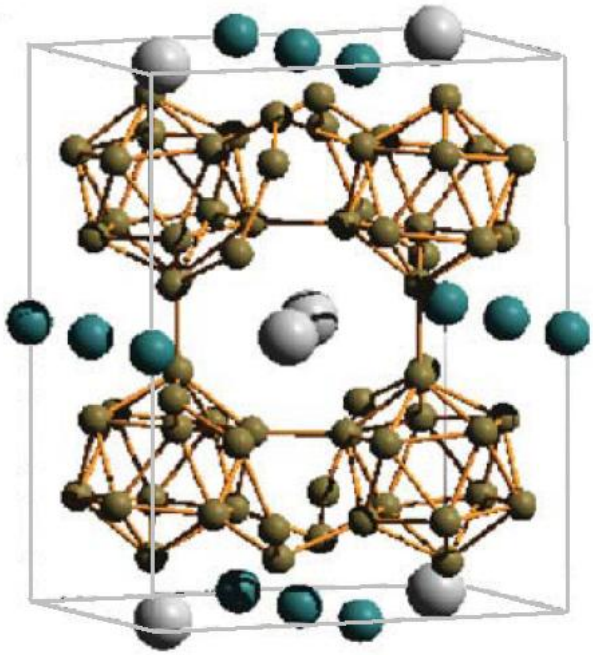

Figure 1.2: Proposed structure for $AlMgB_{14}$. Boron atoms are brown, aluminum atoms are green and magnesium atoms are gray.[27]

The hexagonal crystal structures of materials like LiB,[28-29] MgB_2, and AlB_2 are of interest since they are not composed of icosahedra but alternating layers of boron and metal atoms as shown in Figure 1.3.[30] These layered structures have planar sp^2 hybridized boron bonding instead of icosahedral covalent bonds, and decompose at relatively low temperatures. Presently, it is unclear whether there is a preferred crystal structure for energetic borides.

The effects of crystal structure and bonding on metal boride materials are reflected in their phase diagrams. Hexagonal AlB_2 decomposes at the relatively low temperature of 975°C[8] while the tetragonal (icosahedral) AlB_{12} doesn't decompose until ~2150°C (although there is still debate as to whether AlB_{12} melts congruently or decomposes). The decomposition of AlB_2 results in a significant amount of liquid aluminum, given by the equation

$$6AlB_2 \rightarrow AlB_{12} + 5Al \qquad (1.4)$$

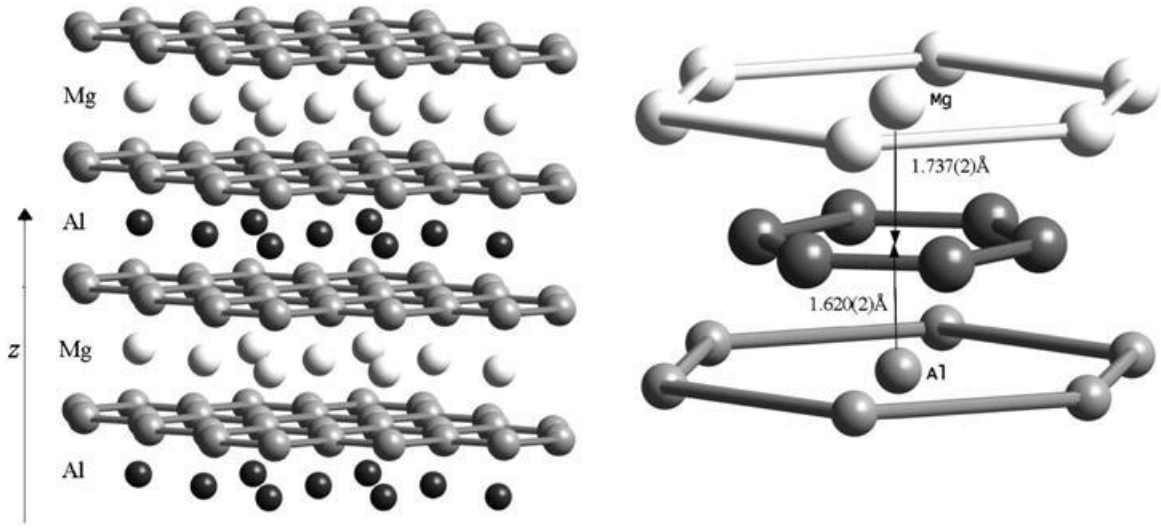

Figure 1.3: Proposed structure of $Al_{0.5}Mg_{0.5}B_2$.[30] AlB_2 and MgB_2 have the same structure.

The presence of liquid aluminum at higher temperatures may aid the oxidation process through rapid exothermic reactions and increased transport. The Mg-B phase diagram is similar to that of the Al-B system, with the lower temperature diboride phase decomposing into higher borides (MgB_4, MgB_7, MgB_{12}) as the temperature is increased.[8] Due to the relative similarity in structure, the magnesium and aluminum borides have a degree of solid solubility. While magnesium was not one of the top candidates for energetic elements based on its enthalpy of combustion, its high reactivity with air make it an interesting material for further investigation, especially in conjunction with aluminum.

The boride compounds selected for testing in this study were AlB_2, MgB_2, AlB_{12}, $Mg_{0.5}Al_{0.5}B_2$, $AlMgB_{14}$, and SiB_6. These compounds were selected on the basis of cost, availability, ease of synthesis, and potential energetic performance. The selection of five aluminum and/or magnesium borides allowed for a number of comparisons to be made, including the role of magnesium and aluminum in synthesis and oxidation, metal-to-boron ratio, hexagonal versus icosahedral structure, the role of decomposition temperature and the presence of a liquid at high temperatures. Silicon and boron do not form a diboride compound, but SiB_3 and SiB_6 decompose at ~1300 and 1850°C, respectively.[8] As a material with a higher decomposition temperature and lower metal-to-boron ratio than the diborides and an icosahedral boron structure, SiB_6 provided an interesting comparison to the aluminum/magnesium boride materials.

Materials were selected to incorporate a range of physical, chemical and thermodynamic properties in order to determine which properties had the greatest correlation to sensitivity and energetic performance. Stoichiometric mixtures of the

starting powders for each compound were also tested in an effort to understand the role of bonding and crystal structure on energetic performance.

All powders were synthesized from mixtures of elemental powders, which included the aluminum baseline material, boron, magnesium, aluminum-magnesium alloy, silicon and boron carbide. Synthesis and characterization were conducted at Ceramatec, Inc. These powders were then supplied to ARDEC for sensitivity testing, screening, and energetic testing. Due to budgetary constraints and organizational setbacks at ARDEC the full battery of tests were not conducted. Nonetheless, valuable results were obtained through the characterization process warranting continued investigation into metal borides for insensitive energetics.

1.3 References

1. Kubota, Naminosuke. "Propellants and Explosives," Wiley-VCH, Weinheim, Germany (2007)

2. J. Macek and M. Semple, "Combustion of Boron Particles," *Combust. Sci. Tech*. **1**, 181-191 (1969)

3. L. Yeh and K. K. Kuo, "Ignition and Combustion of Boron Particles," *Prog. Energy Comb. Sci.*, **22**[6] 511-41 (1996)

4. W. Zhou, R. A. Yetter, F. L. Dryer, H. Rabitz, R. C. Brown, and C. E. Kolb, "A Comprehensive Physical and Numerical Model of Boron Particle Ignition," *26th Int. Symposium on Combustion*, The Combustion Institute, 1909-1917 (1996)

5. B. Hussman and M. Pfitzner, "Extended Combustion Model for Single Boron Particles Part I: Theory," *Combust. and Flame* **157** 803-821 (2010)

6. B. Hussman and M. Pfitzner, "Extended Combustion Model for Single Boron Particles Part 2: Validation," *Combust. and Flame* **157** 822-833 (2010)

7. T. Mitani and M. Izumikawa, "Combustion Efficiencies of Aluminum and Boron in Solid Propellants," J. Spacecraft 28[1] 79-84 (1991)

8. H. T.-S. Hsia, "Air-Augmented Combustion of Boron and Boron-Metal Alloys," AFRTL-TR-71-80 (June 1971)

9. I. Barin, Thermochemical Data of Pure Substances, (VCH, New York, 1993)

10. R. L. Mazzi and B. E.Warren, "The Structure of Vitreous Boron Oxide," *J. App Crystallography* **3**[4] 251-257 (1970)

11. E. L. Dreizin, D. G. Keil, W. Felder, and E. P. Vicenzi, "Phase Changes in Boron Ignition and Combustion," *Combustion and Flame,* **119** 272-290 (1999).

12. R. O. Foelsche, R. L. Burton and H. Krier, "Boron Particle Ignition and Combustion at 30-150 atm," *Combust. and Flame* **117** 32-58 (1999)

13. R. Ulas, K. K. Kuo, and C. Gotzmer, "Ignition and Combustion of Boron Particles in Fluorine-Containing Environments," *Combustion and Flame,* **127** 1935-1957 (2001)

14. W. Zhou, R. A. Yetter, F. L. Dryer, H. Rabitz, R. C. Brown, and C. E. Kolb, "Effect of Fluorine on the Combustion of "Clean" Surface Boron Particles," *Combustion and Flame,* **112** 507-521 (1998)

15. Y.-S. Kwon, A. A. Gromov, A. P. Ilyin, E. M. Popenko, and G.-H. Rim, "The Mechanism of Combustion of Superfine Aluminum Powders," *Combust. and Flame* **133** 385-391 (2003)

16. L. Meda, G. Marra, L. Galfetti, F. Severini, and L. De Luca, "Nano-Aluminum as Energetic Material for Rocket Propellants," *Mater. Sci. Eng. C* **27** 1393-1396 (2007)

17. R. D. Lee, K. Park, and M. R. Zachariah, "Importance of Phase Change of Aluminum in Oxidation of Aluminum Nanoparticles," *J. Phys. Chem. B* **108** 14793-14795 (2004)

18. M. A. Trunov, S. M. Umbrajkar, M. Schoenitz, J. T. Mang, and E. L. Dreizin, "Oxidation and Melting of Aluminum Nanoparticles," *J. Phys. Chem. B* **110** 13094-13099 (2006)

19. M. M. Mench, K. K. Kuo, C. L. Yeh, and Y. C. Lu, "Comparison of Thermal Behavior of Regular and Ultra-Fine Aluminum Powders (Alex) Made from Plasma Explosion Process," *Combust. Sci. and Tech.* **135** 269-292 (1998)

20. C. L. Yeh and K. K. Kuo, "*8th Int. Symp. on Transport Phenomena in Combust."* (1995)

21. S. P. Luh, H. C. Perng, T. K. Liu and H. S. Chu, "Influence of Boron Coating on its Fuel-Riched Solid Propellant," *Xiyou Jinshu Cailiao Yu Gongcheng* **38**[1] 172-175 (2010)

22. A. Leibu, D. Gany and D. W. Netzer, "*8th Int. Symp. on Transport Phenomena in Combust.*" (1995)

23. I. Leibu, V. Rosenband and A. Gany, "The Boron/Titanium Composite Particle: A Novel Approach for Ignition Enhancement," *31st AIAA/ASME/SAE/ASEE Joint Propulsion Conference and Exhibit,* **1995** 2988-3004

24. T.-K. Liu, S.-P. Luh and H.-C. Perng "Effect of Boron Particle Surface Coating on Combustion of Solid Propellants for Ducted Rockets," *Propellants, Explosives and Pyrotechnics* **16** 156-166 (1991)

25. P. Q. Flower, P. A. Steward, L. R. Bates, A. J. Shakesheff and P. W. Reip, "Improving the Efficiency of Metallised Explosives," Insensitive Munitions European Manufacturers Group (2006)

26. J. M. Mota, J. Abenojar, Martinez, F. Velasco and A. J. Criado "Borides and Vitreous Compounds Sintered as High-Energy Fuels," *J. Solid State Chem.* **177** 619–627 (2004)

27. T. Letsoalo and J. E. Lowther, "Systematic Trends in Boron Icosahedral Structured Materials," *Physica B: Cond. Matt*.,**403**[17] 2760-67 (2008)

28. Z. Li, Q. Z. Qu, B. Huang, and Z. Li, "Crystal Structure and Morphology of a New Compound, LiB," *J. Alloys Comp*. **311** 256-264 (2000)

29. A. N. Kolmogorov and S. Curtarolo, "Prediction of Different Crystal Structure Phases in Metal Borides: A Lithium Analog to MgB_2," *Phys. Rev. B*, **73**[18] 180501-4 (2006)

30. D. A. Andersson, L. Casillas, M. I. Baskes, J. S. Lezama and S. D. Conradson, "Modeling of the Phase Evolution in $Mg_{1-x}Al_xB2$ ($0 < x < 0.5$) and Its Experimental Signatures," *J. Phys. Chem. B* **113** 11965–11976 (2009)

2. SYNTHESIS AND CHARACTERIZATION OF BORIDES

2.1 Characterization Procedure

Twenty powders were selected for characterization and energetic testing. All powders were mixed or synthesized from five raw powders. The raw powders used for this study were Valimet H3 aluminum 99.99% (herein called Al), H. C. Starck amorphous boron 95% (B) with 2.0% oxygen and 0.4% magnesium as chemical impurities, -325 mesh Atlantic Co. magnesium (Mg), Valimet 55wt.% Mg-44wt.% Al alloy (Al-Mg) with 0.4% Fe, Elkem silicon 99% (Si) and UK boron carbide (B_4C).

From these raw powders the starting mixtures for the various reacted boride compounds were mixed. Raw powders with the desired stoichiometric composition were added to 1.5 or 2 liters of hexane and milled in a stainless steel mill with 10 kg spherical WC-Co media at 80 rpm for 1 hour. Batches of 500 g or 750 g were made. The hexane was evaporated by air convection for at least 24 hours.

Reacted borides were synthesized from the starting powders. There were many references in the literature on the synthesis of the borides of interest, including AlB_2,[1-3] AlB_{12},[4] MgB_2[5-14], $Mg_{0.5}Al_{0.5}B_2$,[15-17] $AlMgB_{14}$,[18-19] and SiB_6.[20] Three or four 20mm diameter by 20mm high cylindrical pellets (approximately 10g) of the starting powders were pressed at 50 MPa using a uniaxial press and loaded into a graphite crucible with a threaded lid. The materials were then fired in an argon atmosphere according to the temperature schedules listed in Table 2.1. The temperature schedules were determined

Table 2.1

Temperature Schedules for Reacted Powders

Starting Powder	Ramp Rate (°C/min)	Hold Temp (°C)	Soak Time (min)
Al + 2B	30	900	240
Al + 12B	33	1500	60
Mg + 2B	30	900	240
½Al-Mg + 2B	30	900	240
Al-Mg + 14B	33	1500	60
Si + 6B	33	1500	60
2Al + B_4C	30	900	240

based on the literature and on phase diagrams for the respective systems (Chapter 1). A more detailed investigation of the synthesis of AlB_2 is given in Chapter 3. The reacted pellets were removed from the crucible and crushed with a mortar and pestle. They were then screened through a 230 (63μm) mesh stainless steel screen.

The compositions of the starting and reacted powders were evaluated using X-ray diffraction (XRD) on a Phillips Analytical X'Pert-MPD PW 3040/00 X-Ray diffractometer with Cu-K_α radiation. The data were collected over a 2θ range of 15-75° with a step size of 0.02° and a counting time of 1 s/step. A commercially available software package (X'Pert, Phillips) was used for Rietveld fitting. The particle size and surface area of the particles were analyzed using laser light scattering (Beckman model LS 230) and multipoint N_2 adsorption surface area analysis (Micromeretics, Tristar model). Scanning electron microscopy (SEM) and energy dispersive spectroscopy (EDS) were used to analyze particle morphology and phase distribution.

2.2 Starting Powder Characterization

Diffraction patterns of raw powders were generally as expected. Due to the low atomic mass of boron and the large fraction of amorphous material, patterns containing

high molar ratios of boron registered fewer counts by the X-ray detector. Accordingly, the X-ray pattern for boron showed relatively few counts in relation to the background and boron was not easily detected in the starting powder mixtures with heavier elements. An XRD pattern for boron can be seen in Figure 2.1. Of the crystalline boron phases, the predominant polytype was rhombohedral (space group R3m [166]). There was also a detectable amount of boron oxide (B_2O_3, hexagonal, space group P31 [144]), which was expected to be present as a thin layer on the surface of the fine boron particles.

Aluminum, magnesium, and the aluminum-magnesium alloy were not scanned, but their patterns were reflected in the starting powder scans containing the respective raw powder. Aluminum, magnesium and oxygen were more easily distinguished by XRD than boron and therefore the crystal structure of powders containing higher molar ratios of these elements were more easily identified. The pattern for Al + 2B (Figure 2.2)

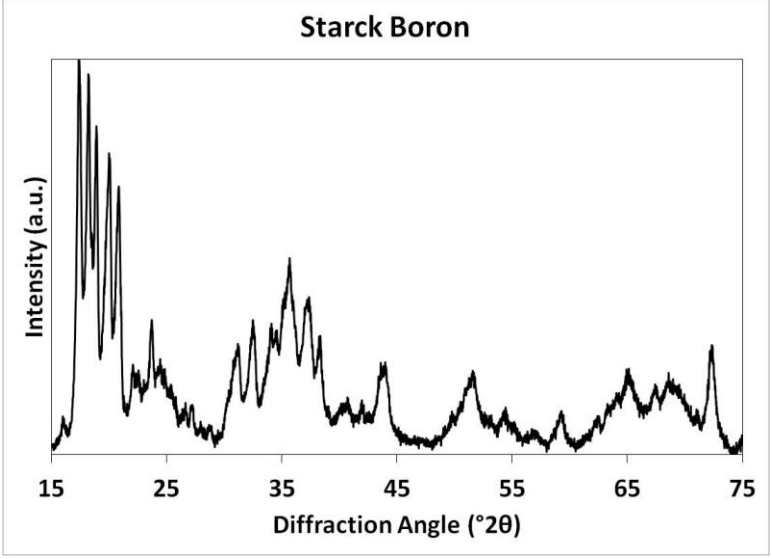

Figure 2.1 XRD scan of Starck boron powder. Most of the powder was amorphous and not detectable by XRD. Of the crystalline polytypes, rhombohedral boron was predominant. Broad peaks reflect small crystallite size.

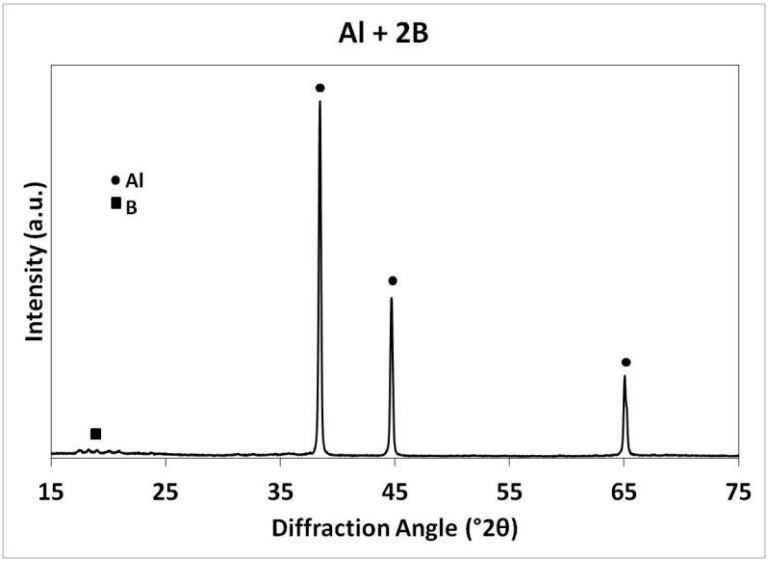

Figure 2.2: XRD pattern of Al + 2B. The largest peaks (at 38.5^0, 44.8^0 and 65^0 2θ) are aluminum peaks. Boron is difficult to resolve due to its amorphous structure and small atomic size.

almost exclusively showed cubic aluminum (space group Fm3m [225]), with trace amounts of rhombohedral boron. As expected, the pattern for Al + 12B (not shown) was very similar to that of Al + 2B but with less intense aluminum peaks due to dilution by the boron. Similarly, the pattern for Mg + 2B (Figure 2.3) showed large magnesium peaks (space group P63mmc [194]) with trace amounts of crystalline boron. MgO was expected to be seen on the magnesium powder but was not detected. The Al-Mg + 2B powder (Figure 2.4) contained the compound $Mg_{17}Al_{12}$ with space group I43m. The different space group from that of Mg or Al confirmed that the Al-Mg powder was an alloy and not a simple mixture of the two metals. This distinction is important because Al-Mg has a lower melting temperature (~450°C) than aluminum or magnesium. This may have implications for the oxidation behavior of this powder as well as for the synthesis of compounds using Al-Mg.

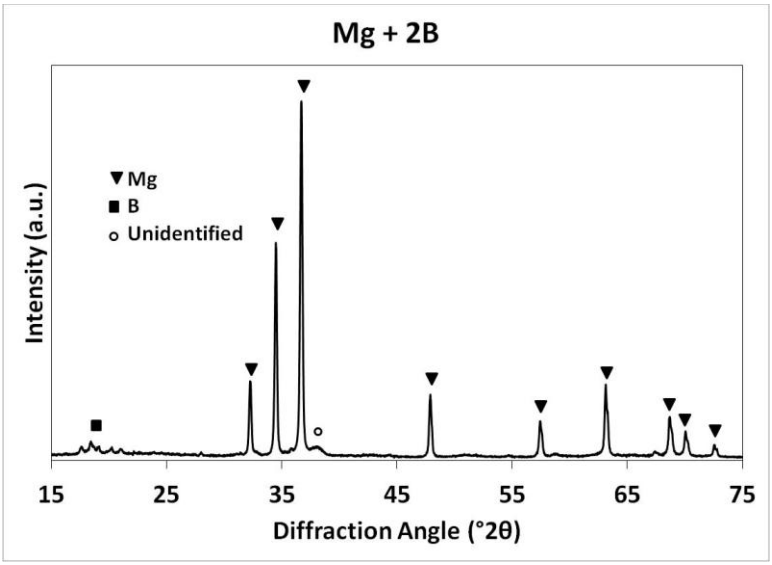

Figure 2.3: XRD scan of Mg + 2B powder. As with the other starting powders, boron was not easily detected.

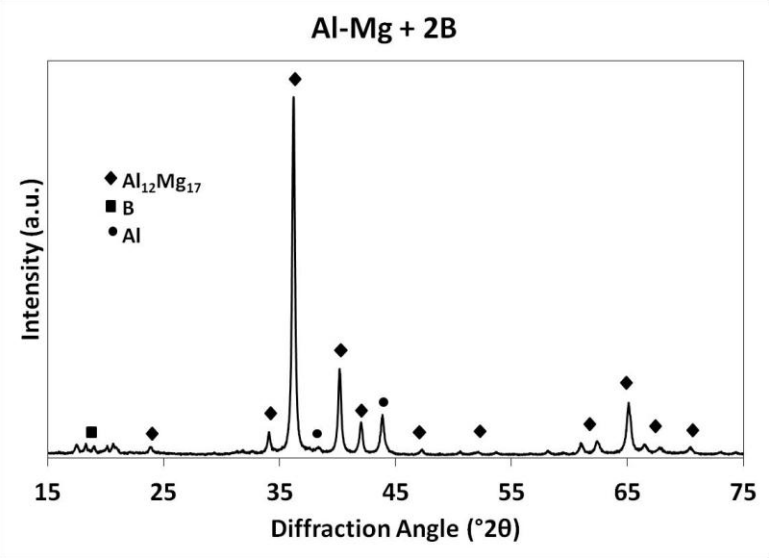

Figure 2.4: XRD scan of Mg-Al + 2B. The magnesium-aluminum alloy ($Al_{12}Mg_{17}$) had space group I43m, confirming the presence of a true alloy and not a mixture.

Al-Mg + 14B showed the same peak positions for the magnesium-aluminum alloy as Mg-Al + 2B but with reduced signal due to the larger amount of boron and therefore is not shown. Si + 6B (Figure 2.5) had the expected silicon peaks and a small amount of rhombohedral boron. 2Al + B_4C had aluminum peaks similar to Al + 2B with rhombohedral boron carbide peaks clearly present in Figure 2.6.

Table 2.2 summarizes particle characteristics for raw and starting powders. Particle size and surface area data showed that the raw boron powder was submicron in size. Consequently, powder mixtures with boron powder were also very fine. Milling helped to mix powders but did not alter the average particle size much. The measured particle size was compared to a calculated particle diameter, d, given by the equation

$$d = \frac{6}{\rho \cdot SA} \tag{2.1}$$

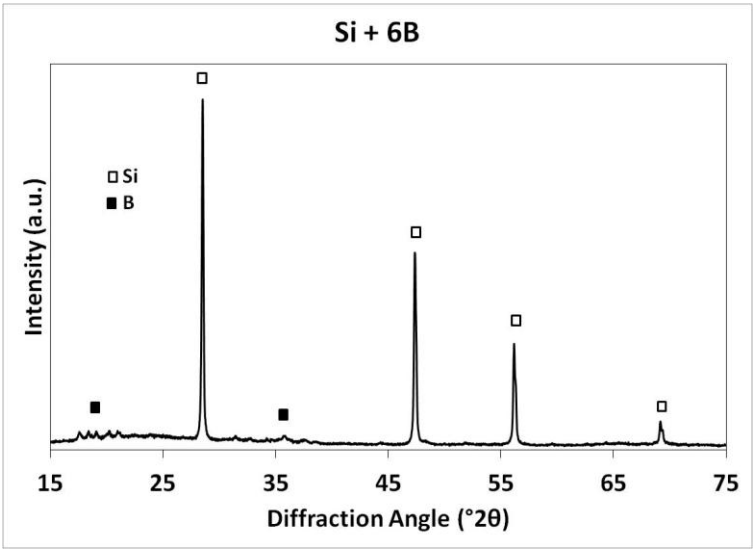

Figure 2.5: XRD pattern for Si + 6B.

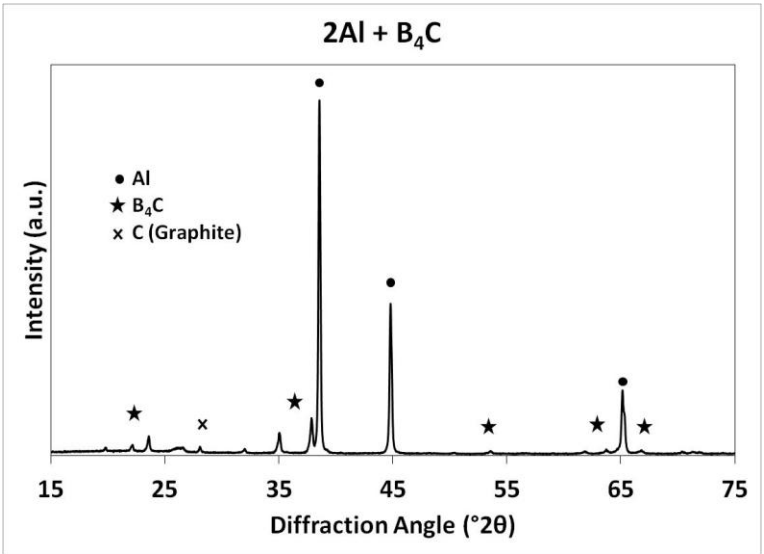

Figure 2.6: XRD pattern for $2Al + B_4C$. The three main aluminum peaks can be seen clearly, with rhombohedral B_4C peaks also present.

Table 2.2

Raw and Starting Powder Characteristics

Material	Surface Area (m^2/g)	Particle Size (μm) d_{10}	d_{50}	d_{90}	Mean	Calculated* Average (μm)
B	10.88	0.1	0.2	3.2	1.2	0.2
Al	1.39	0.2	2.9	7.8	3.4	1.6
Mg	0.82	11.8	38.2	66.5	38.6	3.9
Mg-Al	0.40	2.0	10.0	25.9	12.4	6.8
Si	3.56	0.2	2.7	5.9	2.7	0.7
B_4C	6.92	0.1	1.4	3.8	1.7	0.3
Al + 2B	6.23	0.2	2.3	6.5	2.8	0.4
Al + 12B	9.11	0.1	0.4	3.2	1.3	0.3
Mg + 2B	6.73	0.3	8.6	65.4	24.0	0.4
½ Al-Mg + 2B	5.85	0.1	1.6	5.1	2.0	0.4
Al-Mg + 14B	7.75	0.1	1.3	4.4	1.8	0.3
Si + 6B	9.10	0.1	0.4	2.6	0.9	0.3
B_4C + 2Al	4.30	0.2	2.0	5.4	2.4	0.6

*Based on Equation (2.1)

in which ρ is the density in g/cc and SA is the surface area in m^2/g. This equation assumes perfectly spherical, monosized particles, so the calculated diameter is generally an underestimation of the average particle diameter. From Table 2.2 it is clear that the calculated particle size does not agree with the measured average particle size, though the surface area and particle size should correlate for relatively equiaxed, well-dispersed particles. In addition to the spherical particle assumption, factors such as dispersion liquid (2-propanol in this case), dispersant used and solubility of the particles in the liquid also affected the measurements. Figure 2.7 and Figure 2.8 show SEM images of the starting powder mixtures. The powder mixtures were a distribution of metal powders in a boron matrix, in which the smaller boron particles tended to fill void spaces between the larger metal particles. The Al, Al-Mg and Si powders were made by gas atomization and were spherical. The Mg was less homogeneous in size and much larger most other particles used.

The SEM images in Figure 2.7 and Figure 2.8 give secondary electron images on the left and backscattered electron images on the right. The secondary electron images (SEI), which tended to have higher resolution, gave clear views of the particle morphology and surface characteristics. The backscattered images (BEC) gave insight into the distribution of phases in the powders. Light regions in BEC images corresponded to heavier elements (magnesium, aluminum and silicon) while darker regions corresponded to light elements (boron and carbon). It is clear from these images that particles tended to agglomerate, as expected, affecting the particle size measurement and quite possibly the synthesis of boride compounds, TGA results, and energetic testing described below.

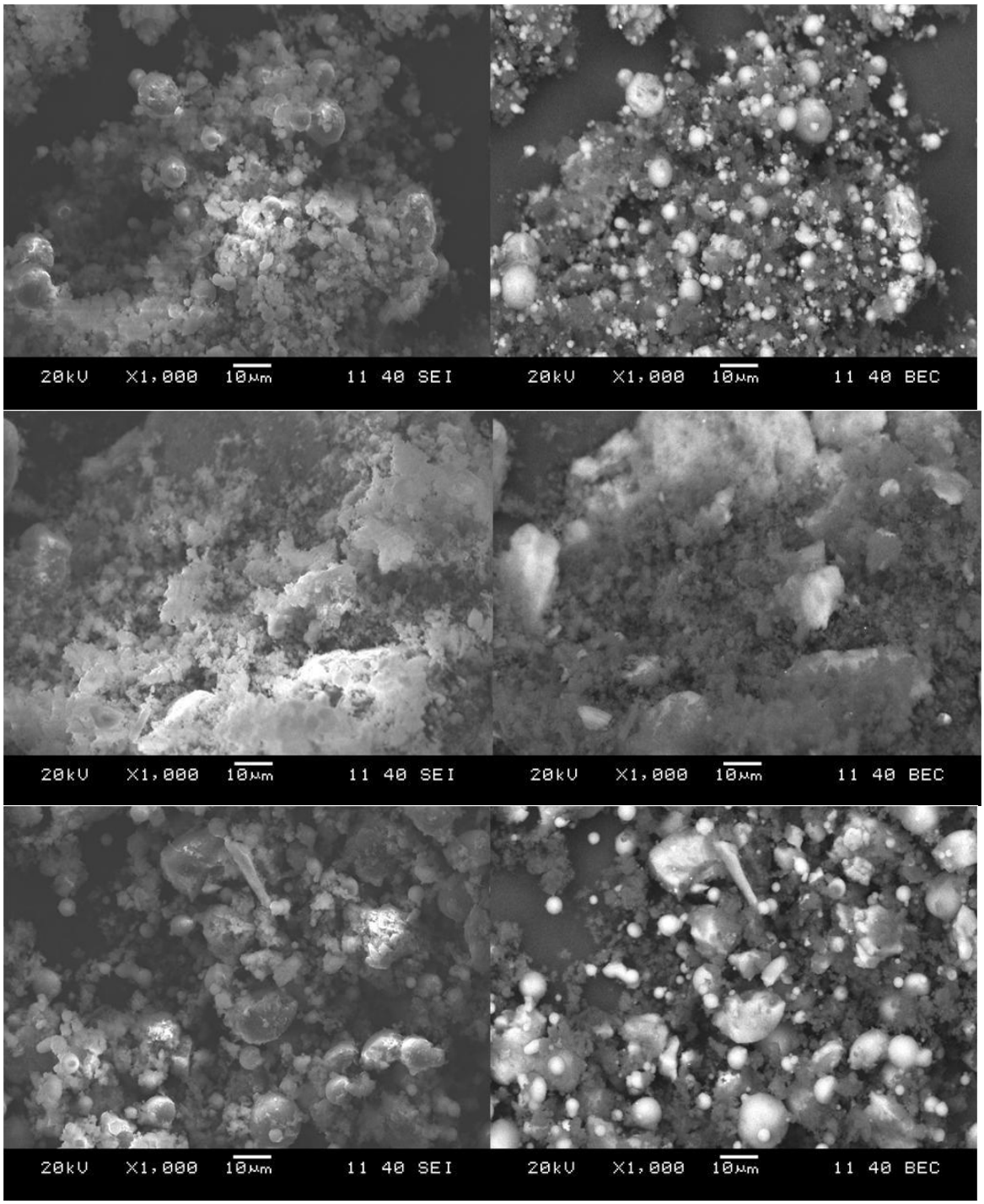

Figure 2.7: SEM images of starting powders. From top to bottom: Al + 2B, Mg + 2B and Al-Mg + 2B. Markers are 10 μm. Secondary images on left and backscattered images on right.

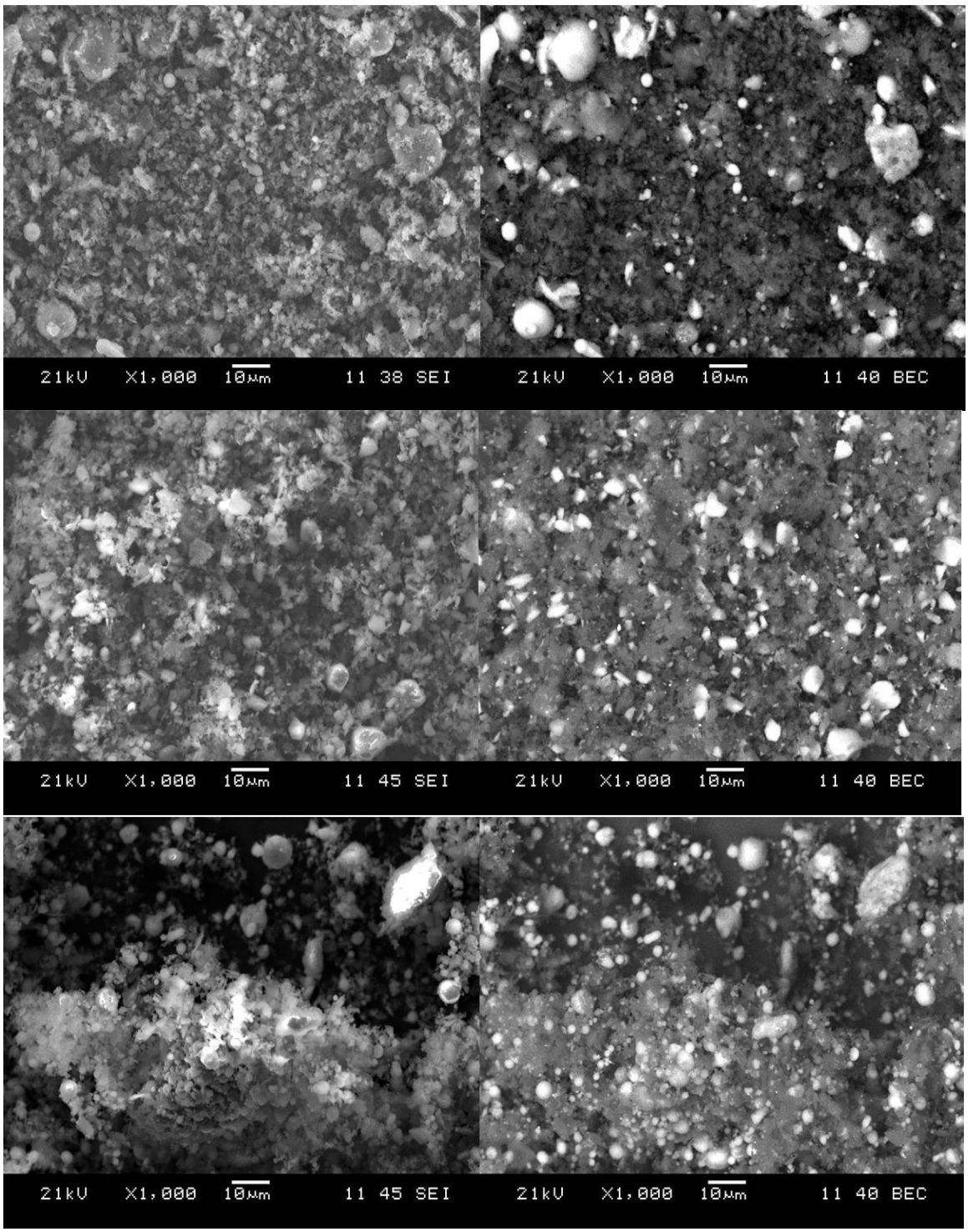

Figure 2.8: SEM images of starting powders. From top to bottom: Al-Mg + 14B, Si + 6B and $2Al + B_4C$. Markers are 10 μm. Secondary images on left and backscattered images on right.

2.3 Reacted Powder Characterization

In general, boride compounds were much easier to identify in XRD patterns than boron. The reaction of Al + 2B at 900°C for four hours produced AlB_2 (hexagonal, space group P6-mmm) with some free aluminum and a small amount of Al_2O_3 as shown in Figure 2.9. Rietveld analysis was used to calculate the relative weight percent of phases in the reacted powders. By this analysis, the reaction of Al + 2B produced 76.0% AlB_2 (by weight), 19.1% Al, 3.8% Al_2O_3 and 1.1% Al_3BC. The aluminum-to-boron ratio appeared to increase after the reaction because of incomplete conversion of aluminum and boron to AlB_2. Free boron was not accounted for in the Rietveld analysis, so the given composition is not correct. Assuming that all aluminum-containing phases were detected by XRD and that the initial stoichiometry was preserved, a calculation was made for the amount of free boron that must have been present. The adjusted composition was 64.9 % AlB_2, 16.3% Al, 14.6% B, 3.2% Al_2O_3, and 0.9% Al_3BC.

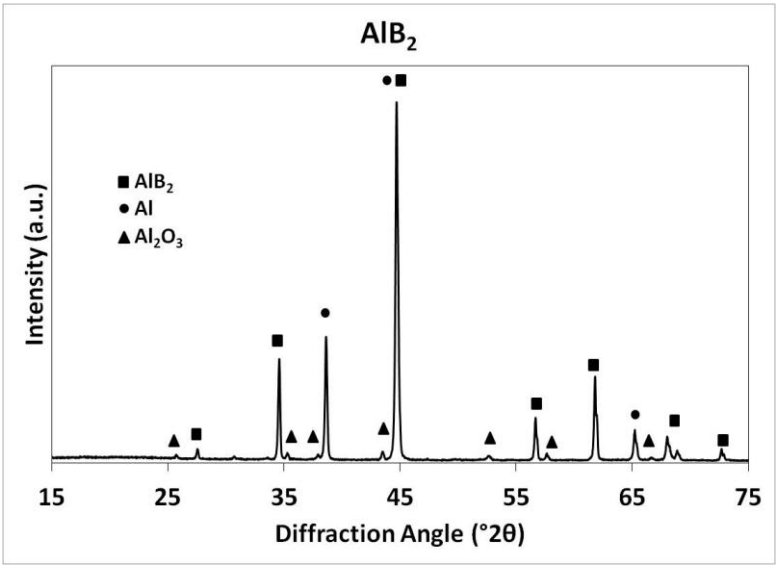

Figure 2.9: XRD pattern of Al + 2B reacted at 900°C for 4 hours. The pattern shows that AlB_2 was formed, along with some free aluminum and a small amount of Al_2O_3.

The oxide in this powder resulted partially from native oxide layers that coated both starting powders, partially from oxygen in the reaction atmosphere and partially from surface oxidation after removal from the inert reaction environment. The relative significance of each is discussed in detail in Chapter 3.

Reaction of Mg + 2B in the same conditions as Al + 2B resulted in MgB_2 with the same hexagonal structure (P6-mmm) as AlB_2 but with slightly different lattice parameters. Figure 2.10 shows that MgO was present as a contaminant in the reacted powder. The oxygen likely came from the same sources as for AlB_2 but the higher reactivity of magnesium with oxygen led to a higher amount of oxide. Rietveld analysis gave the composition as 83.6% MgB_2 and 16.1% MgO.

Reacted $Al_{0.5}Mg_{0.5}B_2$ was isostructural with AlB_2 and MgB_2. A few sources in the literature[17, 22] describe the $Al_xMg_{1-x}B_2$ structure in detail, with alternating layers of hexagonally close packed aluminum and magnesium separated by hexagonal boron

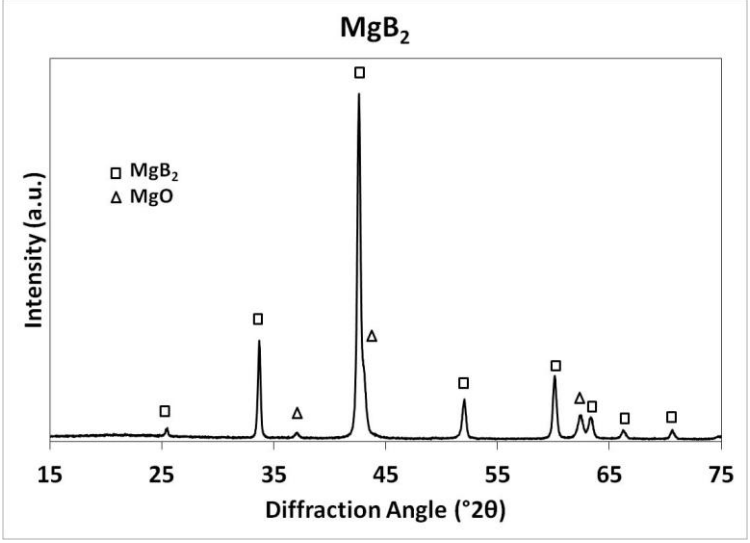

Figure 2.10: XRD pattern of Mg + 2B reacted at 900°C for 4 hours. MgB_2 was formed, with MgO present as a contaminant.

layers. A comparison of the three XRD patters in Figure 2.11 showed that the peak locations of $Al_{0.5}Mg_{0.5}B_2$ were intermediate to those of AlB_2 and MgB_2, due to a slight variation in lattice parameters between the three materials. The Rietveld software did not have structure data for this compound, so its composition could not be calculated.

Reacted Al + 12B (Figure 2.12) differed greatly from reacted Al + 2B. The phase diagram of the Al-B system (Chapter 1) predicts the formation of α-AlB_{12}, a tetragonal phase, at temperatures above ~980°C. The XRD pattern for reacted Al + 12B reflected this tetragonal structure, with Al_2O_3 and Al as minor impurities. A lower signal intensity compared to the diboride materials was due to the large molar ratio of boron to metal in this system, just as it was for the powder mixtures.

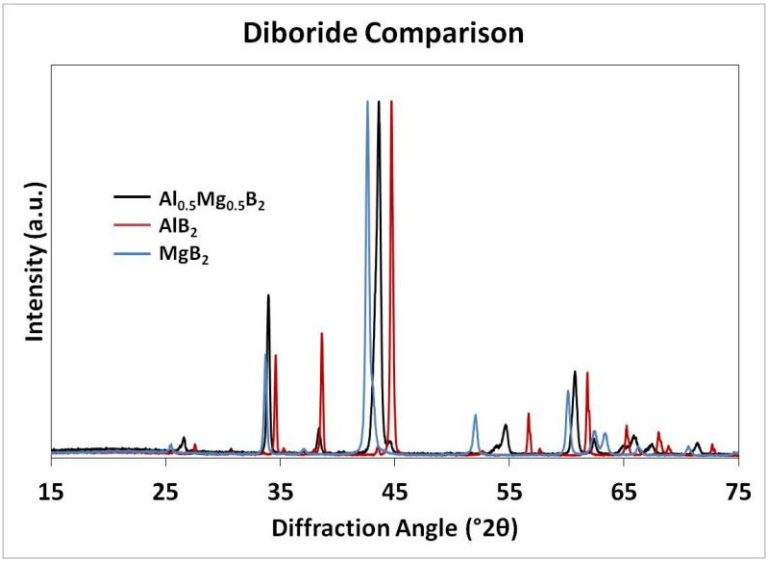

Figure 2.11: Comparison of XRD patterns for $Al_{0.5}Mg_{0.5}B_2$ (black), AlB_2 (blue), and MgB_2 (red). Notice the shift in peak location for the three diborides (corresponding to shifted lattice parameters) at 33-36° 2θ, 41-46° 2θ, 51-57° 2θ and 59-62° 2θ.

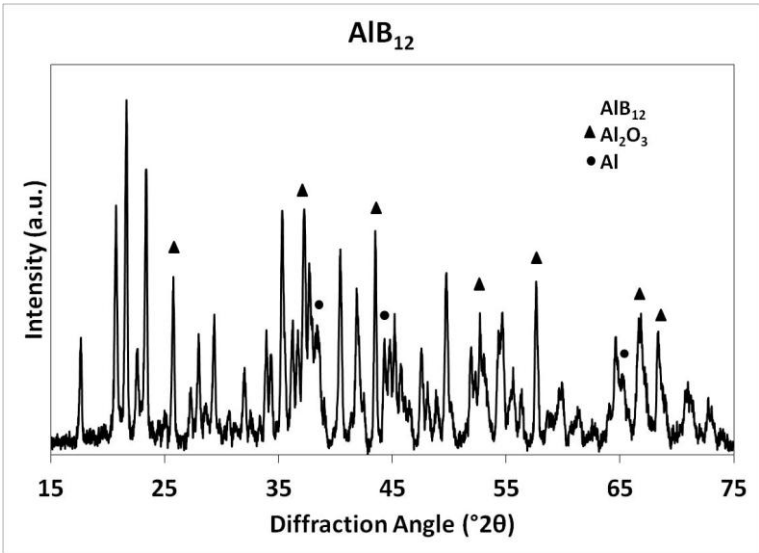

Figure 2.12: XRD pattern of Al + 12B reacted at 1500°C for one hour. Tetragonal AlB_{12} was formed with some Al_2O_3 and Al present.

The structure of $AlMgB_{14}$ was orthorhombic (space group Imam, Figure 2.13). It contained aluminum and spinel ($MgAl_2O_4$) as impurities. The compound is not perfectly stoichiometric,[23] with 75% aluminum occupancy and 78% magnesium occupancy, giving a true formula of $Al_{0.75}Mg_{0.78}B_{14}$. However, it will be referred to as $AlMgB_{14}$ in this thesis.

When reacted at 1500°C, Si + 6B gave the XRD pattern in Figure 2.14. The software was only able to index the pattern up to 40° 2θ, but the indexable peaks corresponded well to SiB_6 with no major impurities.

The reaction products of 2Al + B_4C were the least predictable. It was reacted under the same conditions as AlB_2, in an attempt to form AlB_2 and volatile carbon byproducts, thereby establishing a precedent for using boron carbide in place of boron.

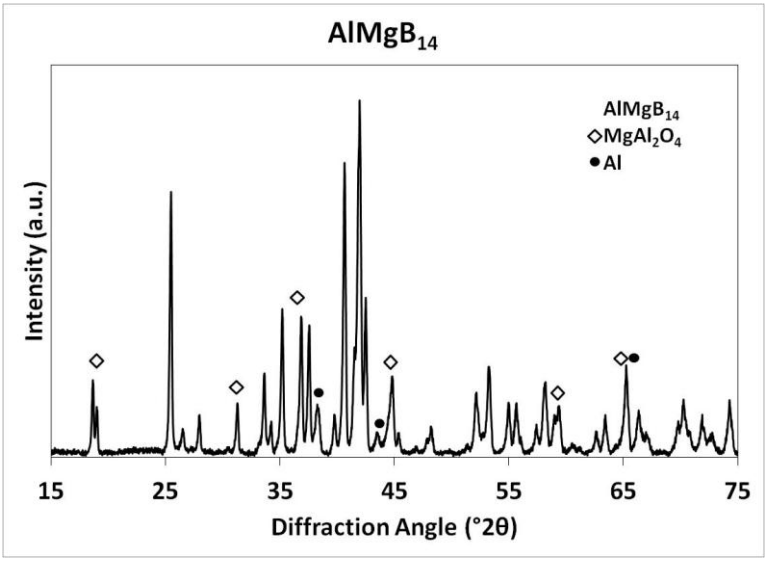

Figure 2.13: XRD pattern for Al-Mg + 14B reacted at 1500°C for one hour. $MgAl_2O_4$ and Al were present in the final product.

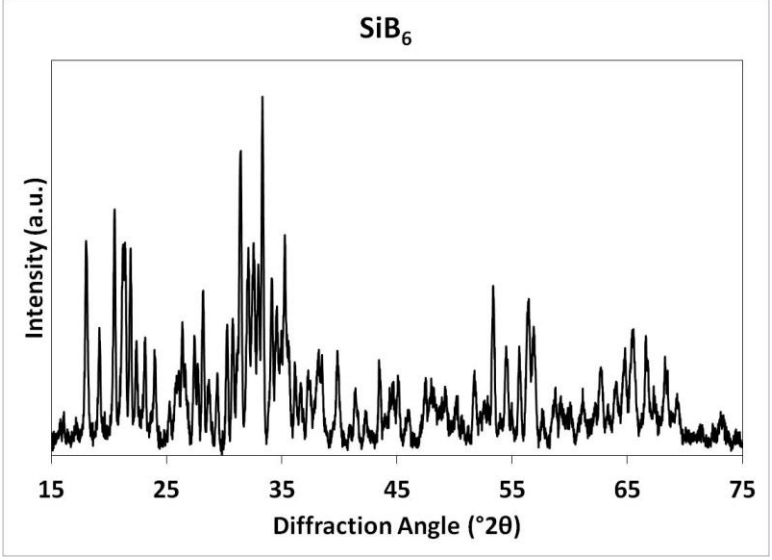

Figure 2.14: XRD pattern of Si + 6B reacted at 1500°C for one hour.

Figure 2.15 shows that the major products formed were AlB_2 and Al_3BC, suggesting that B_4C does have some promise as a boron replacement in synthesizing AlB_2. However, some aluminum and B_4C remained unreacted, similar to, but to a greater extent than, Al + 2B. Methods for increasing the extent of reaction between Al and B_4C would have to be devised in order for replacement of B with B_4C to be realized in the synthesis of AlB_2. Such methods were not explored in this thesis due to time and budgetary constraints.

A summary of the raw and starting powders used to make each boride compound can be found in Table 2.3. The characteristics of the reacted powders, including particle size and surface area, were affected by the characteristics of the raw powders and by the processing temperature of the reacted compounds. Table 2.4 includes the particle size and surface area measurements for the reacted powders. Powders reacted at 1500°C tended to have lower surface areas than those reacted at 900°C due to increased diffusion and

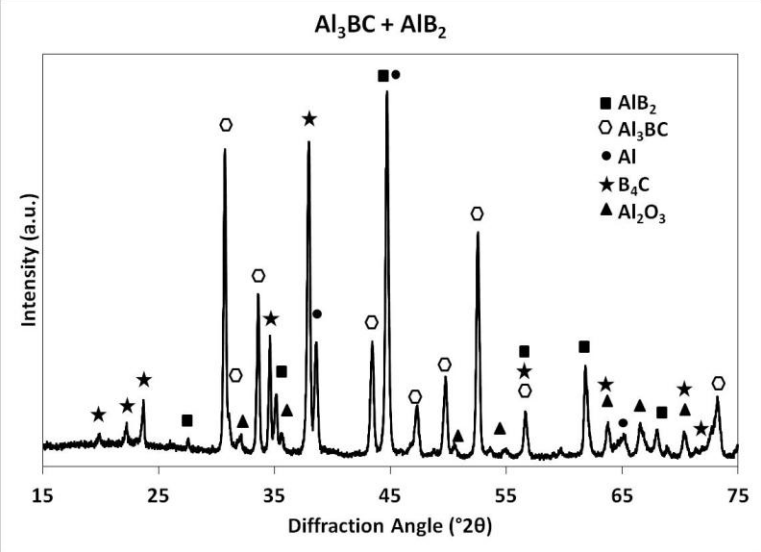

Figure 2.15: XRD pattern of 2Al + B_4C reacted at 900°C for 4 hours.

Table 2.3

Synthesized Powder Summary

Raw Powder(s)	Starting Powder	Reacted Powder
B, Al	Al + 2B	AlB_2 + Al + B
B, Al	Al + 12B	AlB_{12}
B, Mg	Mg + 2B	MgB_2
B, Al-Mg	½Al-Mg + 2B	$Al_{0.5}Mg_{0.5}B_2$
B, Al-Mg	Al-Mg + 14B	$Al_{0.75}Mg_{0.78}B_{14}$
B, Si	Si + 6B	SiB_6
B_4C, Al	2Al + B_4C	Al_3BC + AlB_2

Table 2.4

Boride Powder Characteristics

	Surface Area	Particle Size (μm)				Calculated*
Material	(m^2/g)	d_{10}	d_{50}	d_{90}	Mean	Average (μm)
AlB_2	1.64	0.5	8.4	28.8	11.9	1.2
AlB_{12}	1.38	1.3	6.4	17.5	8.6	1.8
MgB_2	4.78	0.7	9.2	46.0	17.4	0.5
$Mg_{0.5}Al_{0.5}B_2$	2.30	0.9	7.3	27.5	11.4	0.9
$Mg_{0.78}Al_{0.75}B_{14}$	0.55	4.8	14.7	28.2	16.0	4.1
SiB_6	0.71	3.2	14.9	38.4	20.8	3.9
Al_3BC + AlB_2	2.60	0.3	4.3	17.7	7.2	0.9

*Based on Equation (2.1)

particle coarsening at higher temperatures. SEM images in Figure 2.16 and Figure 2.17 revealed that the average particle size was <10 μm for all reacted powders but the small particles tended to form large agglomerates, over 100 μm in size.

2.4 Summary

Elemental powders of boron, aluminum, magnesium, aluminum-magnesium, silicon and boron carbide were used to synthesize the boride compounds AlB_2, MgB_2, $Al_{0.5}Mg_{0.5}B_2$, AlB_{12}, $AlMgB_{14}$, SiB_6 and Al_3BC through high temperature reaction under

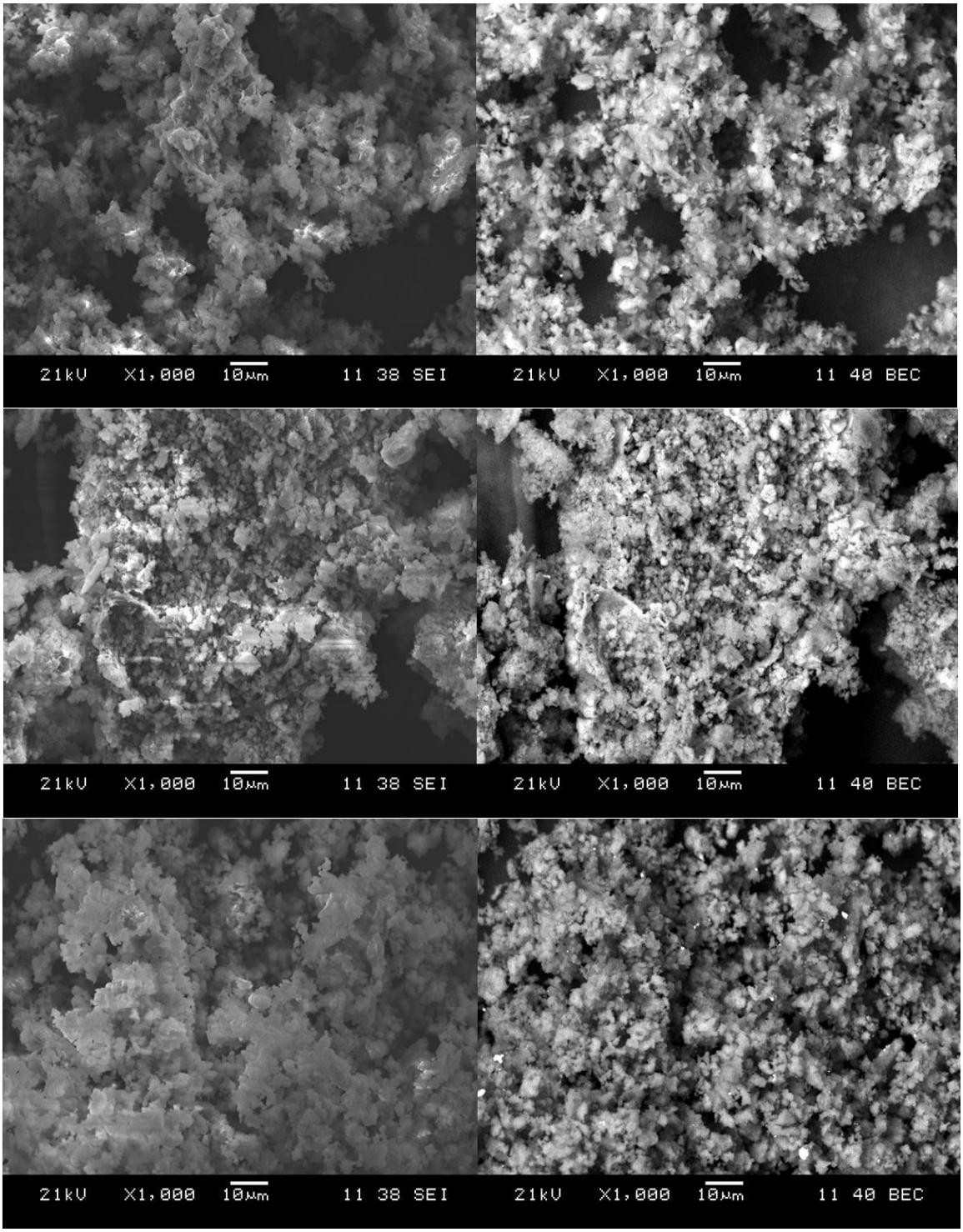

Figure 2.16: SEM images of reacted powders. From top to bottom: AlB_2, MgB_2 and $Al_{0.5}Mg_{0.5}B_2$. Markers are 10 μm, with secondary images on left and backscattered images on right.

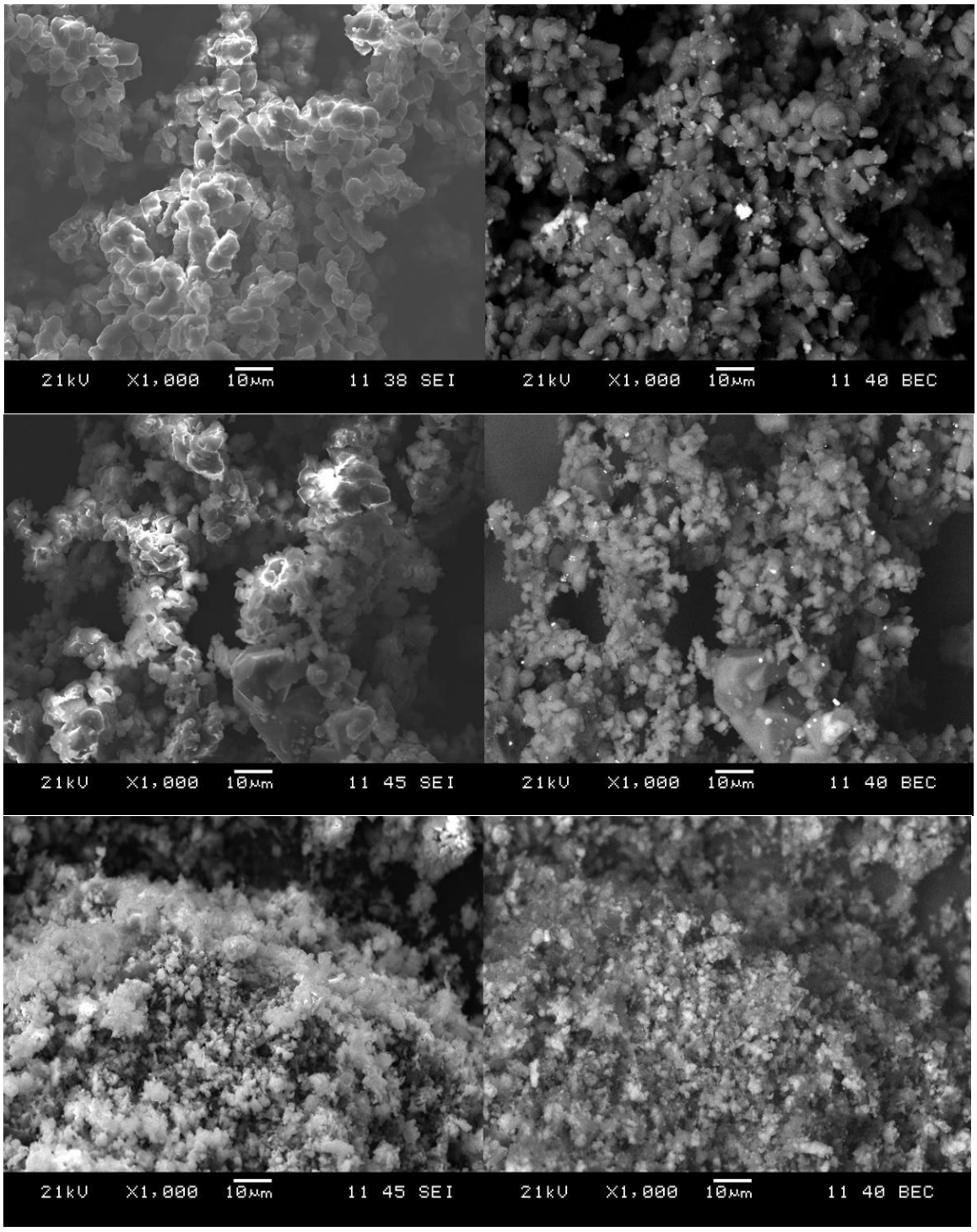

Figure 2.17. SEM images of reacted powders. From top to bottom: $AlMgB_{14}$, SiB_6 and $Al_3BC + AlB_2$. Markers are 10 μm with secondary images on left and backscattered images on right.

inert conditions. The raw powders were generally single phase by XRD but contained some impurities, especially oxygen, resulting from native oxides on the starting powders, reaction with oxygen during synthesis, and exposure to oxygen after reaction. AlB_2 also had carbon contamination that probably came from carbon in the starting boron, although none of the other borides had carbon impurities. Reduction of oxygen contamination is desired for energetic materials because the inert oxides do not participate in the energy producing oxidation reactions and essentially reduce the energy density of a given material. Carbon contamination is not as significant a problem, as carbides and borocarbides can oxidize with the rest of the fuel.

Most of the powder mixtures did not react completely during synthesis. It is not clear whether this will impact their energetic performance. Pure compounds are desired so that the effect of composition and crystal structure on sensitivity and performance can be investigated, but if there is little difference between a compound with 70% boride and 80 or 90% boride, the synthesis methods described above may be satisfactory for large scale production with no major adjustments needed. It may also be possible that powder mixtures have comparable performance to reacted compounds and the reaction process can be omitted altogether. Methods for improving the purity of AlB_2 are described in Chapter 3.

Laser light scattering showed that the reacted powders had a range of particle sizes resulting from differences in size of the raw powders; materials with large fractions of boron generally had smaller particle sizes than those with lower boron contents. SEM images suggested that materials that were reacted at higher temperatures had more particle coarsening than those reacted at lower temperatures. Images also revealed

particle agglomeration, leading to a disparity between particle size measurements and surface area analysis. Because agglomeration occurred to a different degree in each powder and the morphology of each was slightly different, surface area was a better method of comparison for the relative size of each powder.

The surface area of energetic powders is known to be a significant factor in their sensitivity and performance. High surface area powders are more susceptible to accidental discharge because there is more active area for a reaction to take place. This also makes them desirable in energetic systems, where their high reactivity leads to better performance than the same material with a lower surface area. Because the materials investigated had different surface areas, direct comparisons of sensitivity or performance without further qualifications cannot be made. However, energetic particles range in size from a few nanometers to hundreds of microns and can be made with almost any surface area. The materials studied in this thesis were fairly similar in surface area (0.5-11 m^2/g) because of the boron powder and can be compared qualitatively. Subsequent in-depth studies of any promising materials can be conducted on powders with the same surface area.

Characterization of the composition and morphology of these energetic fuel additives was critical for the study of AlB_2 synthesis in Chapter 3, oxidation behavior described in Chapter 4, activation energy determination in Chapter 5 and for the energetic testing conducted by ARDEC. The exact composition of the powders, including impurity content, was needed for accurate calculations of the theoretical weight gain from oxidation. Furthermore, secondary phases (if present in large enough quantities) may affect the oxidation behavior of a material, such as large amounts of free aluminum and

boron in AlB_2. The particle size distribution is necessary to implement higher-accuracy oxidation models that account for the size and surface area of all particles in the system. This becomes especially important for the powder mixture systems that have a bimodal particle size distribution.

Due to high interest in AlB_2 by ARDEC and the difficulty in making this particular material react completely, an in depth study aiming to increase the extent of reaction of aluminum and boron was conducted. The results of this study are presented in Chapter 3.

2.5 References

1. J. Fjellstedt, A. E. W. Jarfors and L. Svendsen, "Experimental Analysis of the Intermediary Phases AlB_2, AlB_{12} and TiB_2 in the Al–B and Al–Ti–B Systems," *J. Alloys and Compounds* **283** 192–197 (1999)

2. D. Mirkovi´c, J. Gröbner, R. Schmid-Fetzer, O. Fabrichnaya and H. L. Lukas, "Experimental Study and Thermodynamic Re-Assessment of the Al–B System," *J. of Alloys and Compounds* **384** 168–174 (2004)

3. M. J. van Setten and M. Fichtner, "On the Enthalpy of Formation of Aluminum Diboride, AlB_2," *J. of Alloys and Compounds* **477** L11–L12 (2009)

4. I. Hiashi, **"**Crystal Chemistry of α-AlB_{12} and γ-AlB_{12}**,"** Journal of Solid State Chemistry 154, **168-**176 (2000)

5. X. Wang, "The Formation of AlB2 in an Al–B Master Alloy," *J. of Alloys and Compounds* **403** 283–287 (2005)

6. R. A. Fisher, G. Li, J. C. Lashley, F. Bouquet, N. E. Phillips, D. G. Hinks, J. D. Jorgensen and G. W. Crabtree, "Specific heat of $Mg^{11}B_2$," *Physica C* **385** 180–191 (2003)

7. E. Bauer, C. Paul, S. Berge, S. Majumdar, H. Michor, M. Giovannini, A. Saccone and A. Bianconi, "Thermal Conductivity of Superconducting MgB_2," *J. Phys.: Condens. Matter* **13** L487–L493 (2001)

8. A. Bharathi, S. J. Balaselvi, S. Kalavathi, G. L. N. Reddy, V. S. Sastry, Y. Hariharan and T. S. Radhakrishnan, "Carbon Solubility and Superconductivity in MgB_2," *Physica C* **370** 211–218 (2002)

9. S. L. Bud'ko, P. C. Canfield and V. G. Kogan, "Magnesium Diboride: Basic Physical Properties and High Upper Critical Field Anisotropy," *Physica C* **382** 85–92 (2002)

10. D. G. Hinks, J. D. Jorgensen, H. Zheng, S. Short, "Synthesis and Stoichiometry of MgB_2," *Physica C* **382** 166–176 (2002)

11. J. D. Jorgensen, D. G. Hinks, and S. Short, "Lattice Properties of MgB_2 Versus Temperature and Pressure," *Phys.Rev.B* **63**, 224522 (2001)

12. Z.-K. Liu, D. G. Schlom, Q. Li and X. X. Xi, "Thermodynamics of the Mg–B System: Implications for the Deposition of MgB_2 Thin Films," *Appl. Phys. Lett.* **78**[23], 4 (2001).

13. I. Maurin, S. Margadonna, K. Prassides, T. Takenobu, Y. Iwasa and A. N. Fitch, "Carbon Miscibility in the Boron Layers of the MgB_2 Superconductor," *Chem. Mater.* **14** 3894-3897 (2002)

14. M. Pranthaman, J. R. Thompson and D. K. Christen, "Effect of Carbon-Doping on Bulk Superconducting MgB_2 Samples," *Physica C* **335** 1-5 (2001)

15. J. Shimoyama, K. Hanafusa, A. Yamamoto, Y. Katsura, S. Horii, K. Kishio and H. Kumakura, "Dramatic Effects of Ag Addition on Low Temperature Synthesis of MgB_2," *Journal of Physics: Conference Series* **97** 012255 (2008)

16. H. E. Calderóna, R. G. I. Hidalgo, Z. H. Melgarejoc and O. M. Suárez, "Effect of AlB_2–Mg Interaction on the Mechanical Properties of Al-Based Composites," *Materials Science and Engineering A* **527** 2258–2264 (2010)

17. S. Margadonna, K. Prassides, I. Arvanitidis, M. Pissas, G. Papavassiliou and A. N. Fitch, "Crystal Structure of the $Mg_{1-x}Al_xB2$ Superconductors near x=0.5," *Physical Review B* **66**, 014518 (2002)

18. J. S. Slusky, N. Rogado, K. A. Regan, M. A. Hayward, P. Khalifah, T. He, K. Inumaru, S. M. Loureiro, M. K. Haas, H. W. Zandburgen and R. J. Cava, "Loss of Superconductivity with the Addition of Al to MgB_2 and a Structural Transition in $Mg_{1-x}Al_xB_2$," *Nature* **410** 343-345 (2001)

19. B. A. Cook, J. L. Harringa, T. L. Lewis, and A. M. Russell, "A New Class of Ultra-Hard Materials Based on $AlMgB_{14}$," *Scripta Mater* **42**[6] 592-602 (2000)

20. S. Okada, T. Shishido, T. Mori, K. Iizumi, K. Kudou and K. Nakajima, "Crystal Growth of $MgAlB_{14}$-type Compounds Using Metal Salts and Some Properties" *J. of Alloys and Compounds* **458** 297–301 (2008)

21. S. K. Dutta and G. E. Gazza, "Properties of Hot Pressed SiB_6," *Ceramic Bulletin*, **52**[7] 552-554 (1973)

22. D. A. Andersson, L. Casillas, M. I. Baskes, J. S. Lezama and S. D. Conradson, "Modeling of the Phase Evolution in $Mg_{1-x}Al_xB2$ ($0 < x < 0.5$) and Its Experimental Signatures," *J. Phys. Chem. B* **113** 11965–11976 (2009)

23. T. Letsoalo and J. E. Lowther, "Systematic Trends in Boron Icosahedral Structured Materials," *Physica B: Cond. Matt*.,**403**[17] 2760-67 (2008)

3. HIGHER PURITY AlB_2

3.1 In-House Synthesis

The synthesis of AlB_2 has been attempted a number of times using various techniques since Funk reported the first method in 1925.[1] His general procedure of heating an aluminum-boron mixture in a nonoxidizing environment (that produced an "AlB_2" compound by chemical analysis) has been used in this paper, with improvements. Felten[2] reported a method of heating a stoichiometric ratio of aluminum and boron powders to 800^0C overnight in a graphite crucible. This method resulted in AlB_2 with the minor impurities aluminum, graphite, and boron carbide as detected by XRD. Variations of this method were used in this thesis, with a number of steps taken to minimize the impurities accompanying AlB_2 in the final product. Methods for making large quantities of high purity boron have not been described in the literature.

A study of synthesis atmosphere was conducted to determine the effect of atmosphere on AlB_2 formation and impurity content. Approximately 5g samples of a stoichiometric Al + 2B mixture (55.51% aluminum – 44.49% boron by weight) were pressed into pellets and heated at a rate of 200°C/hour to 900°C, held for 1 hour and returned to room temperature at 900°C/hour. This was done in argon, He-6%H_2 and vacuum (~60 mtorr). It was hypothesized that the incomplete reaction of boron and aluminum was due to the surface oxides on one or both of the powders. He-6%H_2 was expected to reduce the oxides (particularly B_2O_3) and aid in their removal by forming

volatile species. Because B_2O_3 has a finite vapor pressure at the reaction temperature, it was thought that reaction under vacuum would remove B_2O_3 through vaporization. [3]

XRD and subsequent Rietveld analysis of the powders showed that the synthesis atmosphere had little impact on AlB_2 formation and impurity content. Because boron was virtually undetectable by XRD due to the much higher intensities of aluminum and AlB_2, the amount of free boron had to be calculated. Assuming that the initial powder composition had a molar ratio of 2:1 boron to aluminum, the final composition could be calculated based on the knowledge that all the phases containing aluminum were detectable by XRD. Back-calculating for the amount of boron that must have been present was then a trivial matter. The sample heated in argon had the highest amount of Al_2O_3 impurity, while the sample heated under vacuum had the least, but both were within 1.5%. The sample heated under the reducing atmosphere of He-6%H_2 had the greatest amount of AlB_2 with 84%. This corresponded to the lowest levels of unreacted aluminum and boron. These differences in composition were relatively small and all three environments produced a similar product as shown in Table 3.1 and the XRD patterns in Figure 3.1.

Although the atmospheres investigated did not have much effect on the formation of AlB_2, it was not clear whether surface oxides were limiting the reaction rate. The

Table 3.1

Atmosphere Comparison

	Rietveld Analysis* (Weight %)				
Atmosphere	**AlB_2**	**Al**	**B**	**Al_2O_3**	**Al_3BC**
Argon	86.1 [78.9]	8.5 [7.8]	[8.4]	3.4 [3.1]	1.9 [1.7]
He-6%H_2	89.7 [84.0]	6.4 [6.0]	[6.4]	2.6 [2.4]	1.3 [1.2]
Vacuum	88.1 [81.4]	8.1 [7.5]	[7.6]	1.9 [1.8]	1.9 [1.8]

* Rietveld analysis adjusted for free boron in brackets.

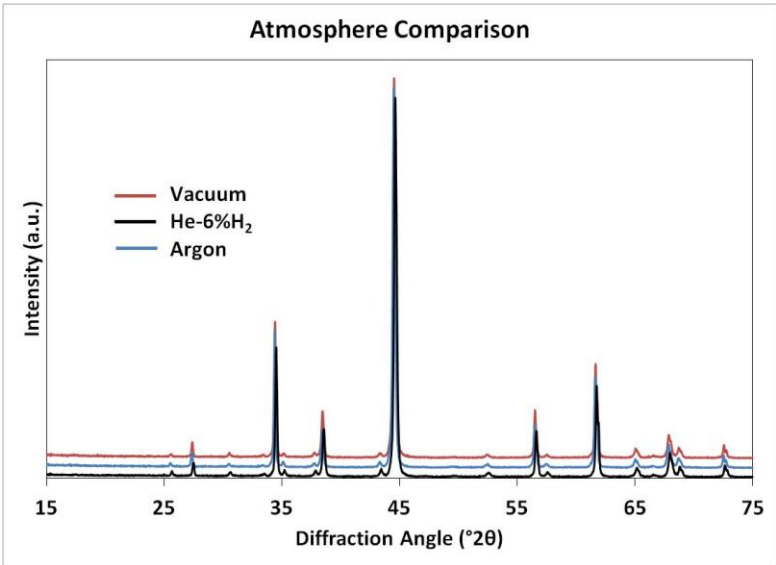

Figure 3.1: XRD patterns for samples reacted in argon (black), He-6%H_2 (black) and vacuum (red). Scans are nearly identical.

atmospheres did not significantly change the oxide content. The sample run in He-6%H_2 had the most AlB_2, but more Al_2O_3 than the sample under vacuum. While H_2 may reduce B_2O_3, it did not reduce Al_2O_3. In the presence of aluminum B_2O_3 may be reduced by aluminum to form Al_2O_3, (ΔG_f^o = -320 kJ/mol) which would explain the presence of Al_2O_3 in every AlB_2 X-ray pattern when it was not found on the aluminum by itself or as a mixture. B_2O_3 may have volatilized somewhat under vacuum, but the lower amount of Al_2O_3 did not correspond to higher AlB_2 content.

It is possible that significant reactions were taking place during the ramp up to temperature before the material reached its isothermal condition. Adsorbed gases, including water and O_2, have been seen to change the physicochemical properties of fine boron powders.[4] Measured weight loss from the compacted boron pellets in the previous studies may have been due to the volatilization of B_2O_3, carbon species, or adsorbed vapors. Removal of any or all of these species prior to reaching the reaction temperature by using various ramp rates and isothermal holds was investigated. Figure 3.2 clearly

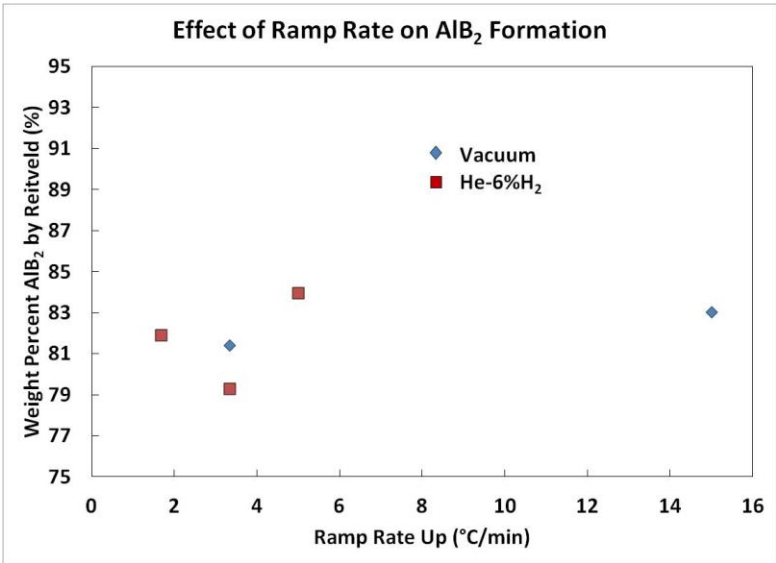

Figure 3.2: Effect of ramp rate on AlB_2 formation. Ramp rate does not appear to have an effect on AlB_2 formation in either vacuum or reducing atmospheres.

shows that ramp rate did not have an effect on AlB_2 formation in He-6%H_2 or vacuum, the most likely atmospheres for a changing ramp rate to be effective. Separately, an isothermal hold was implemented at 350°C with no improvement in the extent of reaction.

Due to the incomplete reaction of aluminum and boron in all reaction environments, it was thought that the reaction was diffusion limited. One hour at 900°C may not have been sufficient, and it was thought that a longer hold may lead to more complete reaction. Because diffusion increases parabolically with time, a much longer hold time was investigated. A sample was heated at 200°C/hour to 900°C and held for 12 hours before being cooled to room temperature at 900°C/hour. There was very little difference in the amount of AlB_2 formed between the sample held for one hour and the one held for 12 (see Figure 3.3 and Table 3.2). Both of the samples oxidized slightly more than samples in the atmosphere comparison study because the furnace chamber was not evacuated before heating.

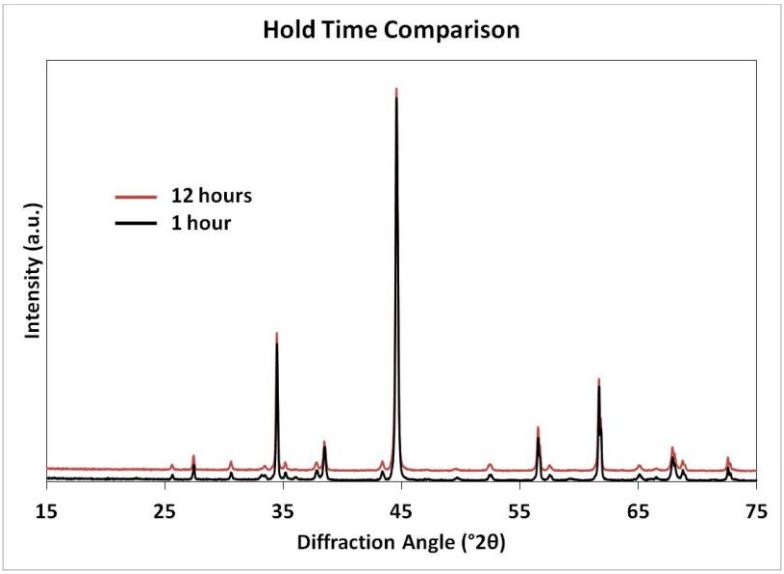

Figure 3.3: XRD of sample reacted for 1 hour and 12 hours. Scans are nearly identical.

Table 3.2

Hold Time Comparison

Time (hours)	Rietveld Analysis* (Weight %) AlB_2	Al	B	Al_2O_3	Al_3BC
1	84.3 [77.3]	4.2 [3.9]	[8.3]	5.8 [4.2]	5.3 [4.9]
12	85.5 [75.9]	4.7 [4.2]	[11.3]	4.6 [4.1]	5.2 [4.6]

* Rietveld analysis adjusted for free boron in brackets.

Phase diagrams for the aluminum-boron system[5-7] place the decomposition temperature of AlB_2 between 972 and 985°C. The decomposition of AlB_2 is described by the following reaction[7]

$$6AlB_2 + 14.4kJ \rightarrow AlB_{12} + 5Al \qquad (3.1)$$

Based on the literature it was assumed that a temperature around 900°C would be sufficient to form AlB_2 without too closely approaching the limit of decomposition into

AlB_{12}, from which the kinetics to return to AlB_2 are very slow.[7] As there was ~75°C in between 900°C and the decomposition temperature, the effect of changing the hold temperature was examined in order to determine if higher reaction temperatures were possible. Samples was heated to 700, 800, 850, 900, 925, 950 and 975°C at 300°C/hour in He-6%H_2 and held for one hour before being cooled at 900°C/hour. The extent of reaction between aluminum and boron was seen to increase up to 900°C, where it did not change significantly until 975°C, at which point decomposition was observed. These results are summarized in Figure 3.4 and Table 3.3. An XRD pattern of these materials is presented in Figure 3.5.

Temperature was found to be a very significant factor controlling the reaction of aluminum and boron. It was expected that at temperatures below 660°C, the melting point of aluminum, little reaction would occur. At a temperature of 700°C, approximately 50 weight percent AlB_2 formed. As the temperature increased, the amount of AlB_2

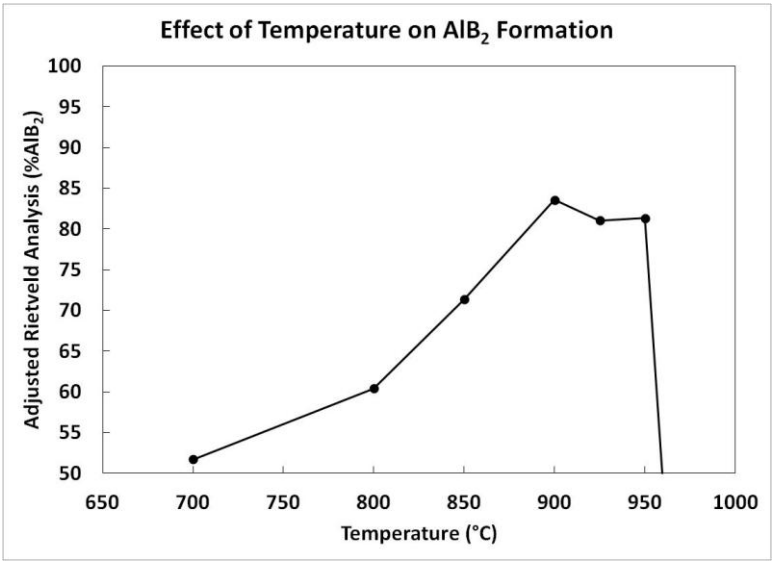

Figure 3.4: Temperature dependence of AlB_2 formation. Higher temperatures favor AlB_2 formation up to 900°C, where a maximum in the extent of reaction is reached.

Table 3.3

Temperature Comparison

Temp (°C)	Rietveld Analysis* (Weight %) AlB_2	Al	B	Al_2O_3	Al_3BC
700	65.4 [51.7]	32.3 [25.5]	[20.9]	0.4 [0.3]	2.0 [1.6]
800	72.4 [60.4]	22.3 [18.6]	[16.5]	3.7 [3.1]	1.6 [1.3]
850	80.9 [71.3]	14.3 [12.6]	[11.8]	3.4 [3.0]	1.5 [1.3]
900	89.7 [83.1]	7.2 [6.7]	[6.8]	1.0 [0.9]	2.2 [2.0]
925	87.5 [81.0]	6.3 [5.8]	[7.4]	3.4 [3.1]	2.8 [2.6]
950	87.8 [81.3]	7.2 [6.7]	[7.4]	3.4 [3.1]	1.6 [1.5]
975	Decomposed				

* Rietveld adjusted for free boron in brackets.

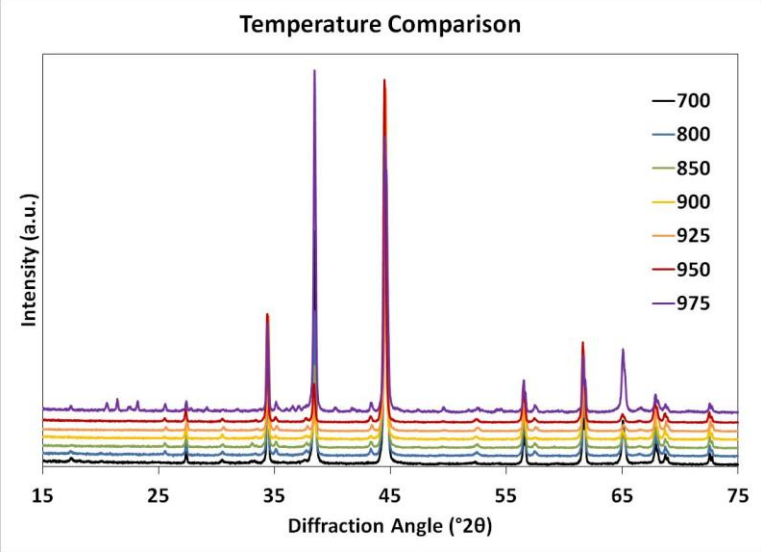

Figure 3.5: XRD of samples reacted at 700, 800, 850, 900, 925, 950 and 975.
exponentially, but this does not explain the abrupt leveling off of the extent of reaction.

increased exponentially to a maximum of around 83 weight percent. It would be expected that the trend from Figure 3.4 continue to 100% AlB_2 at a temperature of ~925°C if not for the plateau above 900°C. The reason for this is unclear.

As well as increasing parabolically with time, diffusion increases exponentially with temperature. It was speculated that increasing the temperature would increase diffusion and hence AlB_2 formation. Temperature did increase the formation of AlB_2

Nor does it correlate with the results of the increased hold time study, which suggested that diffusion was not limiting the reaction.

One possibility is that wetting of boron particles by molten aluminum was limiting the reaction. It is generally known that most molten metals do not wet oxides well.[8] From the results above, it is clear that there was Al_2O_3 present in the final product and, at least initially, amorphous B_2O_3. The literature does not contain much information regarding the contact angle of aluminum on boron or B_2O_3, but it has been well characterized for Al_2O_3.[9] The aluminum contact angle ranges from 103-83° over the temperature range 660-1000°C, which represents poor wetting but does indicate that better wetting is achieved at higher temperatures. While this correlates with the increase in AlB_2 formation as a function of temperature, the contact angle decreases linearly as a function of temperature[9] whereas the observed rise was exponential.

Wetting of AlB_2 by aluminum is not reported either, but wetting of AlB_{12}, aluminum borocarbides, and other metal diborides has been examined.[10-11] The contact angle of aluminum on α-AlB_{12} has been reported as 157° at 900°C and is no lower than 115° for any aluminum borocarbide phase below 1000°C.[10] Wetting by aluminum of TiB_2, ZrB_2 and HfB_2 at 900°C results in contact angles of 140°, 106° and 134°, respectively.[11] There has been a time dependence reported for most of these contact angles, but at temperatures below 1000°C aluminum does not achieve 'good wetting' on any substance similar to boron, Al_2O_3 or AlB_2. The contact angles decrease sharply with temperature, but the reaction cannot be carried out at higher temperatures due to the decomposition of AlB_2.

Based on this data, it was hypothesized that aluminum wet boron moderately well, but did not wet AlB_2 or any oxide surface. As the reaction progressed it became more difficult for aluminum to reach unreacted boron, leaving segregated aluminum and boron in the product regardless of hold time. To investigate this hypothesis a small pellet of aluminum was heated on a boron substrate to 900°C in argon. Due to the increasing vapor pressure of aluminum at higher temperatures, this test had to be stopped before data could be collected.

To verify if wetting of aluminum was indeed an issue, AlB_2 was synthesized with six different aluminum particle sizes. Changing the aluminum particle size was expected to change the extent of reaction between aluminum and boron by changing the aluminum distribution throughout the pellet. If aluminum was dewetting from an oxide or boride surface, samples with smaller aluminum particles were expected to react to a higher extent due to the higher frequency of aluminum-boron particle interactions and smaller diffusion distances. Al + 2B samples with nominal average aluminum particle sizes of 3, 5, 12, 30, 60 and 90 μm were milled in a 500 mL HDPE bottle filled with hexane and 2 kg of WC-Co media for 4 hours at 40 rpm. The powders were dried by air convection for 24 hours, pressed into pellets, and fired at 900°C for 4 hours in under argon. The longer hold time was used to minimize any effects that may have been caused by limited diffusion of larger aluminum particles in order to isolate the effects of wetting.

Figure 3.6 shows EDS elemental maps of the aluminum particle distribution for the six different particle sizes. It is clear that the 3 μm particles of aluminum (red) were well distributed in a matrix of much finer boron (dark). The distribution became less homogeneous as the particle size increased. It was expected that if wetting were a

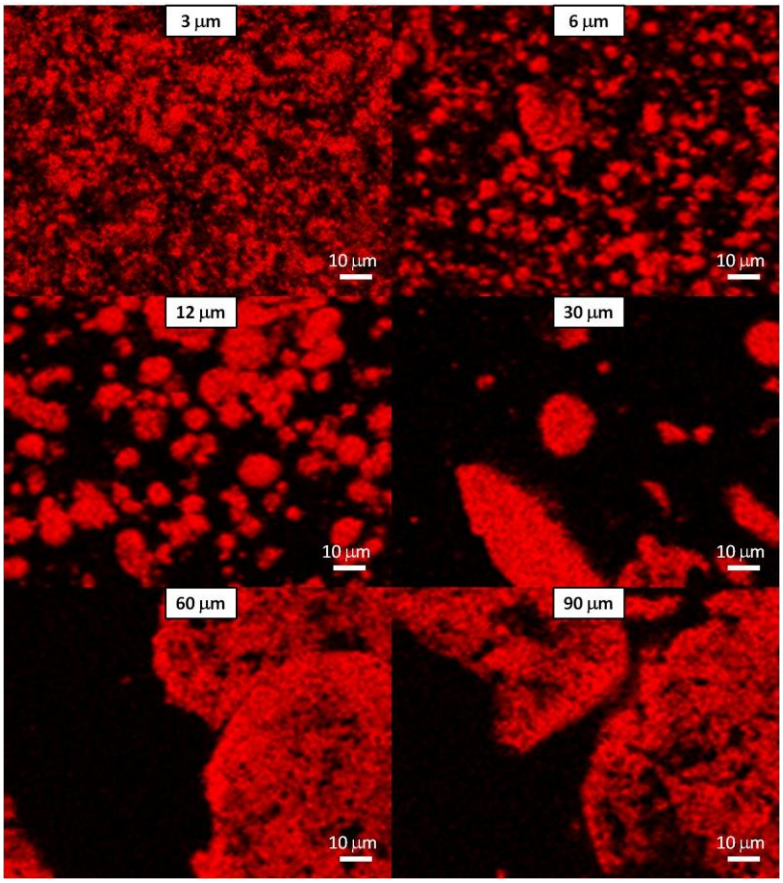

Figure 3.6. Aluminum particle distribution (red) in boron matrix (black) in pressed Al + 2B pellets for six average particel sizes.

problem, the EDS maps of the larger particles would remain less homogeneous because the aluminum was not spreading across the boron surfaces.

After reaction the distribution of aluminum grew somewhat less homogeneous as the aluminum particle size increased, but it was difficult to determine from the EDS maps (Figure 3.7) if aluminum was wetting boron or not. The aluminum did redistribute throughout the reacted product. There appeared to be regions of unreacted aluminum but they may have also been caused by the surface topography, which was not completely flat. Using EDS on individual light and dark regions of the EDS maps did not give a clear chemical distinction between the two; boron and aluminum were present in relatively

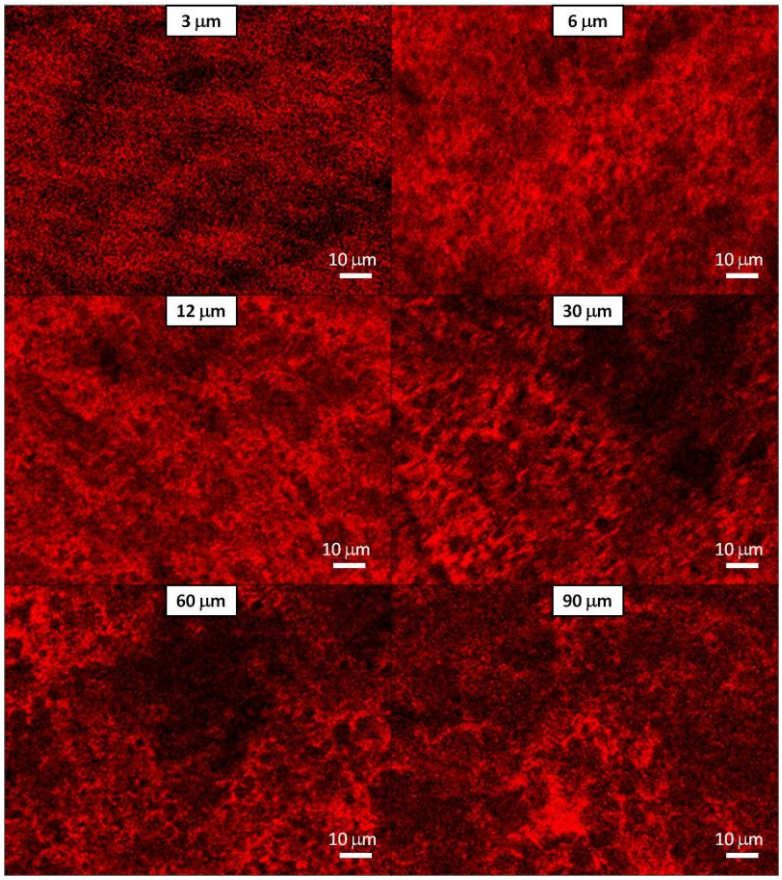

Figure 3.7. Aluminum distribution after reaction at 900°C for 4 hours. The aluminum spread through the pellet after melting, but resulted in less homogeneous distributions as the aluminum particle size increased.

similar amounts. Once again, boron was difficult to detect. Maps of the boron distribution had less contrast and were generally uniform.

The composition fluctuations in Figure 3.7, seen as brighter and darker red, may be caused by surface roughness. While generally inconclusive, the redistribution of 30, 60 and 90 μm aluminum particles is the strongest evidence for decent wetting of boron by aluminum. Local fluctuations in composition may have existed, but it does not appear that liquid aluminum had trouble wetting and diffusing during the reaction.

X-ray diffraction of each sample (Table 3.4 and Figure 3.8) indicated that

Table 3.4

Al Particle Size Effect on AlB_2 Formation

Aluminum	Rietveld Analysis* (Weight %)				
Size (μm)	AlB_2	Al	B	Al_2O_3	Al_3BC
3	71.0 [58.8]	23.4 [19.4]	[17.2]	3.7 [3.1]	1.9 [1.6]
6	73.5 [61.8]	20.8 [17.5]	[15.9]	3.8 [3.2]	1.9 [1.6]
12	73.4 [61.7]	20.3 [17.1]	[15.9]	3.4 [2.9]	2.9 [2.4]
30	78.3 [67.9]	16.5 [14.3]	[13.3]	3.3 [2.9]	1.9 [1.6]
60	72.4 [60.3]	22.6 [18.8]	[16.6]	3.1 [2.6]	1.9 [1.6]
90	69.9 [57.4]	24.1 [19.8]	[17.9]	2.7 [2.2]	3.3 [2.7]

* Rietveld adjusted for free boron in brackets.

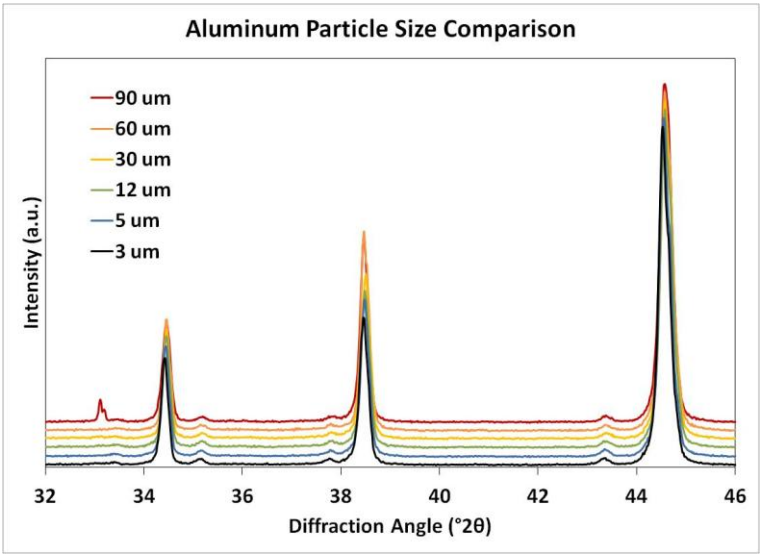

Figure 3.8: Two major peaks in the XRD scans of AlB_2 made with different size Al. The Al_2O_3 peak does not seem to be impacted by Al particle size.

increasing aluminum particle size had little correlation with extent of AlB_2 formation. All of the materials reached roughly the same extent of reaction, with the 30 μm sample having a slightly higher percentage of AlB_2 than the 3 μm sample. This is surprising in light of the EDS maps in Figure 3.7. While the maps do not clearly show which material should have the highest AlB_2 content, the differences in aluminum distribution were thought to reflect differences in composition. This does not appear to be the case. The assumption that the smallest particle size would result in the highest AlB_2 fraction was

not correct.

The amount of Al_2O_3 decreased with increasing particle size, an expected result if a nontrivial amount of Al_2O_3 were present on the surface of aluminum particles. Larger particles with lower surface to volume ratios would be expected to have less Al_2O_3. An unidentified peak was found in the 90 μm aluminum scan but it is unclear what caused this peak.

Results of the wetting study suggest that aluminum wetting was probably one of the limiting processes in the synthesis of AlB_2. It is most likely that a combination of diffusion and wetting were the rate limiting processes in the reaction of aluminum and boron as the temperature approached 900°C. Repeating the hold time study at lower temperatures and observing a time dependence for AlB_2 formation would confirm this, as both diffusion and wetting are time dependent, but a more significant pursuit would be to identify any systematic factors that halted the reaction above 900°C.

The consistent appearance of contaminates (Al_2O_3 and Al_3BC) across all test conditions meant that oxygen and carbon contamination prevented the synthesis of a completely phase pure material. However, the incomplete reaction of boron and aluminum was reduced by optimizing the reaction temperature, so achieving complete reaction of aluminum and boron, with minor impurities still present, would be a significant improvement. It was hypothesized that adjustments in the systematic experimental conditions would help increase the extent of boron and aluminum reaction further and that one or more of these conditions, not the material properties, was limiting the formation of AlB_2.

The effect of pressing pressure on the pellets was examined. In the previous studies, cylindrical pellets of Al + 2B were made by uniaxial compaction. In this study the pressing pressure was adjusted to determine the impact of compaction on the extent of reaction. Pellets were pressed at 34, 103 and 207 MPa using a uniaxial press and compared to loose powder. All samples were reacted at the same time under vacuum (~60 mtorr) using the same temperature profile as the atmosphere comparison study. The results are presented in Figure 3.9-Figure 3.12. Modest consolidation greatly improved the conversion of the aluminum-boron mixture to AlB_2 and reduced the amount of Al_2O_3. Figure 3.10 shows that consolidation decreased the amount of boron and aluminum identically, suggesting that the larger contact area that resulted from pressing led to increased reaction. Further increase in pressure did not increase the extent of reaction of aluminum and boron nor did they reduce the amount of impurities.

The weight loss of the samples was recorded and is shown in Figure 3.12. The loose powder gained 1% of its initial weight, while all pressed pellets lost around 1% of their initial weight. According to Figure 3.11 and 3.12, the loose powder gained weight and oxidized more, while the pressed pellets lost weight and oxidized less. This demonstrated that the reaction atmosphere was a major source of oxygen in these powders and that most of the oxygen was not coming from the starting powders themselves. Because both pressed and loose powders had the same amount of oxygen initially, any disparity in oxygen content must have come from the reaction environment. A larger quantity of Al_2O_3 in the loose powder reflected the higher surface area in contact with the atmosphere, whereas the lower amount in the pressed pellets was a result of reduced transport of oxygen to the interior of the pellet.

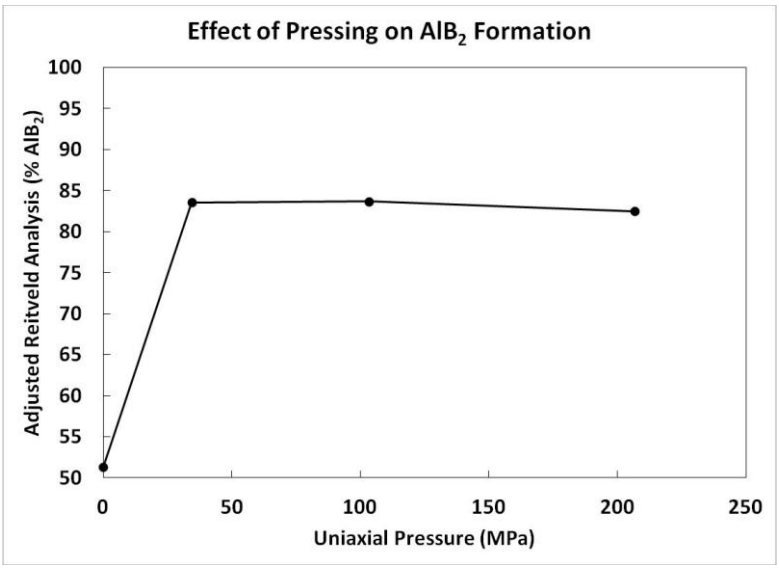

Figure 3.9: Effect of uniaxial pressure on AlB_2 formation. Modest consolidation greatly improved the conversion of aluminum and boron to AlB_2, but further pressure did not help.

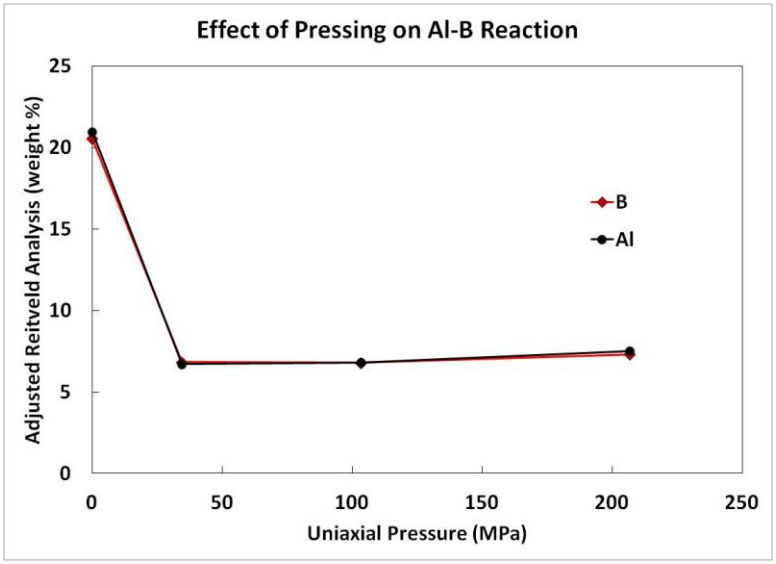

Figure 3.10: Effect of uniaxial pressure on unreacted aluminum and boron. It is clear that compaction increases the extent of aluminum and boron reaction, but increasing the pressing pressure has no effect.

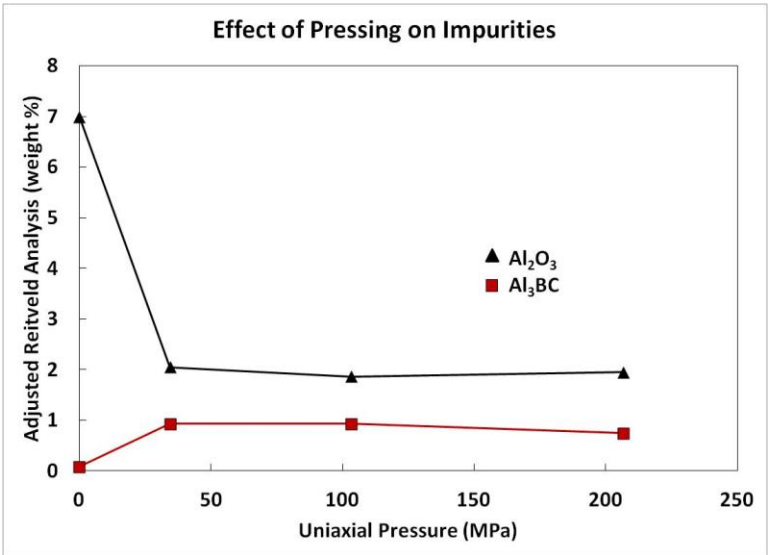

Figure 3.11: Effect of uniaxial pressing pressure on impurity formation.

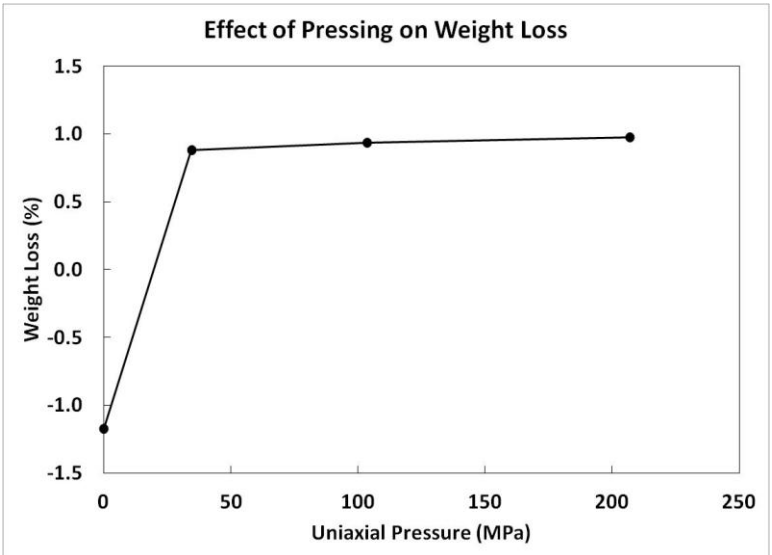

Figure 3.12: Effect of uniaxial pressing pressure on weight loss (in vacuum). Powder that was not consolidated gained weight, while powder that was pressed into pellets lost weight.

To confirm the claim that transport of oxygen to material closer to the center of a pellet was reducing the oxidation of the material, a composition profile of a pellet was created. X-ray scans were taken at five heights, removing a fraction of the AlB_2 material with SiC sandpaper after each scan. As Figure 3.13 shows, AlB_2 formation was highest at the center of the pellet and decreased towards the ends. Accordingly, free boron and aluminum were highest at the ends of the pellets and less abundant at the center, with the exception of one outlying aluminum data point near the top of the pellet. Interestingly, the amount of Al_2O_3 did not change much over the height of the pellet. The top of the pellet had the highest weight percent Al_2O_3 and the interior had the lowest, but the variation was less than one weight percent. Because of the cylindrical shape of the pellet, oxygen was able to diffuse towards the center of the pellet radially as well as from the top and bottom so that each height had a similar weight fraction. However, it appears significant that the top of the pellet (where gas flow was greatest) had more Al_2O_3 than the bottom (where there was little flow). The slightly higher Al_2O_3 content on the top of the pellet most likely indicates that the consolidation of Al + 2B into a pellet provided some protection from oxidation in addition to reducing diffusion distances.

The most puzzling finding from the pellet composition profile is the high weight fraction of Al_3BC at the ends of the pellets. The appreciable difference in composition from the bulk material suggests that most of the carbon at the ends of the pellet was not coming from the starting powders but from an outside source. This source was probably oleic acid that was applied to the pellet die as a lubricant and would generally only contact the top and bottom of the pellet. Nonetheless, a background concentration of Al_3BC remained at the center of the pellet which most likely arose from carbon in the

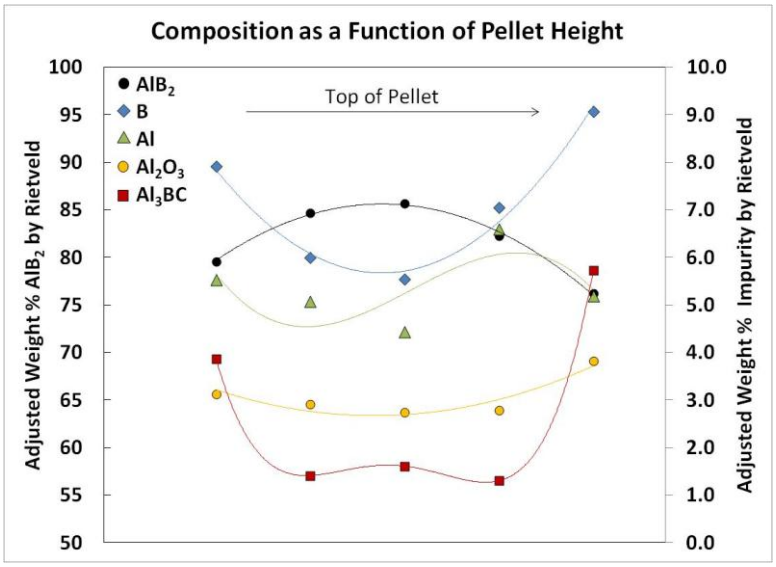

Figure 3.13. Composition of reacted Al+2B pellet as a function of height.

starting boron. Interestingly, the loose powder did not have any Al_3BC. It was assumed that the loose powder's increased exposure to oxygen allowed the carbon to oxidize to CO or CO_2, but the high Al_3BC content at the ends of the pellet does not support that hypothesis. Further studies on Al_3BC would shed light on its role in AlB_2 synthesis, but because it occurs in relatively small quantities and because it is not energetically inert like Al_2O_3 its presence can be tolerated.

Although it was expected to give higher weight fractions of Al_2O_3, re-milling and a second reaction of the final powder was conducted in an attempt to react the remaining aluminum and boron. The reacted powder was put in a 100 mL WC Spex mill with 50g of 3mm WC-Co media, filled with hexane and shaken vigorously for five minutes. The sample was then dried by air convection and reacted at 900°C for 4 hours in argon. Table 3.5 and Figure 3.14 show that the additional milling and reaction helped reduce the amount of free aluminum at the expense of forming more Al_2O_3. While Al_2O_3 increased by 2.8% on a mass basis, on a molar basis it only increased by 1.1% (from 1% to 2.1%).

Table 3.5

Effect of Remilling and Second Reaction on AlB_2 Formation

	Rietveld Analysis* (Weight %)				
Sample	**AlB_2**	**Al**	**B**	**Al_2O_3**	**Al_3BC**
As Reacted	76.0 [64.9]	19.1 [16.3]	[14.6]	3.8 [3.9]	1.1 [0.9]
Remilled	84.6 [76.4]	7.4 [6.7]	[9.7]	6.6 [6.0]	1.4 [1.3]

* Rietveld adjusted for free boron in brackets.

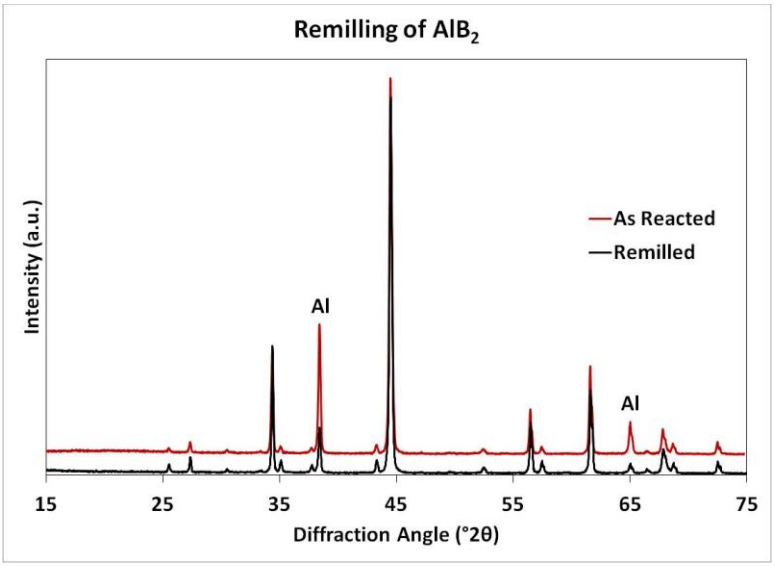

Figure 3.14. X-ray scan of AlB_2 after reaction (red) and after milling and second reaction (black).

On a molar basis the amount of free aluminum decreased 9.3%, from 18.2% to 8.9%, much more than would have been removed from oxidation alone. This clearly demonstrates that remilling and reacting AlB_2 increased the extent of reaction between aluminum and boron. On its own, this is not a surprising result. Remilling the reacted powder was expected to redistribute aluminum and boron so that unreacted material had a higher probability of coming in contact. Because a significant amount of AlB_2 formed in the first reaction cycle, it was assumed that all aluminum and boron in intimate contact

would react to form AlB_2. Accordingly, remilling seemed to be an obvious choice. But in light of the diffusion and wetting studies, which suggest that longer hold times would not allow aluminum to diffuse farther and that aluminum is distributed relatively evenly in the reacted material, this result is puzzling.

Another proposed cause of incomplete reaction is the decomposition of AlB_2 into AlB_{12} and aluminum due to local temperature fluctuations above 975°C produced by the inhomogeneous exothermic reaction of aluminum and boron. Equation (3.1) indicates that the enthalpic barrier to decomposition is very small (~2.4 kJ/mol) and it has been previously discussed that the kinetics of the reverse reaction are very slow. Once an area of AlB_2 had decomposed, it would remain as AlB_{12} and aluminum. Because AlB_{12} is nearly as difficult to detect as boron, the only product observed in X-ray scans would be aluminum. It would appear as though aluminum and boron hadn't reacted when in fact they had and then subsequently decomposed.

3.2 Commercial Powder

In an effort to identify possible routes to a more phase-pure product, a commercial AlB_2 powder (H. C. Starck Grade A AlB_2) was purchased. X-ray diffraction was performed on this powder and compared to a sample synthesized in-house. The diffraction patterns are compared in Figure 3.15. The patterns are remarkably similar, with the only major distinction being that the powder synthesized in-house had slightly more AlB_2 (85.7%) than the commercial powder (82.4%). The chemical analysis preformed on the commercial powder was reported as 54.9% aluminum, 42.8% boron,

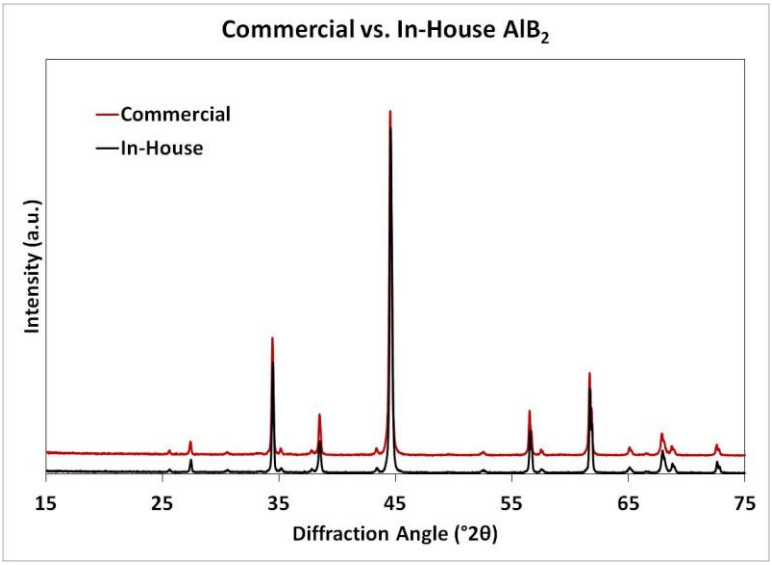

Figure 3.15. Comparison of commercially available AlB_2 power with the highest purity powder synthesized in-house. The powders are nearly identical in phase assemblage, with the in-house powder having slightly less free aluminum than the commercially available powder.

0.2% carbon, 0.1% nitrogen, 0.1% iron and 1.9% oxygen. The compositions of each powder are detailed in Table 3.6. The surface areas of the powders were nearly identical, with a surface area of 2.05 m^2/g for the in-house sample and 2.09 m^2/g for the commercial powder.

3.3 Conclusions

AlB_2 was synthesized by high temperature reaction of fine aluminum and boron powders. Phase pure AlB_2 was not achieved due to impurities in these powders. Incomplete reaction between aluminum and boron led to products that were a maximum of 90.7% AlB_2 by weight as determined by Rietveld analysis of X-ray diffraction patterns (when the assumption that free B is associated with the remaining unreacted Al, the amount of AlB_2 formed is less than 86 wt. %). It was determined that reaction

Table 3.6

Commercial vs. In-House AlB_2 Comparison

	Rietveld Analysis* (Weight %)				
Sample	**AlB_2**	**Al**	**B**	**Al_2O_3**	**Al_3BC**
In-House	90.7 [85.7]	4.7 [4.4]	[5.5]	2.9 [2.7]	1.7 [1.6]
Commercial	88.5 [82.4]	6.7 [6.2]	[6.9]	3.4 [3.2]	1.4 [1.3]

* Rietveld analysis adjusted for free boron in brackets.

atmosphere, time at temperature, ramp rate, and aluminum particle size did not have appreciable effects on the extent of reaction of aluminum and boron. Reaction temperature and compaction did affect the final composition, with temperatures between 900-950°C giving the highest extent of reaction for powders that were consolidated with at least 34 MPa of pressure. Molten aluminum wet boron, but incomplete spreading occurred such that remilling of reacted powders resulted in improved conversion.

The highest quality powder produced in-house had a higher AlB_2 content and higher purity than a commercially available AlB_2 powder. Based on the chemical analysis of the commercial powder (reported as 98%), the in-house powder had a chemical purity near 99%, although it is unclear whether chemical purity and phase purity translate to the same energetic performance. Further improvements in quality may be achieved through more accurately determining the exact stoichiometry of the AlB_2 compound and reducing carbon and oxygen contamination on the starting boron powder.

3.4 References

1. H. Funk, *Z. Anorg. Allgem. Chem*., 142, 269 (1925)

2. E. J. Felten "The Preparation of Aluminum Diboride, AlB_2,", *J. Am. Chem. Soc.*, **78**[23], 5977–5978 (1956)

3. P. E. Blackburn, A. Buchler and J. L. Stauffer, "Thermodynamics of Vaporization in the Aluminum Oxide-Boron Oxide System,", *J. Phys. Chem* **70**[8] 2469-2474 (1966)

4. V. S. Zenkov, "Adsoprtion-Chemical Activity of Finely Dispersed Amorphous Powders of Brown and Black Boron used in Synthesizing Metal Borides," *Powder Metallurgy and Metal Ceramics*, **45**[5] 279-282 (2006)

5. H. Duschanek and P. Rogl, "The Al-B (Aluminum Boron) System,", *J. Phase Eq*. 15[5] 543-552 (1994)

6. O. N. Carlson, *Bull. Alloys Phase Diagrams*, **11**[6] 560-66 (1990)

7. D. Mirkovic, J. Grobner, R. Schmid-Fetzer, O. Fabrichnaya and H. L. Lukas, "Experimental Study and Thermodynamic Re-Assessment of the Al-B System,", *J. Alloy Comp*. **384** 168-174 (2004)

8. W.D. Kingery, H. K. Bowen and D.R. Uhlman, Introduction to Ceramics, Second Edition (John Wiley and Sons, 1976)

9. V. Laurent, D. Chatain, C. Chatillon, and N. Eustathopoulos "Wettability of Monocrystalline Alumina by Aluminium Between its Melting Point and 1273 K," *Acta Metallurgica* **36**[7], 1797–1803 (1988)

10. A. I. Kharlamov, S. V. Loichenko, V. I. Nizhenko, N. V. Kirillova and L. I. Floka "Wetting of Hot-Pressed Aluminum Borides and Borocarbides by Molten Aluminum And Copper," *Powder Metallurgy and Metal Ceramics* **40[**1-2] 65-70 (2001).

11. A. Passerone, M. L. Muolo and D. Passerone "Wetting of Group IV Diborides by Liquid Metals," *J. Mater Sci* **41**, 5088–5098 (2006)

12. T. Letsoalo and J. E. Lowther, "Systematic Trends in Boron Icosahedral Structured Materials," *Physica B: Cond. Matt*.,**403**[17] 2760-67 (2008)

4. SENSITIVITY AND OXIDATION BEHAVIOR

4.1 Oxidation Characteristics in Air

The insensitivity of an energetic material is imperative to its ultimate implementation. Although sensitivity properties change when a material is incorporated into an energetic system (with oxidizers, binders, plasticizers and other additives) its resistance to accidental discharge by electrostatic shock, friction, impact or temperature must be characterized for the safety of any person who would come in contact with the material. Accidental discharge mechanisms are generally associated with the oxidation behavior of a powder at low (<500°C) temperatures. The oxidation characteristics of several boride powders, physical mixtures, and raw powders were investigated. The high temperature oxidation behavior was also analyzed for the purpose of screening obviously poor performers and identifying potentially promising materials.

Oxidation behavior was analyzed using thermal gravimetric analysis (TGA) and differential thermal analysis (DTA) with a Netzsch (model STA 409) analyzer, heating 25-50 mg of powder in air to 1500°C. Constant heating rate experiments were used to determine the initiation temperature (the temperature at which a material begins to rapidly oxidize) and the extent of reaction (the fraction of theoretical oxidation reached) for a variety of boride powders. Oxidation was detected by TGA as a change in weight and by DTA as a large temperature difference between the sample and a reference.

Samples weighing 25-50 mg were loaded into 1.5 g alumina crucibles and placed on a measurement spindle next to a reference crucible filled with alumina powder. The

measurement spindle was connected to a mass balance to detect changes in weight. Each of the two arms of the spindle (for reference and sample) contained a thermocouple to measure the temperature of each crucible directly under the powder inside. As the temperature was increased, weight gain resulted from oxidation by O_2 in the N_2-20%O_2 mixture flowing into the measurement chamber at 150 cc/min. The diameter of the measurement chamber was approximately 2 cm, giving a molar oxygen flux of approximately 25 millimol cm^{-2} s^{-1}. A 50 mg sample of AlB_2 contains one millimol, which requires 4.5 millimol of O_2 to oxidize completely, so the flux was about five times greater every second than would be needed to completely oxidize the sample. The exothermic oxidation released heat that was detected as a temperature difference between the two thermocouples.

Figure 4.1 shows the conversion, α, as a function of temperature for the Starck boron powder heated at 10°C/min. Conversion is defined as the fraction of powder oxidized compared to the theoretical limit. It is given by the equation

$$\alpha = \frac{m_t - m_i}{m_f - m_i} \tag{4.1}$$

where m_i is the initial mass, m_f is the theoretical final weight and m_t is the mass at a time t during the test. A conversion of zero means that no change has occurred, while a conversion of unity means that the powder has fully oxidized. The theoretical weight change is calculated from the molecular weights, *MW*, of the starting material and final product, as in the equation

$$B + \frac{3}{2}O_2 \rightarrow \frac{1}{2}B_2O_3 \tag{4.2}$$

which results in

$$MW_{products} - MW_{reactants} = \frac{1}{2}\left(69.62\,\frac{g}{mol}\right) - \left(10.81\,\frac{g}{mol}\right) \tag{4.3}$$

giving a total change of 24 g/mol. The gaseous species (O_2 in this case) do not contribute to the weight and are neglected. The total moles of powder were calculated from the initial weight and used to find the total theoretical weight change. Impurities, as determined XRD patterns, were accounted for in such a way that oxides did not change mass and other oxidizable species followed the general form of Equation (4.3).

From Figure 4.1 it is clear that the boron powder did not completely oxidize under the given conditions. This highlights the kinetic limitation of boron discussed previously, where the viscous B_2O_3 skin retards the oxidation of the core of the particle. Although there are two distinct regions, these are not the same as the two stages of combustion described in the introduction. At around 500°C the boron began to rapidly oxidize, corresponding to oxidation of the surface of the fine boron particles. As the conversion approached 0.5, oxidation slowed as a result of the growing oxide layer. Slow diffusion through the oxide layer suppressed rapid oxidation up to 1500°C. In combustion systems the first process happens almost instantaneously, the second process is referred to as the ignition delay and the burning of particles without an oxide layer was not observed.

The conversion for aluminum is plotted alongside that of boron in Figure 4.2. Aluminum reached unity conversion over the same temperature range and heating rate, providing a clear contrast between the oxidation behavior of aluminum and boron.

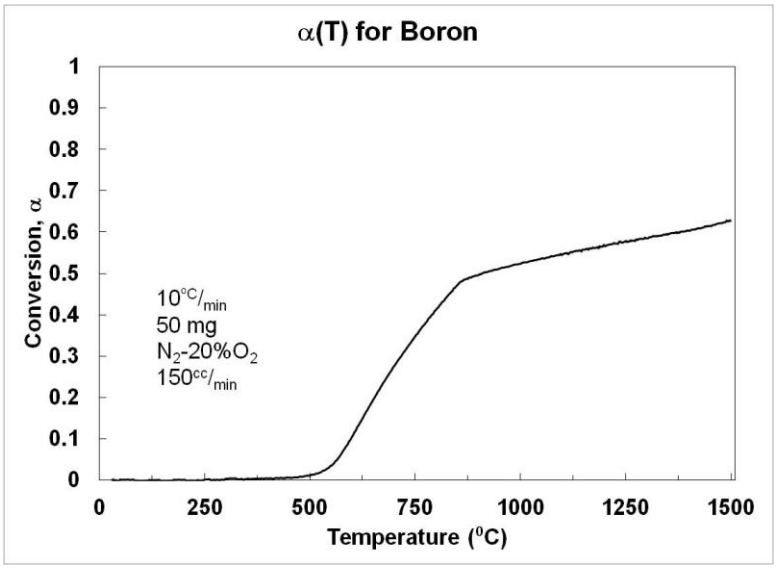

Figure 4.1. Conversion as a function of temperature for boron.

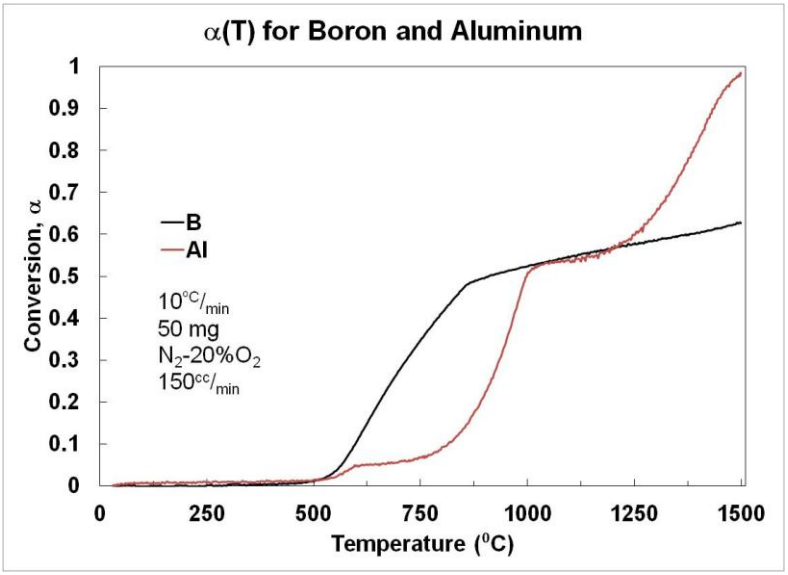

Figure 4.2. Linear heating rate conversion of aluminum and boron.

Interestingly, aluminum appeared to have at least three different processes that controlled the rate of oxidation. The oxidation rate up to 500°C was negligible for aluminum as well. Between 500 and 600°C there was a slight increase in weight. The rate slowed between 600 and 750°C before dramatically increasing to around 1000°C. It slowed again between 1000 and 1150°C and then rapidly increased from 1150 to 1500 °C where all of the initial aluminum had oxidized. This multi-stage oxidation behavior is described in the literature for fine aluminum particles[1-2] and results from a number of phase transformations. Below 660°C, the melting point of aluminum, a thin oxide layer grows on the surface of particles until the Al_2O_3 thickness limits diffusion of oxygen inward to the aluminum particle core. This oxide layer preserves the spherical shape of the particle past the melting point, where thermal expansion of the particle core cracks the oxide skin and exposes molten aluminum to oxygen. SEM images in Figure 4.3 confirm the retention in shape of aluminum particles heated to 750°C. This phenomenon is significant because the core-shell morphology of aluminum at temperatures above 660°C results in much different behavior than would be observed from bulk aluminum or larger particles

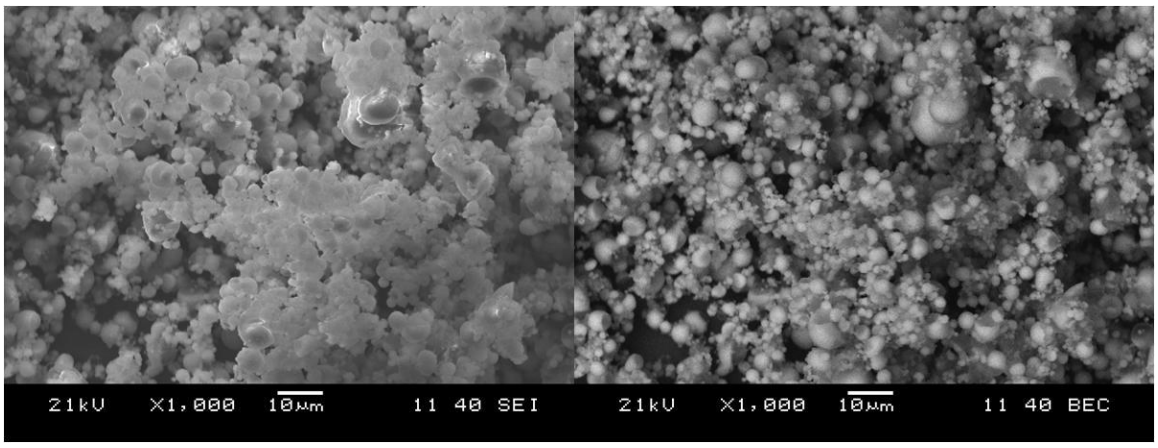

Figure 4.3. Aluminum particles heated to 750°C in air at a heating rate of 10 °C/min. Secondary images on left, backscattered on right.

where the large volume fraction of molten aluminum would dominate the oxidation process. All of the metal particles retained their general shape.

Magnesium is known to be highly reactive with oxygen and the TGA of magnesium and the aluminum-magnesium alloy were much more erratic than those of aluminum or boron. Figure 4.4 illustrates the differences between the three powders. The aluminum-magnesium alloy also had a conversion of unity but underwent most of its oxidation before 1000°C. Magnesium followed the same general trend but stopped oxidizing completely above approximately 900°C, at an α of 0.77. This is not surprising given that the diffusivity of oxygen through MgO is very small[3] and the magnesium particles were larger than the aluminum or aluminum-magnesium.

Boron carbide was investigated as a potential low cost alternative to boron. A TGA comparison of boron and B_4C is shown in Figure 4.5. The calculation for the theoretical weight of oxidized B_4C assumed that all oxidized carbon was converted to CO

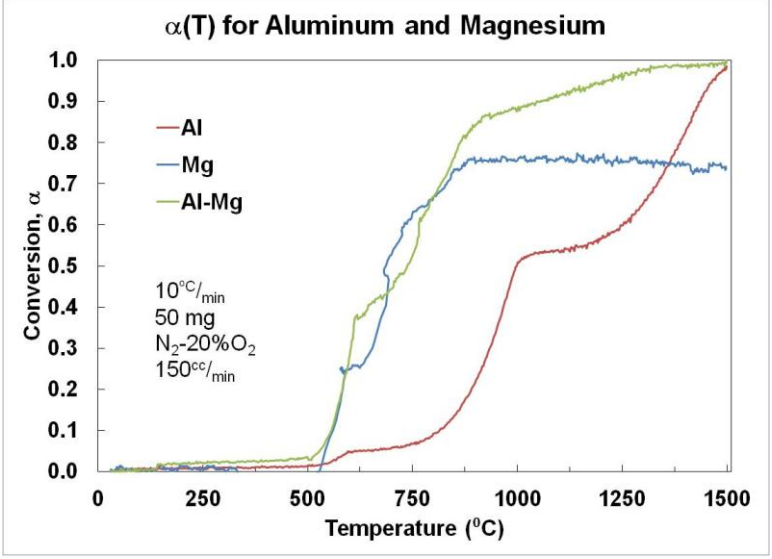

Figure 4.4. Conversion comparison of aluminum, magnesium and the aluminum-magnesium alloy.

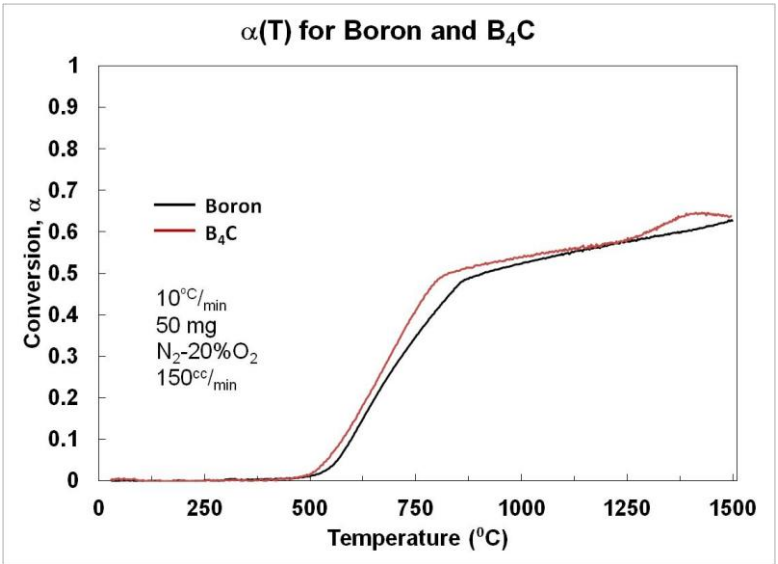

Figure 4.5. Conversion comparison of boron and boron carbide. The boron carbide curve was calculated assuming all carbon was oxidized into a volatile species.

or CO_2 and did not affect the weight of the system. Both materials were nearly identical in oxidation characteristics, suggesting that the B_2O_3 mechanism dominated the B_4C oxidation process and that the carbon was most likely being removed from the system.[4] No information from Figure 4.5 would preclude the use of B_4C as a boron substitute.

Silicon powder was also examined. It only reached one third of its theoretical weight gain due to slow initial oxidation kinetics and the formation of glassy SiO_2 at higher temperatures. The SiO_2 had a similar effect to the B_2O_3 on boron particles – forming a viscous, self-healing diffusion barrier on the surface of the particle – but was more viscous at the temperatures of interest, making silicon a poor energetic material.

Differential thermal analysis complimented the thermal gravimetric analysis by quantifying the temperature and duration of large exothermic events. Both measurements were taken simultaneously under the same conditions. In general, weight gain and heat

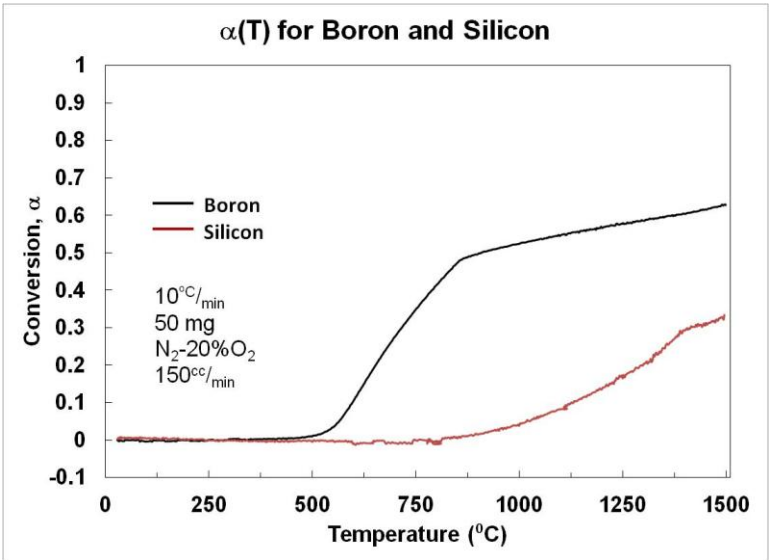

Figure 4.6. Conversion comparison of boron and silicon. The kinetic limitations of boron manifest to an even greater degree in silicon because of the SiO_2 skin that develops.

release (quantified as a change in temperature over the reference) were directly proportional. Figure 4.8 and Figure 4.7 show DTA curves for the raw powders.

The powder mixtures and reacted compounds were analyzed in the same way as the raw powders. Table 4.1 summarizes the TGA data for all powders examined in this study. The initiation temperature is the temperature at which 5% mass gain occurs. While this is not necessarily the temperature at which rapid reaction begins, it gives a point of comparison between materials. The oxidation range is the temperature range between which 5% and 90% of oxidation occur.

The raw powders had the lowest initiation temperatures, with the exception of silicon. Each started to oxidize appreciably before 600°C. Such oxidation at low temperatures contributes to sensitivity, especially for powders with high surface areas like boron (~11 m^2/g) and B_4C (7 m^2/g). Powder mixtures were generally no less sensitive due to the properties of their constituent raw powders and generally to the large

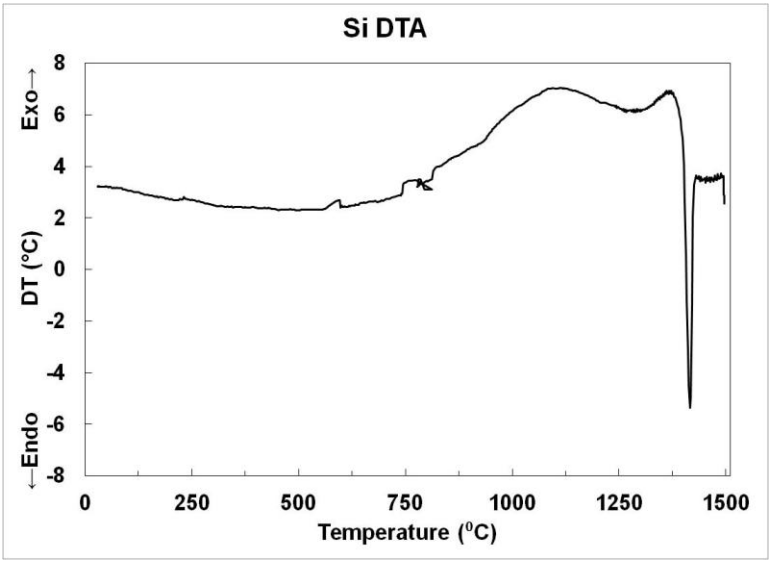

Figure 4.7. Silicon DTA. Silicon oxidized very little and exhibited a large melting endotherm at 1415°C.

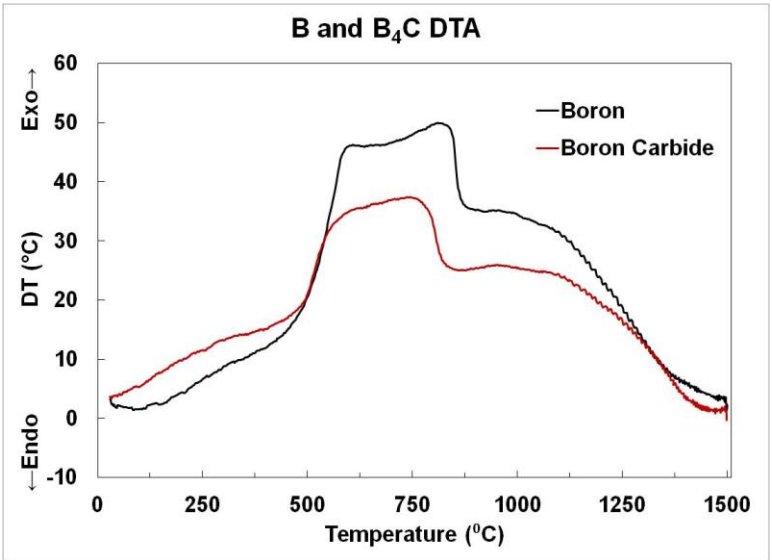

Figure 4.8. Boron DTA.

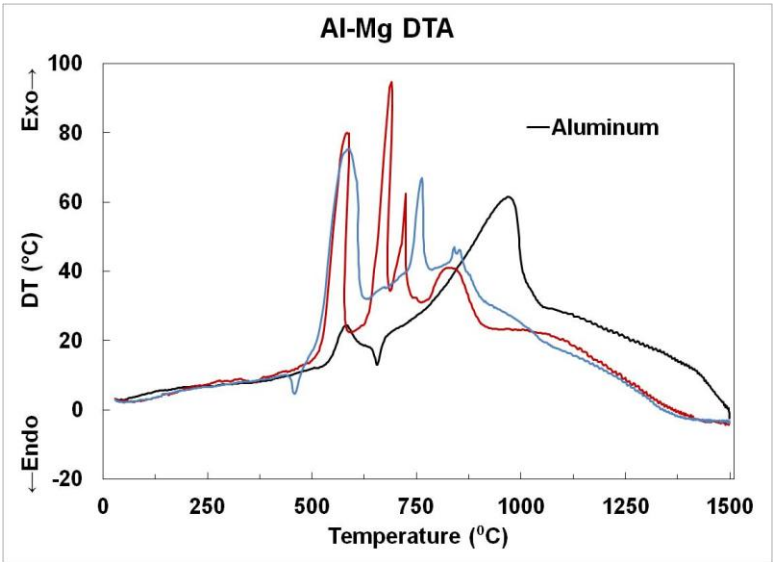

Figure 4.9. DTA of Al, Mg and Al-Mg.

Table 4.1

Boride Powder Oxidation Characteristics

Material	% Weight Change Actual	Theoretical	Conversion α	Initiation Temp (°C)*	Oxidation Range** (°C)
B	152	222	.63	548	905
Al	89	89	1.00	583	804
Mg	51	66	.77	534	292
Mg-Al	78	78	1.00	527	520
Si	47	114	.33	924	573
B_4C	100	152	.65	522	749
Al + 2B	124	149	.84	577	473
AlB_2	145	149	.98	755	505
Al + 12B	147	199	.74	543	566
AlB_{12}	146	199	.74	746	484
Mg + 2B	126	139	.91	597	480
MgB_2	126	139	.90	673	705
½Al-Mg + 2B	122	146	.83	596	765
$Mg_{0.5}Al_{0.5}B_2$	126	146	.86	753	726
Al-Mg + 14B	141	186	.76	573	927
$AlMgB_{14}$	135	186	.73	890	608
Si + 6B	128	189	.68	528	972
SiB_6	116	189	.61	683	818
2Al + B_4C	115	121	.95	535	627
Al_3BC + 2Al	100	121	.83	699	658

* Initiation temperature is reported as the temperature at 5% mass gain.

** Temperature range in which material goes from 5% to 90% mass gain.

percentage of boron in each mixture. The reacted compounds had significantly higher initiation temperatures, as expected. All were above 700°C and some ($AlMgB_{14}$, 890°C) were significantly higher. This makes boride compounds the least sensitive materials.

It is not clear whether the low temperature oxidation characteristics have any bearing on their behavior when integrated into an energetic system. Powders may become more or less prone to oxidation depending on the chemical composition and properties of the oxidizer, binder, plasticizer and other components in the final system. Regardless of any changes in behavior, these data show that on their own boride compounds are generally less prone to oxidation than powders of their constituent elements.

While the high temperature oxidation characteristics of these powders in air may not correlate with their behavior in a complete system, analysis of TGA curves for these powders may still provide useful information. First, it may be an adequate and inexpensive screening test through which obviously poor performers could be eliminated from investigation. Second, it may produce useful results for potentially promising materials that warrant further investigation. This can only be verified through follow-up tests using in situ applications of these materials. If the results of the in situ testing correlate with predictions made from TGA curves, a precedent for using such TGA analysis could be set. Third, while the following analysis may not have any bearing on the specific intended application of these materials by the Army, data gleaned from this work may be useful for other applications, such as ramjet burners and similar applications where operating conditions more closely resemble these test conditions.

None of the boron-metal mixtures reached unity conversion. This is not surprising, as mixtures with boron should have at least partially reflected its low

conversion. Mixtures with high boron contents (Al + 12B, Al-Mg + 14B and Si + 6B) had similar conversions to boron (0.74, 0.76 and 0.61 respectively) while the mixtures with lower boron contents (Al+2B, Mg + 2B, ½Al-Mg + 2B) reached higher conversions (0.84, 0.91 and 0.83). Although an increase in conversion is expected with higher aluminum and/or magnesium content because these elements had higher conversions independently, the improvement was more than would be expected by a simple rule of mixtures. Table 4.1 gives a comparison of the weight gain expected if the powders were not interacting or had no sympathetic effects and the actual percent weight gain of each powder. Based on the TGA data for the elements by themselves, an equation was derived for calculating the expected mass change of the starting powders assuming completely independent oxidation of each species. The equation is

$$\text{Calculated Mass Change} = \sum_{i=1}^{n} Y_i \cdot \Delta M_{T,i} \cdot \alpha_i \tag{4.4}$$

where for a species i, Y_i is the mass fraction, $\Delta M_{T,i}$ is the theoretical mass change and α_i is the conversion. This equation was used to determine what, if any, mutual effects the individual species had on the powders' oxidation.

The change in conversion between the calculated and actual weight gains, presented in Table 4.2, shows that for all powders the difference in conversion from the constituent powders is not simply caused by the addition of a higher conversion material but is the result interactions between the powders as they oxidize. If the powders did not interact with each other, $\Delta\alpha$, the difference between the actual and calculated conversions, would be zero.

Table 4.2

Calculated vs. Actual Weight Gain for Starting Powders

Starting Powder	Calculated % Weight Gain	Actual % Weight Gain	α	Calculated $\Delta\alpha$
Al + 2B	104	124	0.75	+0.09
Al + 12B	129	147	0.66	+0.08
Mg + 2B	93	126	0.67	+0.24
½Al-Mg + 2B	106	122	0.73	+0.10
Al-Mg + 14B	131	141	0.70	+0.06
Si + 6B	136	128	0.72	–0.06
2Al + B_4C	78	115	0.64	+0.19

Silicon was the only material that further inhibited boron oxidation in the mixture. It is clear that the SiO_2 that prevented silicon from reaching conversions higher than 0.33 also had a retarding affect on boron as well. Both B_2O_3 and SiO_2 formed viscous, glassy coatings that acted as a barrier to diffusion and were self-healing. It is very likely that these oxides formed borosilicate phases, although no follow up work was done due to the poor performance of these powders.

For every other mixture the addition of metals to boron provided a significant advantage in reaching high conversions. None of the mixtures would have achieved conversions above 0.75 without beneficial particle-particle interactions. Many different mechanisms could be responsible for this increase. The first possibility examined was the effect of rapid exotherms on weight gain. It was thought that the large exotherms seen in the DTA scans of the metallic powders (Al, Mg and Al-Mg) may have been responsible for the increased conversion of the powder mixtures. Figure 4.10 shows an overlay of TGA and DTA curves for Al + 2B. Exotherms are shown on the secondary axis as positive ΔT, like the peak occurring at 630°C. This peak coincides with the onset of

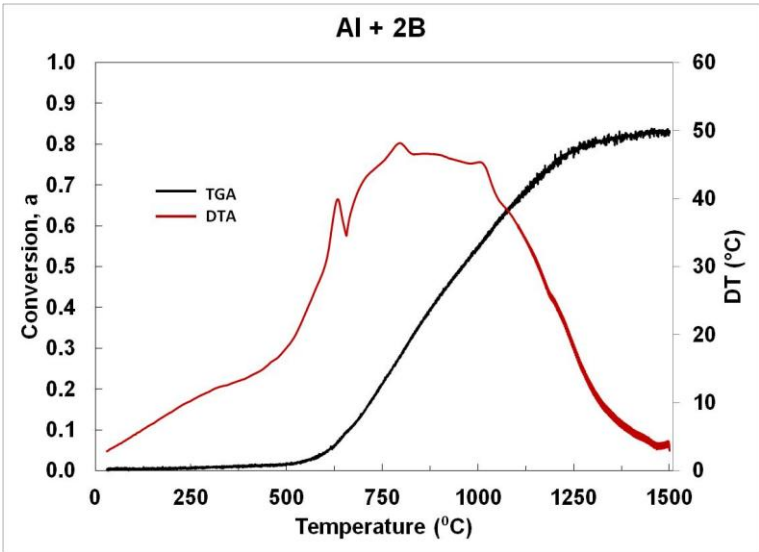

Figure 4.10. TGA and DTA for Al + 2B. Rapid exotherm at 600°C initiated rapid oxidation.

oxidation of Al + 2B. Figure 4.11 displays the same data for Al + 12B. It is very similar to Figure 4.10 but with a slightly smaller exotherm that decreases more rapidly above ~1000°C. Comparable figures are presented below for Mg + 2B, ½Al-Mg + 2B, Al-Mg + 14B and 2Al + B_4C.

The correlation between large ΔT and more rapid oxidation was clear from all figures (Figure 4.11-15). Regions with large temperature differences in DTA corresponded well with regions of higher conversion rate. It is also clear that exotherms in the mixed powder systems were generally not as sharp as those of aluminum, magnesium and the aluminum-magnesium alloy. There did not appear to be any evidence of rapid metal oxidation providing an increase in oxidation rate to boron due to raising the sample temperature. All the mixed samples had fairly broad areas of increased temperature over the reference, more closely tracking the behavior of boron. Because

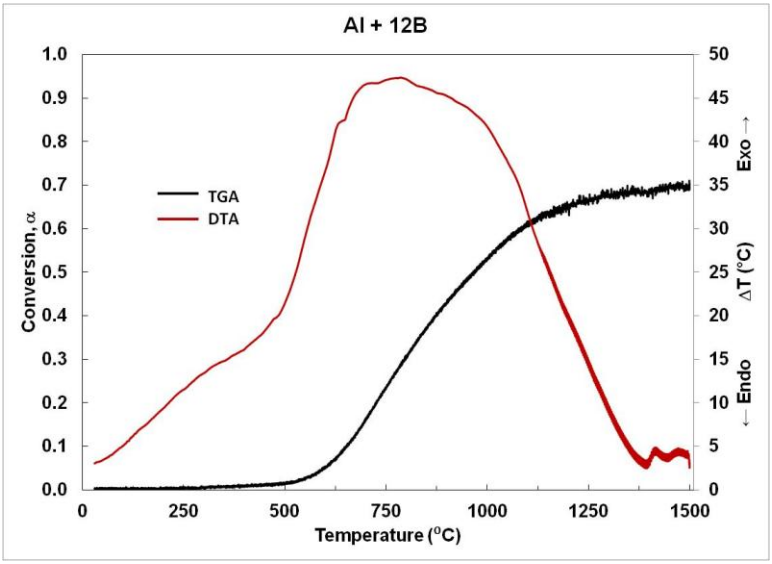

Figure 4.11. TGA and DTA for Al + 12B

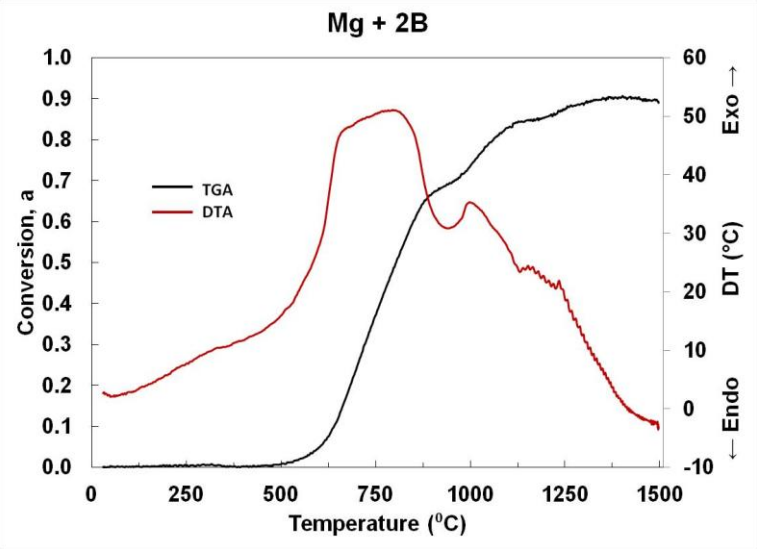

Figure 4.12. TGA and DTA for Mg + 2B.

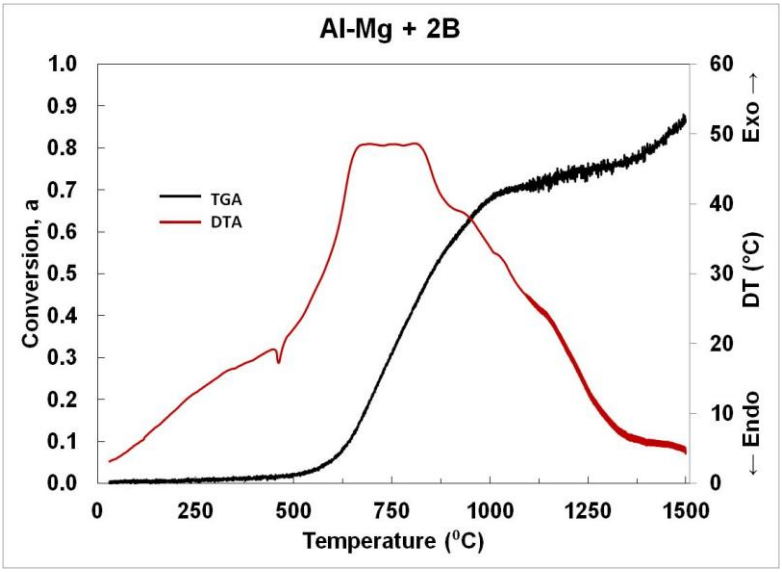

Figure 4.13. TGA and DTA for Al-Mg + 2B. A melting endotherm for the alloy can be seen at 460°C, much lower than either material's melting point.

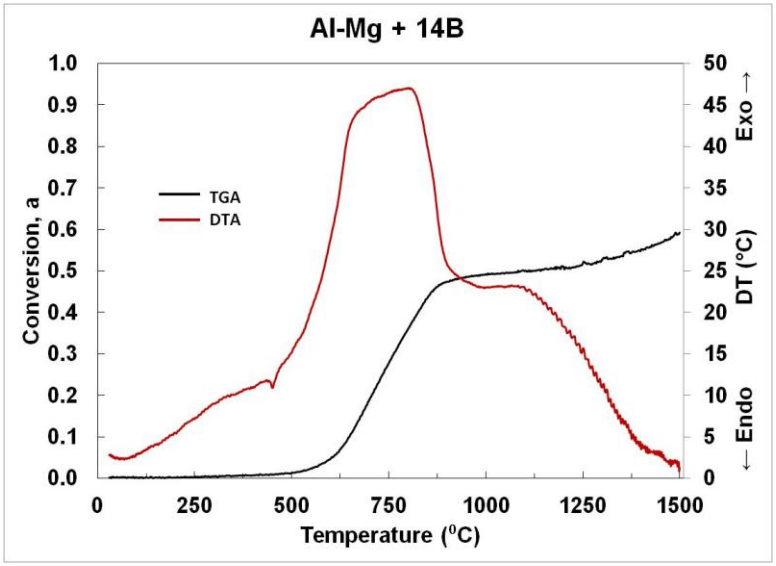

Figure 4.14. TGA and DTA for Al-Mg + 14B.

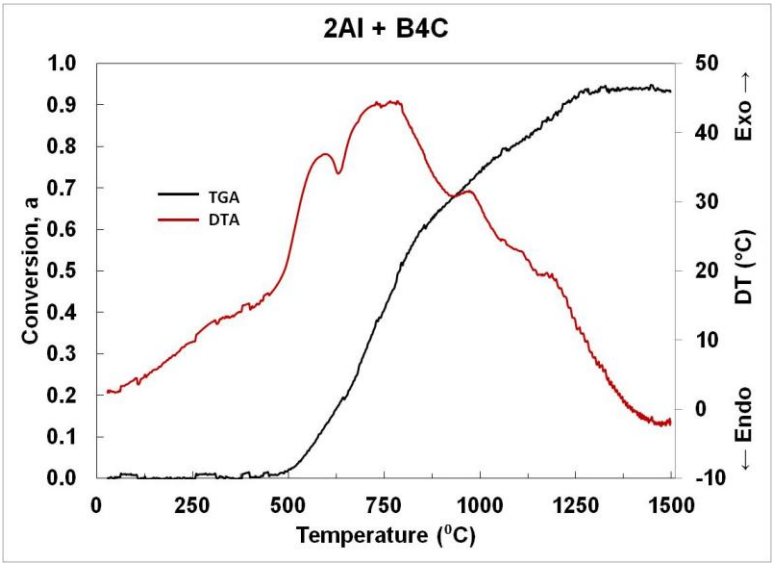

Figure 4.15. TGA and DTA for 2Al + B_4C.

TGA and DTA did not provide clear information about the dominant mechanisms, SEM and XRD were used to investigate the oxidized samples for clues.

Scanning electron microscopy of Al + 2B powder before and after oxidation at 1000°C was conducted to determine the morphology of the oxidized powder. SEM images and EDS revealed that B_2O_3 had formed a continuous layer throughout the powder. Physical manipulation of the oxidized product was more difficult due to its brittle, cohesive nature. Initially added to the crucible as a fine powder, it was difficult to remove and did so in large agglomerates. Figure 4.16 shows Al + 2B powder before and after oxidation at 1000°C. The aluminum particles, which appear as bright spheres before oxidation and lighter spherical regions after oxidation, appear to be coated in B_2O_3 after being oxidized. As B_2O_3 is a liquid at such temperatures, this result is not surprising.

The role of B_2O_3 was investigated by XRD. It is known that aluminum borate phases exist, such as $2Al_2O_3 \cdot B_2O_3$ or $9Al_2O_3 \cdot 2B_2O_3$,[5,6] that are thermodynamically favorable and are also solids at the temperatures examined. X-ray diffraction was used

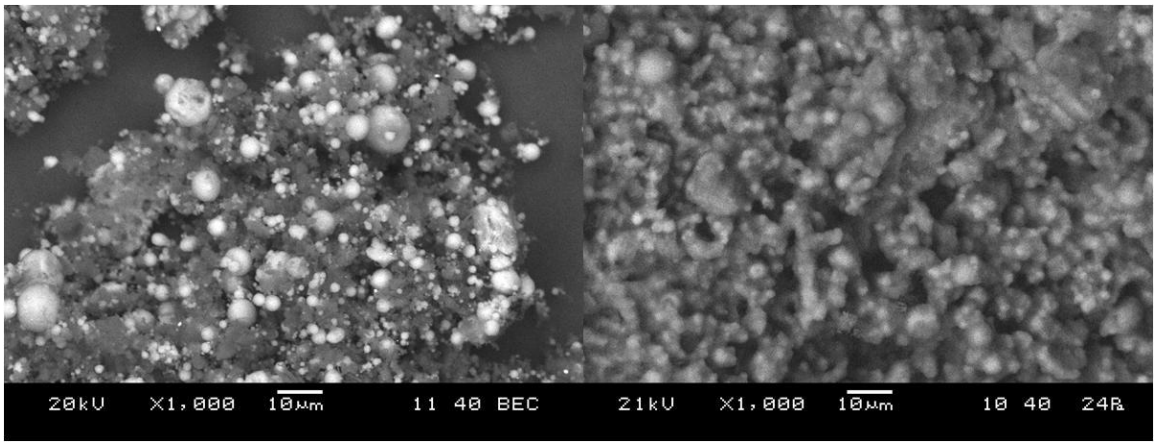

Figure 4.16. SEM backscattered images of Al + 2B before (left) and after (right) oxidation at 1000°C.

to confirm the presence of these phases in the oxidized powder (Figure 4.17). No $9Al_2O_3{\cdot}2B_2O_3$ was observed, but $2Al_2O_3{\cdot}B_2O_3$ was the predominant oxidation product. Al_2O_3 and unoxidized aluminum were also present, along with trace amounts of AlB_{12}. Crystalline B_2O_3 was not observed, indicating that the oxidized boron was amorphous.

The presence of $2Al_2O_3{\cdot}B_2O_3$ is significant. Because liquid B_2O_3 was the rate limiting factor for the oxidation of boron, the removal of B_2O_3 was critical for increasing reaction kinetics. As described in Chapter 1, LiF has been used to remove B_2O_3 from the surface of boron particles with positive results, but the toxicity of fluorine and HF limit its use. In this system, B_2O_3 was essentially removed from the system by forming an aluminum borate with the oxidizing aluminum particles. Liquid B_2O_3, free to diffuse towards aluminum particles as seen in Figure 4.16, reacts with Al_2O_3 on the surface of these particles to form a solid compound, more closely resembling the oxide of aluminum than boron. This provides an inherent mechanism for the increase in oxidation of boron through removal of liquid B_2O_3 and thus reducing the barrier to diffusion of oxidizing species.

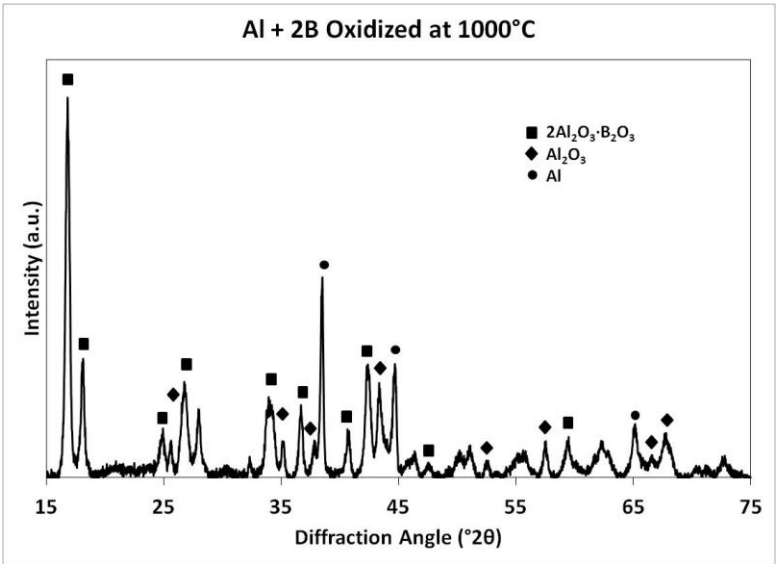

Figure 4.17. XRD of oxidized Al + 2B, showing the formation of aluminum borate. Unidentified peaks are from AlB_{12}, which was formed at temperatures above 975°C, and B_2O_3.

The borate formation mechanism is likely responsible for the $\Delta\alpha$ of +0.09 described in Table 4.2. Al + 12B had a $\Delta\alpha$ of +0.08, which can also be explained by the same mechanism. The benefit of borate formation in this system is nearly identical to the Al + 2B system. Because there was much less aluminum in the Al + 12B powder, the reduction in B_2O_3 was less, leading to a lower overall conversion despite a similar $\Delta\alpha$. A quantification of the phases present in each system after oxidation would be necessary in order to determine exactly how much borate formed, and the expected conversion based on the products would have to be calculated in order to determine if the expected increase in conversion is directly related to the amount of borate formed. Nonetheless, there is strong evidence that this was the dominant mechanism.

B_4C oxidized in much the same way as boron and its increase in conversion upon the addition of aluminum can be explained in the same way. The $\Delta\alpha$ of +0.19 was the second highest of any mixture. The reason for the significant improvement of this

material over Al + 2B is unknown; it is possible that the interactions between carbon and aluminum further assist the oxidation process. It is also possible that the calculation of α leads to an exaggerated $\Delta\alpha$. The calculation assumes that all carbon is removed from the final product, but if aluminum was oxidizing completely while B_4C was only partially oxidized, the carbon remaining in the B_4C would cause the conversion to appear higher than it truly was. While this may happen to some extent, the high conversion of Al + 2B suggests that aluminum and boron are not oxidizing independently and that reaching a high conversion requires both species to oxidize concurrently. It is appropriate to conclude that B_4C + 2Al has a $\Delta\alpha$ greater than Al + 2B, with a maximum of +0.19.

Magnesium oxide also forms a borate with B_2O_3, $3MgO{\cdot}B_2O_3$, and the increase in conversion for Mg + 2B can be explained in a similar way. The $\Delta\alpha$ of +0.24 indicates that not only did magnesium help boron reach higher a conversion but that the formation of a borate also helped magnesium oxidize as well. The relationship between these powders and their borates is described in more detail below.

The benefit of mixing metals and boron has been demonstrated. The decrease in sensitivity of the reacted boride compounds has also been shown in Table 4.1. These data indicate that increased conversions occur with boride compounds too. Not surprisingly, the borate formation mechanism applies equally well for these compounds.

A comparison between Al + 2B and AlB_2 is presented in Figure 4.18. AlB_2 reached a higher conversion over a narrower temperature range and began to oxidize at a higher temperature than Al + 2B. The initial rate of oxidation for both materials appeared to be similar from the slope of the curves, but Al + 2B slowed at higher temperatures, similar to boron, while AlB_2 continued to oxidize until it was almost completely reacted.

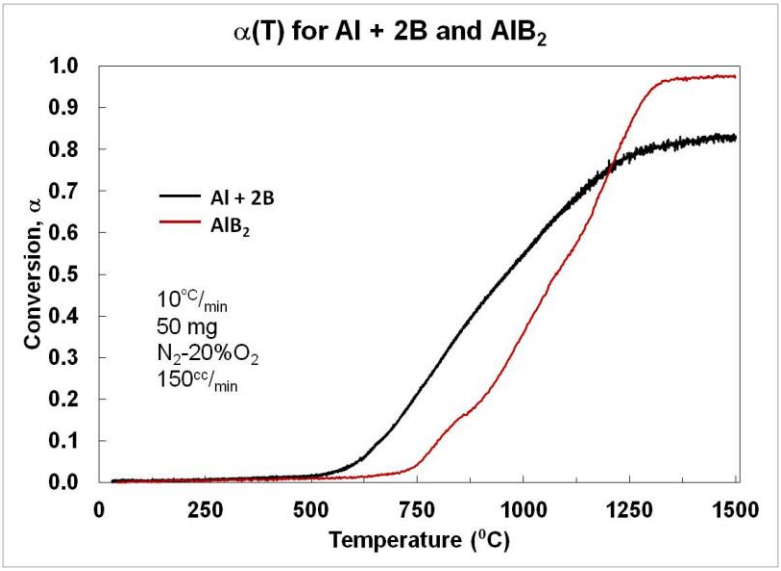

Figure 4.18. Comparison of reacted (AlB_2) and unreacted Al + 2B.

Not only did aluminum borate form on AlB_2 particles, it grew into needle-like structures on the surface of the powder. Figure 4.19 shows how different the oxide growth was between Al + 2B and AlB_2 at 1250°C. Small needles appeared more like a 'fuzz' on the Al + 2B surface, whereas very pronounced, high aspect ratio needles grew on AlB_2. This phenomenon offers a clear explanation for the higher conversion of AlB_2 over Al + 2B. The removal of B_2O_3 occurred on AlB_2 much in the same way it did on Al + 2B, with the key difference being that in the case of AlB_2 the aluminum and boron were atomically close and could rapidly form the borate upon oxidation. The nucleation of borate sites on the particle surface led to the formation of needles as material below the nuclei continued to oxidize. This process also occurred in Al + 2B, but relied on the diffusion of B_2O_3 to particles coated in Al_2O_3 at low conversions or through developing oxide layers at high conversions. The atomic proximity of aluminum and boron seemed to be critical.

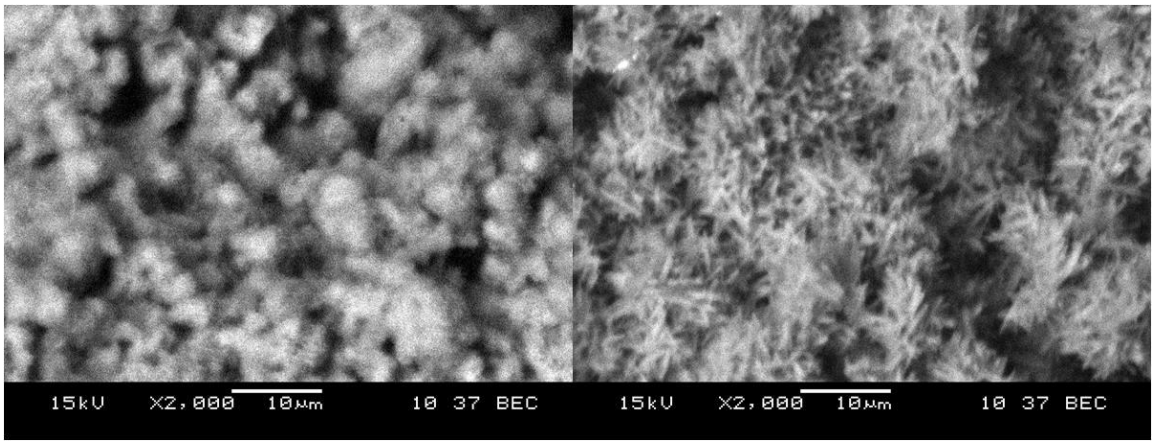

Figure 4.19. SEM backscattered images of Al + 2B (left) and AlB_2 (right) oxidized to 1250°C. $2Al_2O_3 \cdot B_2O_3$ needles grew on the surface of both powders, but are much more developed in AlB_2.

In the Mg-B system shown in Figure 4.20 both powders reached the same ultimate conversion but did so along different paths. The initiation temperature of MgB_2 was higher than Mg + 2B but appeared to originate from a similar temperature range. After the initial oxidation region (below $\alpha \approx 0.33$) both curves shared a similar shape, including kinks around $\alpha=0.7$ and $\alpha=0.8$. The similarity in curve shape suggests a similarity in oxidation behavior. This reinforces the applicability of the borate formation mechanism. Due to lack of interest in this material by the Army, follow up work was not conducted to determine the composition and morphology of the borate on the oxidized powder.

$Al_{0.5}Mg_{0.5}B_2$ was markedly different from either AlB_2 or MgB_2 (Figure 4.21). The initial oxidation was much more gradual than the other diborides, but around 900°C a rapid oxidation occurred with a rate much higher than any other material investigated. At a temperature of 1100°C and a α of 0.6, oxidation nearly halted, then resumed parabolically up to 1500°C. Again, due to lack of interest by the Army these phenomena

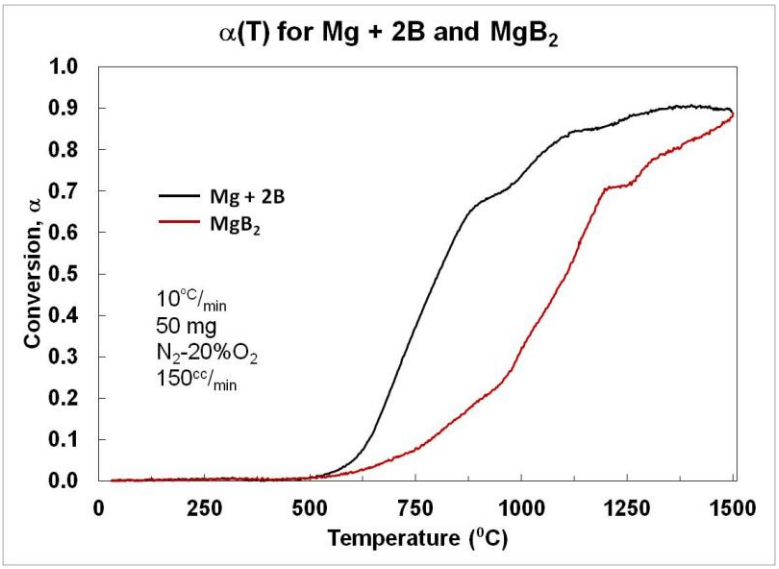

Figure 4.20. Comparison of Mg + 2B and MgB_2.

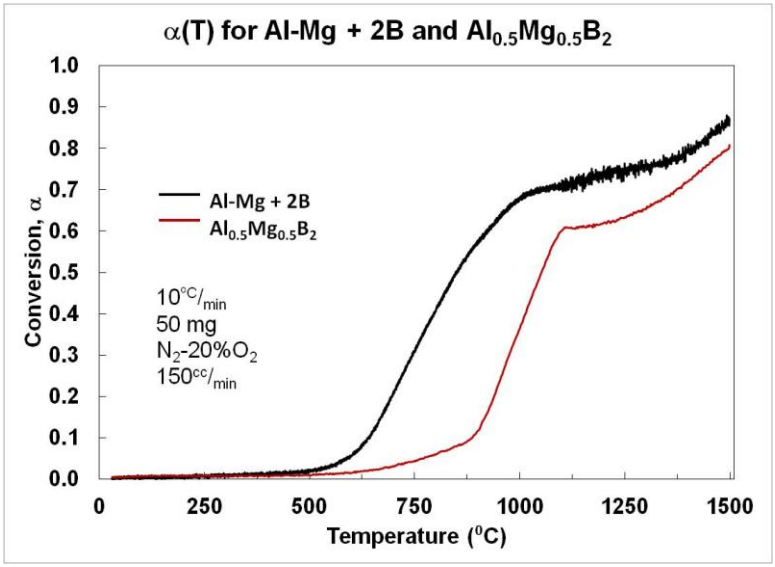

Figure 4.21. Comparison of Al-Mg + 2B and $Al_{0.5}Mg_{0.5}B_2$.

were not studied further, but the rapid oxidation behavior is interesting in the context of energetic materials and may warrant further investigation.

Comparisons of the remaining mixtures and compounds are given in Figure 4.22-25. AlB_{12}, $AlMgB_{14}$, SiB_6 and $Al_3BC + AlB_2$ did not reach high conversions and were no better than their starting powders. $Al_3BC + AlB_2$, which was the incompletely reacted product of $2Al + B_4C$, resembled the $2Al + B_4C$ curve shifted to higher temperatures. It is possible that the reacted material would have reached a high conversion at a similar rate if allowed to continue to higher temperatures. Increasing the extent of reaction of this material and investigating energetic properties are of interest because of its lower cost and the promising results of its physically mixed precursor. The other three materials did not show promise as energetic fuel additives and were not investigated further.

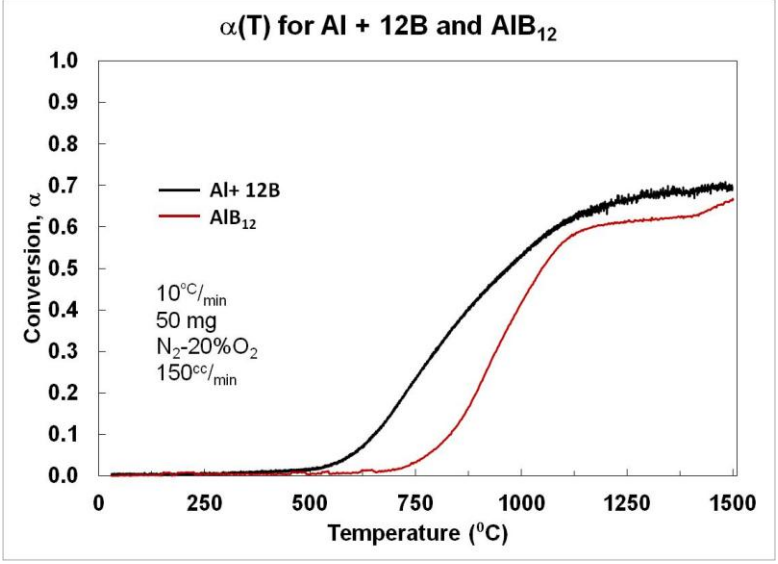

Figure 4.22. Comparison of Al + 12B and AlB_{12}.

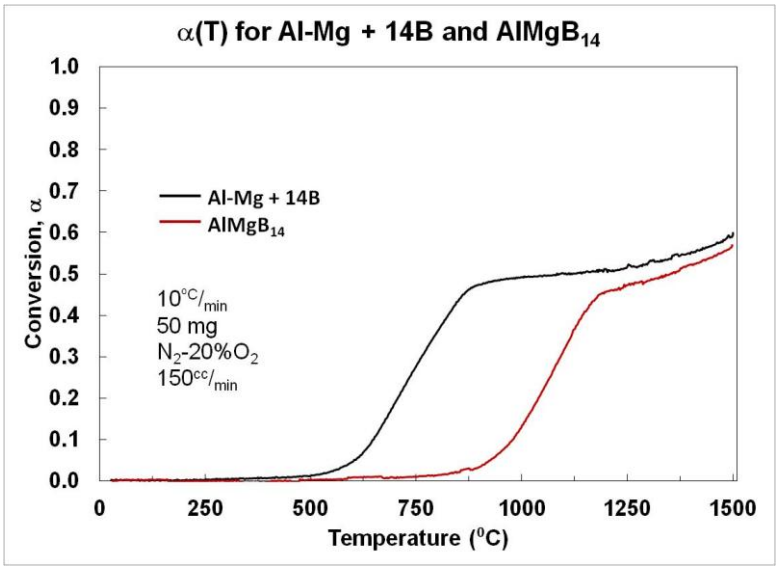

Figure 4.23. Comparison of Al-Mg + 14B and $AlMgB_{14}$.

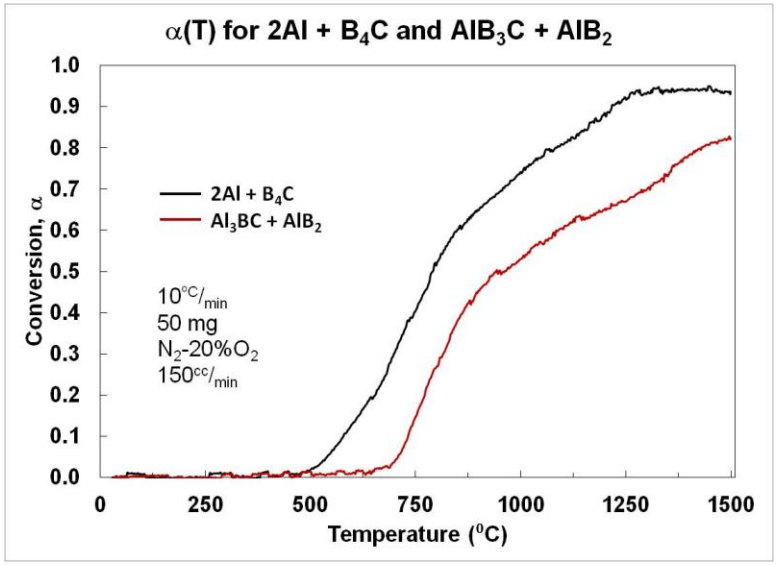

Figure 4.24. Comparison of $2Al + B_4C$ and $Al_3BC + AlB_2$.

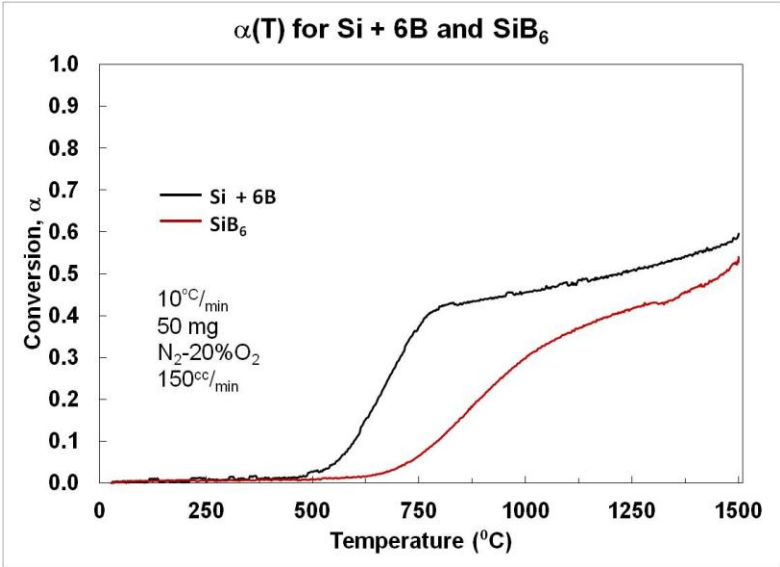

Figure 4.25. Comparison of Si + 6B and SiB_6.

4.2 Conclusions

The rapid oxidation of the metals magnesium and aluminum is desired for energetic applications. Boron is a promising element on the basis of thermodynamic potential, but is too kinetically limited to be effective in most applications. Thermal gravimetric analysis followed by SEM and XRD have confirmed that boron is kinetically limited by a viscous B_2O_3 layer that coats the surface of oxidizing boron particles and slows diffusion. This kinetic limitation was not observed at low conversions, however, due to the high surface area of the power. It is hypothesized that nanometric boron particles with much higher surface areas could oxidize almost completely through surface oxidation without becoming kinetically limited by a thick oxide. Unfortunately, such particles would be difficult to synthesize and keep free of surface oxides and would present a more considerable safety risk.

Differential thermal analysis confirmed that the oxidation of aluminum, magnesium, and magnesium aluminum alloy powders is associated with large exotherms corresponding to rapid oxidation, a desirable energetic characteristic. TGA showed that both aluminum and the magnesium aluminum alloy were fully oxidized by 1500°C. Magnesium only reached a conversion of 0.77 due to the larger particle size of magnesium, which had a thick oxide layer relative to the shrinking particle core. Boron carbide oxidized in nearly the same way as boron, indicating that the process was the same as that described for boron. Silicon reached only 33% of its theoretical value, making it a poor energetic material.

It was demonstrated that mixtures of boron and metal powders oxidized to a higher extent than what was expected using a rule of mixtures calculation. While boron reduced the extent of reaction of aluminum and aluminum-magnesium, the higher extent of reaction of boron (which has a higher enthalpy of oxidation than the metals) achieved through mixing offset the loss. Al + 2B powder reached a higher conversion than expected because of the nucleation of aluminum borate ($2Al_2O_3 \cdot B_2O_3$) needles on the aluminum particle surface. The increase in conversion for Mg + 2B and Al-Mg + 2B is likely caused by borate formation as well, though further investigation is needed. Through the same mechanism, 2Al + B_4C reached the highest conversion (0.95) of the powder mixtures, demonstrating that B_4C may be a viable substitute for boron in energetic systems. Due to the poor performance of silicon, Si + 6B reached a lower conversion than boron alone and does not hold any promise as an energetic mixture.

Reacted diboride compounds of aluminum and magnesium showed the most promise as insensitive energetic materials. They did not rapidly oxidize at low

temperatures, but reached high conversions through the same borate formation mechanism seen in the powder mixtures. Further energetic testing of the diboride materials in comparison to their starting powder mixtures is of great interest. Compounds with higher boron contents, while similarly insensitive, did not reach high conversions and are not likely promising energetic materials.

Ultimately, combustion calorimetry, detonation calorimetry, cylinder expansion testing or another in situ energetic test must determine the viability of these powders. It is not clear yet whether this characterization correlates with performance in an energetic system. This is probably not the case, as the time, pressure, and temperature scales are much different in a combustion or detonation event. However, useful data can be gleaned from thermal analysis. Sensitivity to low temperature oxidation is a critical parameter that must be quantified for safe handling of energetic materials, and when used in conjunction with shock, impact, and friction sensitivity comprises the most critical sensitivity information. Characterization of oxidation products can offer insight into potential reaction mechanisms, both beneficial and detrimental. For example, it is almost certain that Si + 6B and SiB_6 will not make good energetic fuel additives. It is not clear whether the formation of metal borates will impact the in situ performance, but the results that will either confirm or deny this will elucidate the relevance of this work.

4.3 References

1. T. A. Mikhalvo, M. Schoenitz, X. Zhu, E and L. Driezin "Effect of Polymorphic Phase Transitions in Al_2O_3 Film on Oxidation Kinetics of Aluminum Powders," *Combust and Flame* **140**[4] 310-318 (2005)

2. M. M. Mench, K. K. Kuo, C. L. Yeh and Y. C. Lu, "Comparison of Thermal Behavior of Regular and Ultra-Fine Aluminum Powders (Alex) Made from Plasma Explosion Process," *Combust. Sci. and Tech.* **135** 269-292 (1998)

3. K. P. R. Reddy and A. R. Cooper "Oxygen Diffusion in MgO and α-Fe_2O_3," *J. Am. Ceram. Soc.* **66**[9] 664-666 (2006)

4. Y. Q. Li and T. Qiu "Oxidation Behavior of Boron Carbide Powder," *Materials Science and Engineering A,* **444**[1-2] 184-191 (2007)

5. K. V. Logan, J. S. McLemore and J. T. Sparrow, "Particle-Particle Interactions in Aluminum Reduction of Boron Oxide," *AIChE Symposium Series* **84**[263] 59-68 (1988)

6. P. E. Blackburn, A. Buchler and J. L. Stauffer, "Thermodynamics of Vaporization in the Aluminum Oxide-Boron Oxide System," *J. Phys. Chem.* **70**[8] 2469-74 (1966)

5. KINETIC ANALYSIS

5.1 Isothermal Oxidation

Isothermal oxidation studies of AlB_2 and its constituent powders were conducted in order to determine the activation energy of this compound and compare it to that of boron, aluminum and Al + 2B. Thermal gravimetric analysis was used to determine the weight change of the samples upon oxidation, from which the percent conversion of AlB_2 to oxidized product, α, could be calculated. For each run, approximately 25 mg of AlB_2 was heated in N_2-20%O_2 (referred to as air) or industrial grade O_2 flowing at a rate of ~150 cc/min. Samples were brought to temperature as quickly as possible (~75°C/min) and held at temperature for 5-7 hours. Temperatures ranging from 400-1000°C were used.

5.1.1 Model-Free Method I, Air

The data in this chapter were analyzed with a model-free isoconversional method described by Simon.[1] The benefit of this method is that it simplifies the kinetic analysis of complex systems, like Al-B-O, so that processes with multiple steps and different rates can be examined without intricate models. There are only two basic assumptions: 1) The rate of the process is a function of temperature and conversion only, and 2) The activation parameters can be obtained from a set of kinetic runs with the dependence of time vs. temperature. The first assumption can be written mathematically as[1]

$$\frac{d\alpha}{dt} = \Phi(T, \alpha) \tag{5.1}$$

where it is assumed that the temperature dependence of a reaction and the conversion dependence are independent of each other. This leads to[1]

$$\Phi(T, \alpha) = k(T) f(\alpha) \tag{5.2}$$

where *k(T)* is the reaction rate and *f(α)* is a function that describes the conversion process. The rate of the conversion can be written as[1]

$$\frac{d\alpha}{dt} = k(T) f(\alpha) \tag{5.3}$$

Because the reaction's dependence on conversion and temperature are independent, the differential equation in (5.3) can be solved by separation of variables, such that[1]

$$\int_0^{\alpha} \frac{d\alpha}{f(\alpha)} = k \int_o^{t_\alpha} dt \tag{5.4}$$

where t_α is the time at which the conversion α is reached. The rate constant, *k*, has the expected Arrhenius form[1]

$$k(T) = A \exp\left[-\frac{E}{RT} \right] \tag{5.5}$$

in which *A* is the preexponential factor, *E* is the activation energy and *R* represents the ideal gas constant. The solution to Equation (5.4) takes the form[1]

$$g(\alpha) - g(0) = k(T)t_a \tag{5.6}$$

where *g(a)-g(0)* represents the solution to the left hand side of Equation (5.4). Solving this equation for t_α gives[1]

$$t_\alpha = \frac{g(\alpha) - g(0)}{k(T)} \tag{5.7}$$

The expression in the numerator is a solution to the left hand side of Equation (5.4). Substituting k into Equation (5.7) yields[1]

$$t_\alpha = \frac{1}{A_\alpha \exp\left[-\frac{E}{RT}\right]} \tag{5.8}$$

where A_α is given by[1]

$$A_\alpha = \frac{A}{g(\alpha) - g(0)} \tag{5.9}$$

A plot of ln(1/t) vs. 1/T at a given conversion gives a line with the slope –E/R and thus the activation energy can be found. Note that A_α is not the preexponential factor for the global reaction, just at a specific conversion. A model for the $d\alpha/dt$ as a function of α, ($f(\alpha)$ in the differential form or $g(\alpha)$ in the integral form), must be identified before a global value for A can be calculated.

In practice, conditions were not perfectly isothermal. The TGA furnace had to be ramped up to temperature, during which time some oxidation occurred. The ramp was made as quickly as possible to minimize the effects of non-isothermal oxidation on the calculations. The temperature versus time graph in Figure 5.1 shows that the ramp took around 15 minutes to complete for each run. The conversion of boron as a function of time is plotted in Figure 5.2. In this analysis, t=0 when the temperature reached 99% of the average hold temperature. After 5 hours of oxidation at hold temperatures of 600, 650 and 700°C boron had not reached conversions over $\alpha = 0.6$. This was expected from the

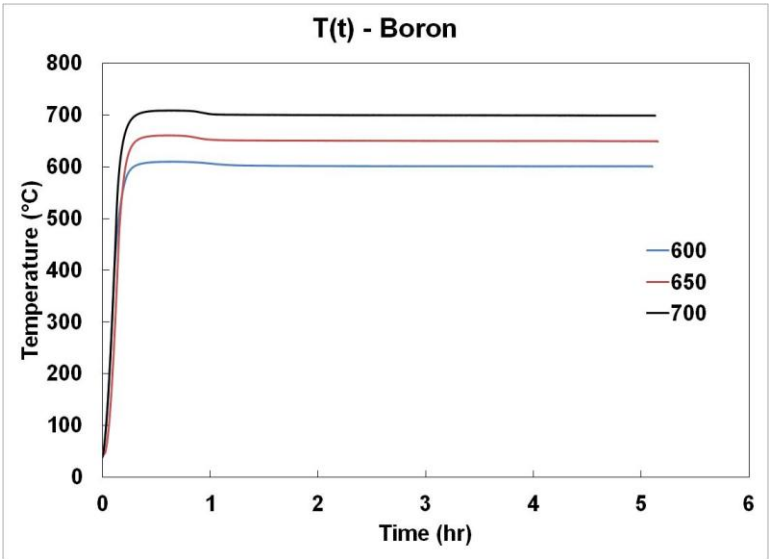

Figure 5.1. Time vs. temperature plot for three isothermal runs of boron in air.

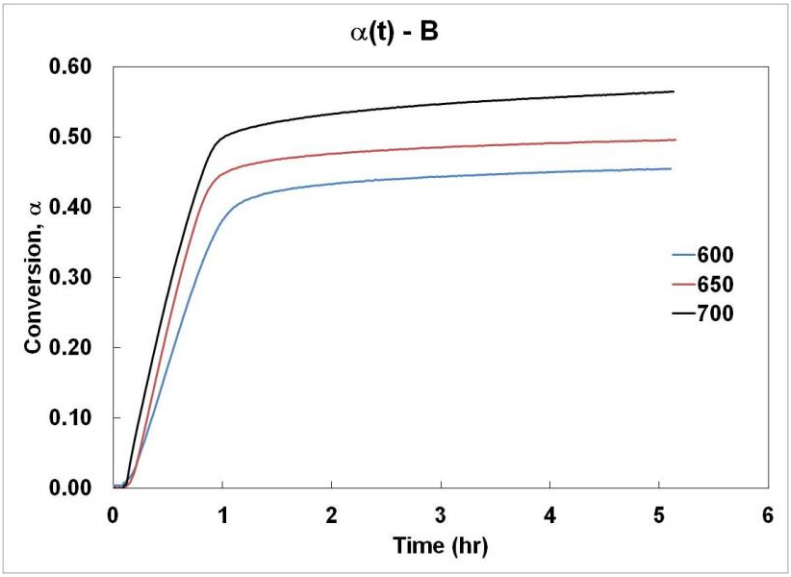

Figure 5.2. Conversion of boron as a function of time at three different temperatures

limitations of boron outlined in previous chapters. Two distinct regions can be seen in the isothermal regime, similar to the constant heating rate regime. Roughly the first half of the oxidation process happened quickly and nearly linearly, while the second half was very slow and somewhat logarithmic. From the linearity of the first oxidation step it is clear that this process corresponded to oxidation of boron with a very thin layer of oxide at the interface of the particle so that diffusion of oxygen to the surface was not the rate limiting step. As the oxide layer grew in thickness, it became a significant barrier to diffusion and slowed the oxidation process. This is the same behavior observed in the linear heating rate study conducted in Chapter 4.

A plot of ln(1/t) vs. 1000/T is given in Figure 5.3. The slope of each line represents the activation energy (in kJ/mol) at a particular α divided by the gas constant. Only conversions up to 0.4 were considered because that is the upper limit for the first linear region. The abrupt change in slope of the $\alpha(t)$ curve above 0.4 represented a

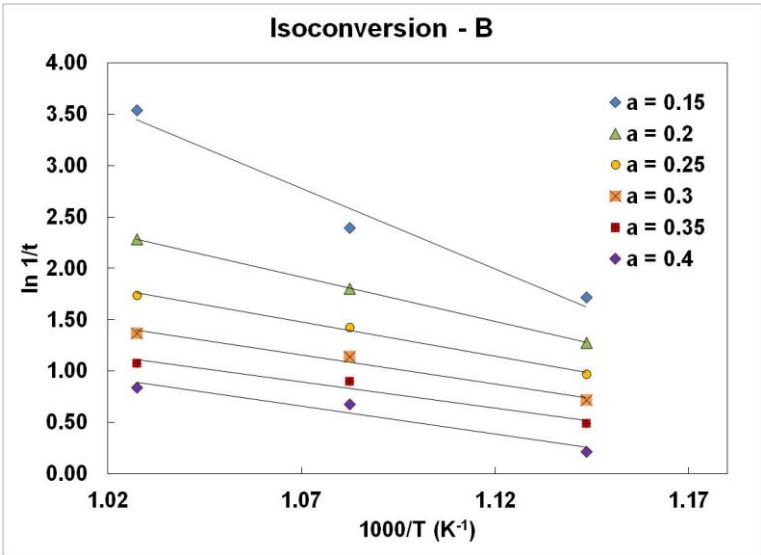

Figure 5.3. Plot of 1000/T vs. ln(1/t). The slope of each line is the activation energy at a particular conversion divided by the gas constant.

change in the oxidation mechanism and hence a change in activation energy. Each α for which three data points were valid (lying in the isothermal regime and not during the ramp) is reported. An average activation energy for these curves is not meaningful because the isoconversion lines have different slopes, indicating that the activation energy is changing as a function of conversion and that the assumption in Equation (5.4) is not valid.

The activation energy at a conversion of 0.15 is clearly affected by the anomalous behavior of high temperature data point (1000/T = 1.027). While this point was located in the isothermal region, it occurred just after the hold temperature was reached. The conversion that this point represents does not reflect processes that occurred isothermally and therefore was eliminated from the analysis. An average of the remaining activation energies, with isoconversion lines that are closer to parallel, gives 53 ± 12 kJ/mol. This gives a first approximation of the activation energy but is fairly imprecise.

It was observed that the conversion specific activation energies (E_α) had a general trend, depicted in Figure 5.4. As conversion increased, the activation energy decreased and appeared to approach a constant value. This is due to the greater contribution of the oxidation during the ramp to the total conversion at low conversions, which decreases as conversion increases. Since the effect of the ramp should not be included in calculations of E, a more accurate representation of the true activation energy is that to which the trend converges. An approximation for this value is the average of the activation energies at 0.30, 0.35 and 0.40, where there does not appear to be significant variation in E with increasing α. The resulting E is 45 ± 2 kJ/mol. A more rigorous approximation was made assuming an inverse relationship between activation energy and conversion in the form

$$E_\alpha = \frac{1}{\alpha^n} + E \tag{5.10}$$

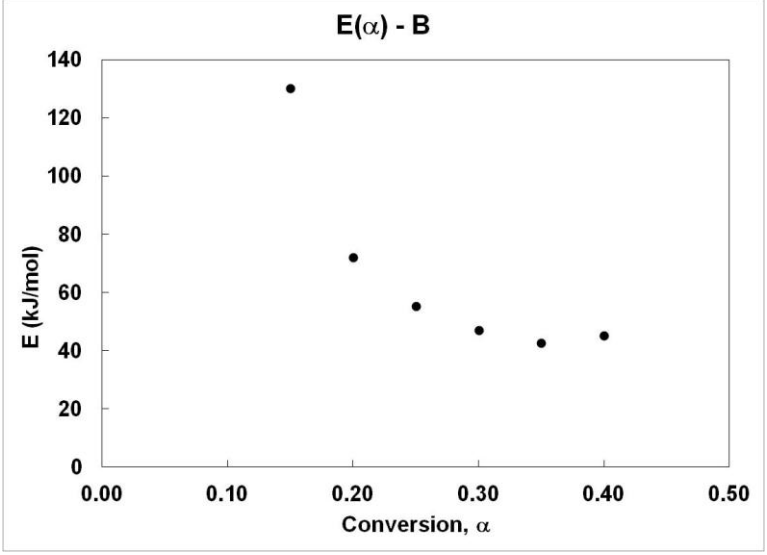

Figure 5.4. Activation energy as a function of conversion for boron.

where E_α is the activation energy at a given conversion, *n* is an adjustable parameter and *E* is the true activation energy. Because this process is simply to identify the best E value, n was adjusted to give the best R^2 value for the straight line that results from plotting E_α versus α^{-n}. The R^2 value as a function of n is presented in Figure 5.5. A value of n=4 gave the highest R^2 value for boron, which led to the linear fit of Equation (5.10) in Figure 5.6. The y-intercept of the line gives the true activation energy, which is 42 kJ/mol. This value agrees well with the approximated value above and represents the activation energy for the interface controlled oxidation of boron.

While it allows for the determination of an activation energy from seemingly confounded data, the method of extrapolation of E_a makes some assumptions that may or may not be valid for the systems investigated. It assumes that there is a single activation energy for the temperature range of interest, which is not necessarily true for complex, multi-component heterogeneous systems. It also assumes that oxidation during the non-

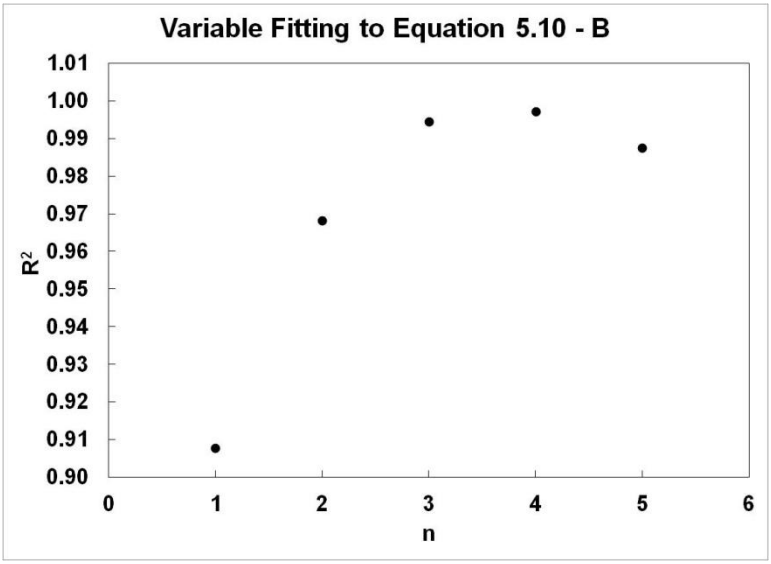

Figure 5.5. Determination of n from Equation (5.10) for boron.

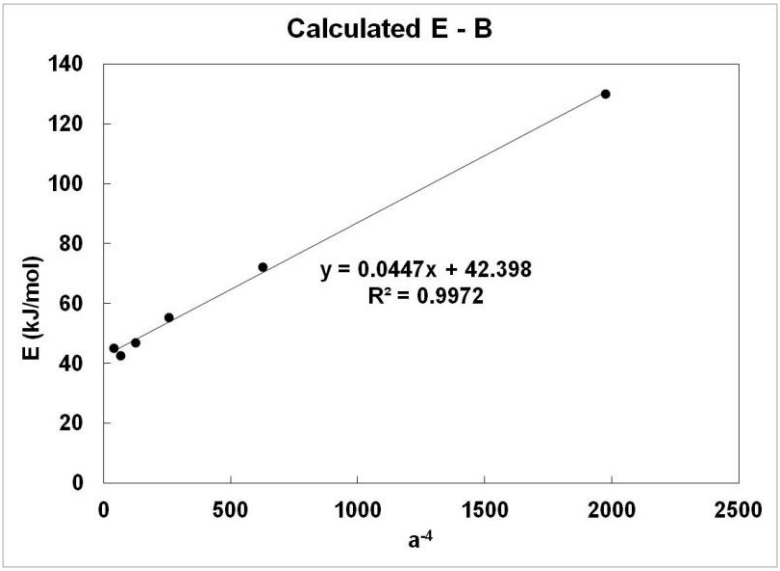

Figure 5.6. Linear fit to Equation (5.10) for boron, where y-intercept is true activation energy.

isothermal ramp is the only factor distorting the calculation of activation energy. This inherently assumes that the data are only taken from a conversion range where one process is dominating. By only using data below α=0.4 in the case of boron, these assumptions are generally valid and the calculated activation energy can be used with confidence. Due to the much slower oxidation in the high α region, an activation energy could not be calculated using the model free method. It would not be practical to continue the test until adequate data was obtained as this would take weeks to complete, so other methods to access the activation energy in this region would have to be used.

A similar process was carried out for aluminum, but the higher initiation temperature and multi-stage oxidation behavior of aluminum made the analysis more difficult. When held at 800°C, aluminum only reached a conversion of 0.17 (Figure 5.7) while the run at 925°C reached a conversion of 0.13 during the ramp alone, and no powder reached a conversion above 0.35. As seen in the case of boron, issues presented

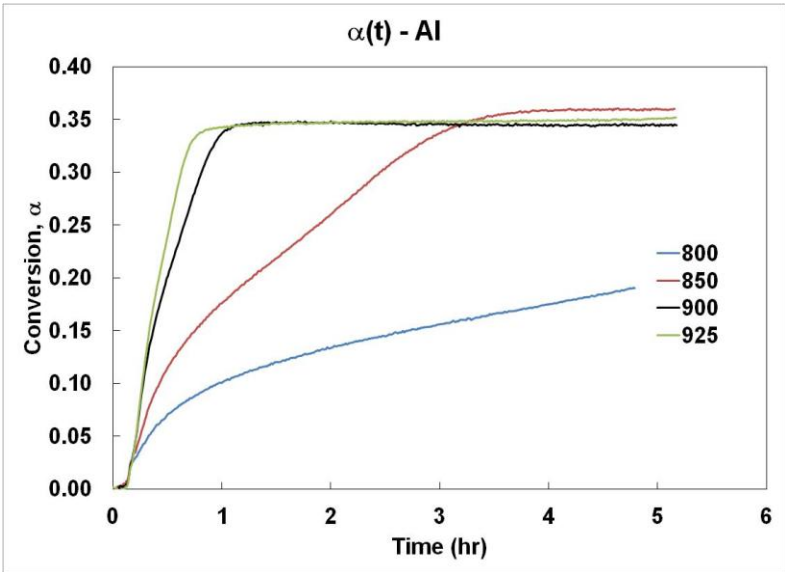

Figure 5.7. Conversion as a function of temperature for aluminum

by the ramp require as many data points as possible to make the most accurate determination of E. There were fewer data than desired for aluminum, but analysis of the available data was conducted.

The plot of ln(1/t) versus 1000/T for aluminum is presented in Figure 5.8. The isoconversion line of 0.15 posed the same problem for this system as it did for boron. A plot of E as a function of α is given in Figure 5.9. Unlike the boron system, the aluminum system did not reach a high enough conversion to dilute the effects of the ramp. The multi-stage oxidation behavior of aluminum described in Chapter 4 prevented the aluminum particles from oxidizing past $\alpha \approx 0.35$ at the temperatures investigated.[2] This was due to the formation of an Al_2O_3 skin on the particle which presented a significant barrier to diffusion. A displacive polymorphic transformation in this oxide layer at higher temperatures resulted in stresses that cracked the Al_2O_3 and exposed aluminum to oxygen in the linear heating rate regime, but in the isothermal cases examined here the temperature was not sufficient to initiate the phase transformation.

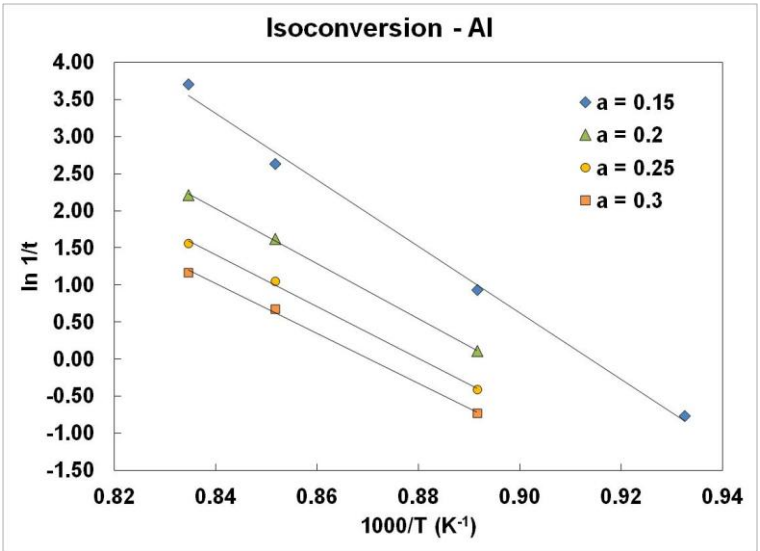

Figure 5.8. Determination of activation energy for aluminum.

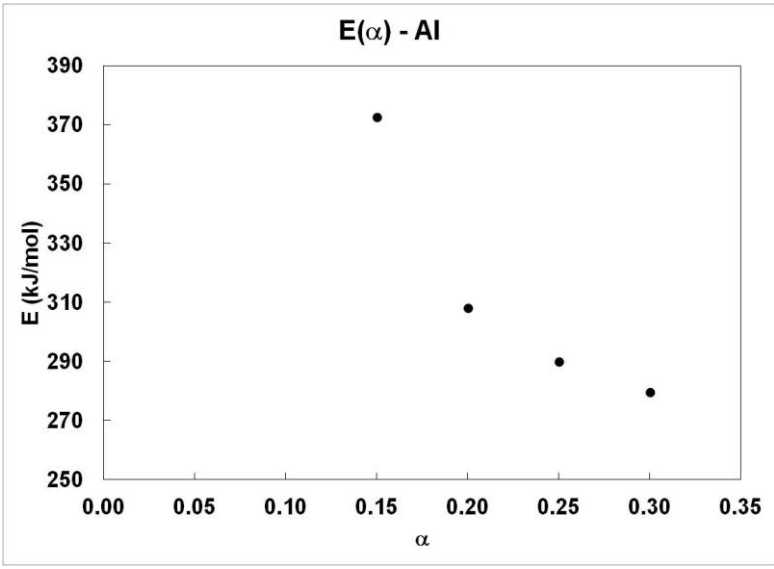

Figure 5.9. Activation energy as a function of conversion for aluminum.

Since the dilution of ramp effects was not sufficient in this system, the activation energy could not be directly obtained from calculated values. However, extrapolation of the trend in Figure 5.9 could be used to approximate the activation energy for the first oxidation process using Equation (5.10). The n that gave the best fit was found to be 3 from Figure 5.10, so n=3 was used. Fitting this equation to the data in Figure 5.11, the activation energy could be read off the graph from the y-intercept as 266 kJ/mol.

Aluminum's interface controlled activation energy was much higher than that of boron. It is at this point that a clarification of the physical meaning of the activation energy for these systems is warranted so that accurate comparisons can be made. On a molecular scale the activation energy represents an energy barrier that must be overcome for a reaction to proceed. This energy barrier is the energy required to form a transition complex between the reactants which, once overcome, for an exothermic reaction, leads to the products of the reaction and a release of energy.[3] It is assumed that this

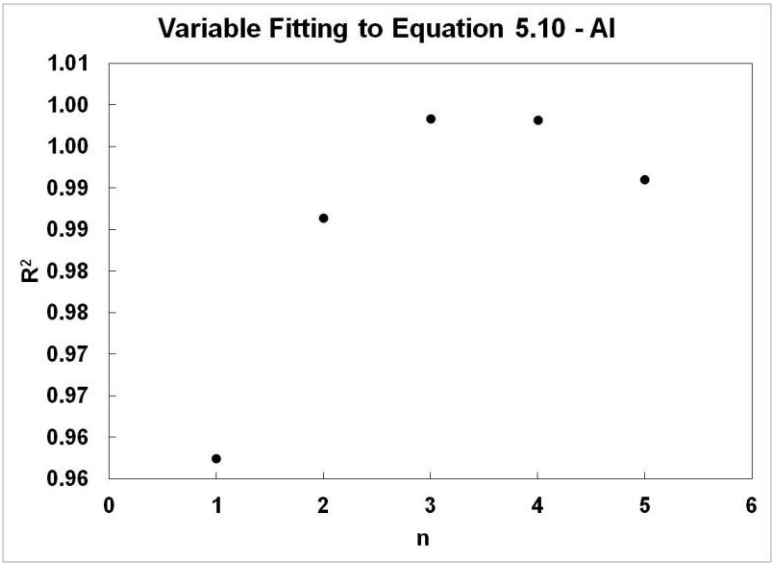

Figure 5.10. Coefficient of determination (R^2) as a function of n in Equation (5.10).

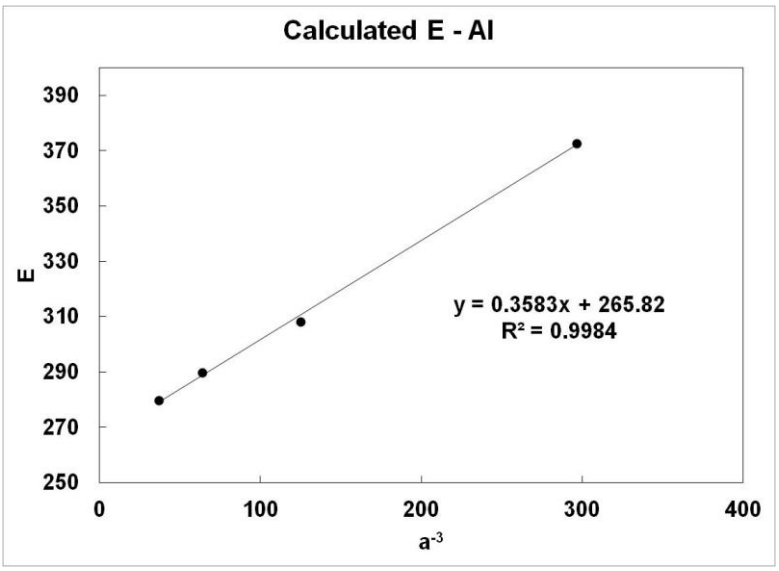

Figure 5.11. Linear fit of Equation (5.10) for n=3. The y-intercept is the true activation energy.

fundamental process is happening for all reactions studied, but the complexity of the systems of interest prevents the activation energy for a single process from being determined. Oxidation in these systems is more than simply the reaction of an oxygen molecule with aluminum or boron through an Al-B-O complex. It is controlled by various mechanisms, including diffusion, viscous flow, nucleation and growth and the complex borate formation mechanisms described in Chapter 4, all of which have a number of activated processes occurring. The activation energy represents the sum of all reactions taking place in the system. These reactions are by necessity temperature dependent, each to a different degree, so that the rate of the overall reaction is determined by the temperature dependence of each reaction. The activation energy, then, is the temperature dependence of the rate limiting step for a given temperature range.

The activation energy of Al + 2B did not approach a constant value, but instead reached a local minimum of approximately 70 kJ/mol at intermediate conversions and began to increase as α approached unity. Figure 5.12 shows the conversion as a function of temperature between 620 and 800°C. The isoconversion plot in Figure 5.13 shows that the E_α values were fairly regular between 0.2 and 0.5, but after 0.5 they became erratic. This is most likely a result of different processes controlling the oxidation behavior of Al + 2B at low and high temperatures as the conversion increased. The $E(\alpha)$ plot in Figure 5.14 would suggest that the minimum activation energy was around 70 kJ/mol. This is much lower than the value expected if the activation energy was simply a rule of mixtures between that of aluminum and boron (116 kJ/mol), indicating that the borate formation mechanism reduced the temperature dependence of the reaction in the temperature range of interest.

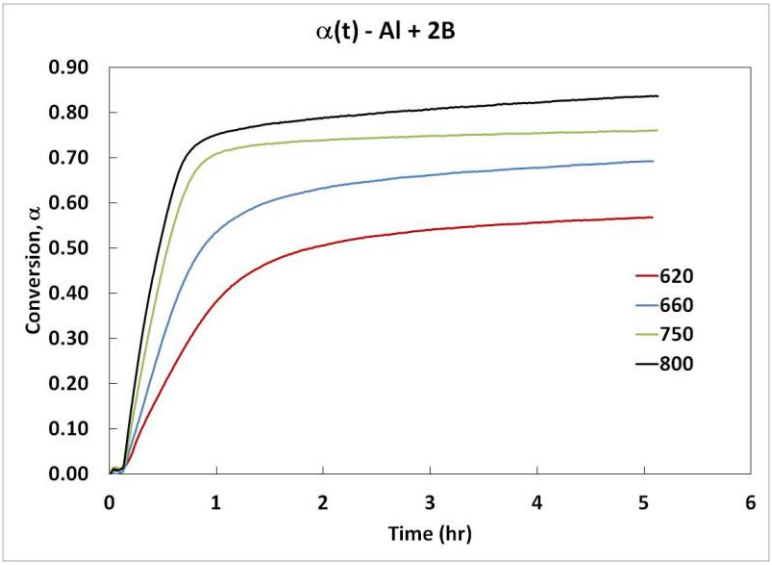

Figure 5.12. Conversion as a function of time for Al + 2B.

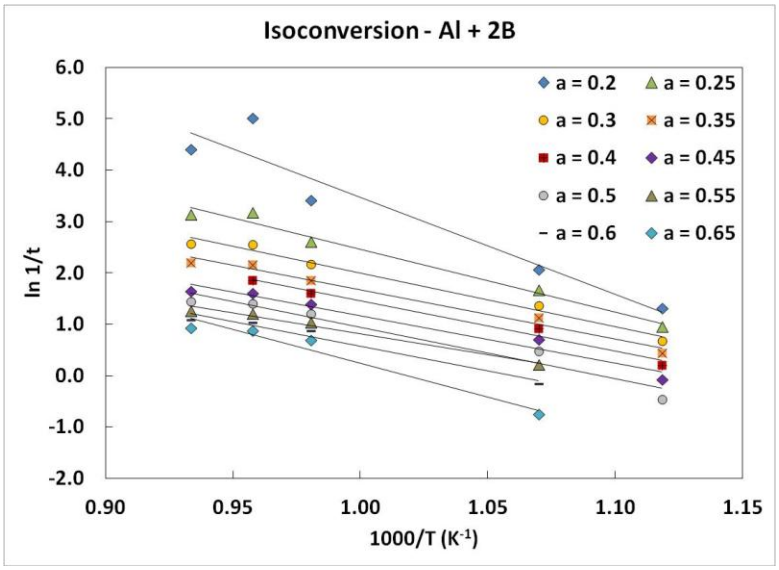

Figure 5.13. Isoconversion plot for Al + 2B in air.

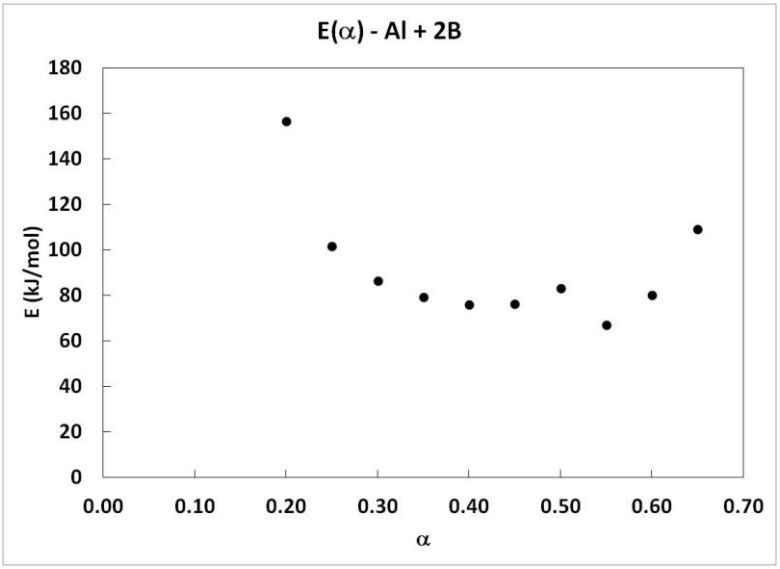

Figure 5.14. E(α) plot for Al + 2B in air.

Aluminum diboride was also analyzed by the model free method, with interesting results. Samples were heated at 900, 925, 950, 975 and 1000°C. The conversion as a function of time is given in Figure 5.15. The oxidation behavior of AlB_2 was much different from that of either aluminum or boron. After an initial parabolic region at the onset of oxidation, each curve assumed linear-type behavior as time progressed. There was no slowing or termination of oxidation as was the case for boron, aluminum or Al + 2B. The isoconversion plot is shown in Figure 5.16. The poor linear fit to the isoconversion line at 0.15 is again a reflection of the effect of ramping on the sample, although the effect is not as pronounced with AlB_2 because there are more data points.

An interesting trend appears from the plot of E as a function of α in Figure 5.17. While the activation energy is not constant with conversion, as it is expected to be in the ideal case, it was not approaching a constant value but instead linearly decreasing with increasing conversion. This behavior is initially surprising, as it does not allow for the

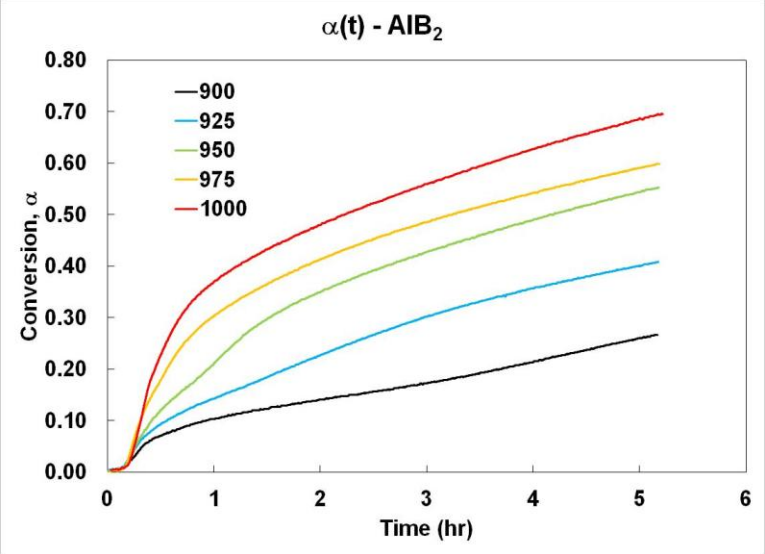

Figure 5.15. Conversion as a function of time for AlB_2.

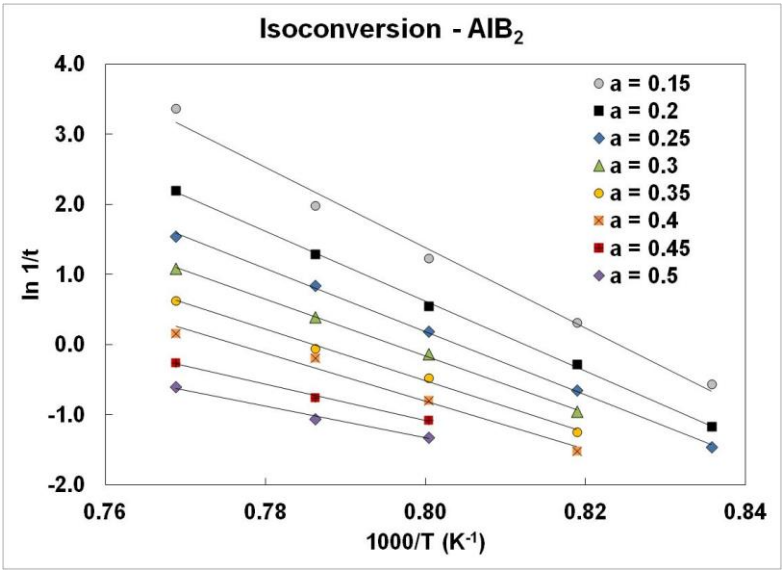

Figure 5.16. Isoconversion plot for AlB_2.

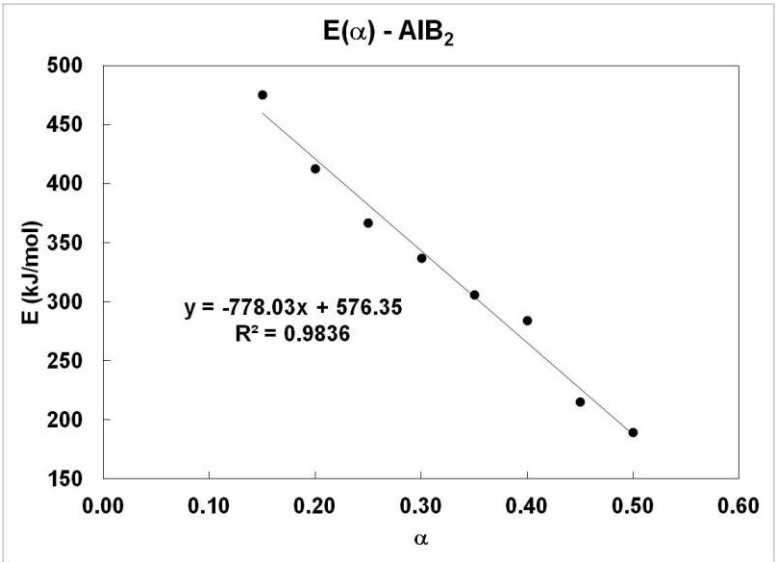

Figure 5.17. Activation energy as a function of conversion for AlB_2.

calculation of an activation energy. The activation energy is best reported as a function of α, given by

$$E(\alpha) = -778\alpha + 576 \tag{5.11}$$

This tells an important story about the oxidation of the AlB_2 system. The initial variation in activation energy may have been caused by residual effects of the ramp on the AlB_2 powder (like boron and aluminum) but did not lead to a converging trend at higher conversions like that of boron and aluminum. Instead, the activation energy continued to decrease with increasing conversion. This suggests that the borate formation mechanism, which is more prominent at higher conversions, reduces the activation energy as oxidation progresses.

The initial oxidation at low conversion follows a parabolic trend that corresponds to the nucleation of aluminum borate sites on the particle surface. This process would manifest as a sigmoidal curve if the experiment were truly isothermal, but the oxidation upon ramping contracted the tail region at the beginning of the curve (as well as skewing the E_α data at low conversions). The nucleation and growth of nuclei continued into higher conversions, but that process was eventually dominated by the radial growth of $2Al_2O_3{\cdot}B_2O_3$ needles, moving oxide material away from the particle surface. The decrease in activation energy as oxidation progressed was likely due to the increasing ease with which particles could oxidize as needles moved oxide away from the particle surface. Although a single value could not be calculated, it is clear from Figure 5.17 that the initial activation energy was greater than 250 kJ/mol.

5.1.2 Model-Free Method II, O_2

In order to obtain more accurate data about the activation energy of aluminum, boron, Al + 2B and AlB_2, the same isothermal study was conducted in oxygen instead of air. Industrial oxygen (99%) was used to minimize any effects caused by oxygen deficiency in the air just outside oxidizing particles and also to attain higher conversions. A small mass of powder (25 mg) was used to increase exposure to oxygen. It was hypothesized that the activation energies would be the same in air and oxygen if the same processes were controlling the rate of oxidation.

From Figure 5.18 a number of differences between runs in oxygen and the previous runs in air can be seen. First, the initial oxidation was very rapid at temperatures above 500°C. . An expansion of the temperature vs. time graph in Figure 5.19 shows large temperatures spikes above 550°C corresponding to rapid exotherms produced by the oxidizing particles. The ease with which this oxidation occurred was a result of the

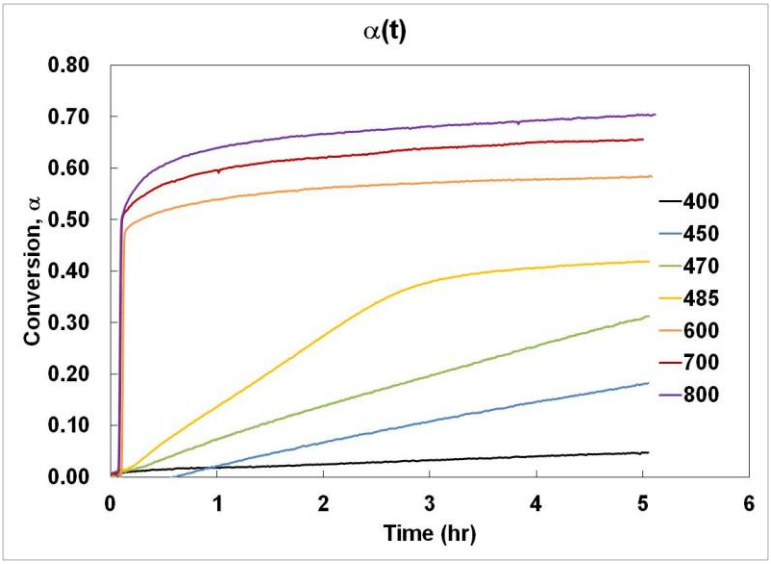

Figure 5.18. Conversion as a function of time for boron in oxygen.

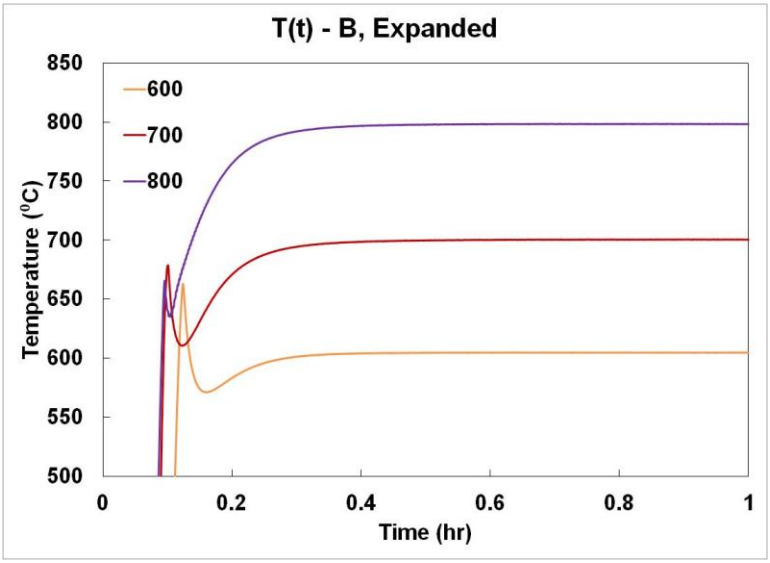

Figure 5.19. Expansion at the top of the ramp portion of the T(t) graph, showing temperature spikes near 650°C.

low activation energy calculated from the run in air. Another interesting feature of these runs is that there was a low temperature region where conversion was a perfectly linear function of time.

Because the low temperature runs (400, 450, 470 and 485°C) each had linear behavior at low conversions, a line was fit to each curve and extrapolated in order to calculate the activation energy of the initial oxidation process. Although the true oxidation curve did not necessarily follow the extrapolated line to complete conversion (as evidenced by the 485°C run), the extra data made it possible to calculate an activation energy for the process controlling the low conversion behavior which was not possible otherwise. A line was fit to the segment of the data between one and two hours after the sample reached 99% of its hold temperature (Figure 5.20) so that isothermal oxidation had enough time to dilute the effects of the ramp and so that each curve could be compared fairly.

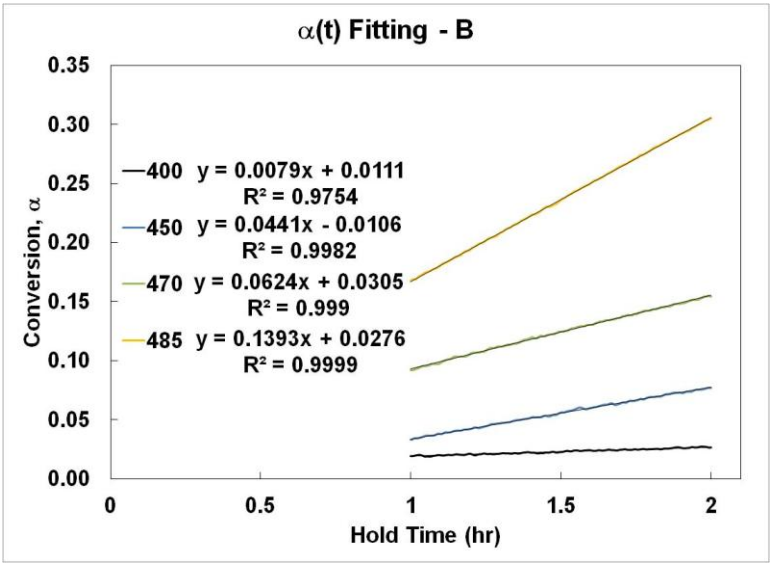

Figure 5.20. Linear fit of $\alpha(t)$ between one and two hours from reaching the hold time.

All curves had R^2 values of 0.998 or higher except for the sample at 400°C, which had an R^2 of 0.975. The linear fit equations were used as calculated (despite non-zero and even negative conversions at t=0) to fairly represent the real behavior. The position of the curve in time is critical to the final value of E, so changing the intercept to zero would give erroneous values. The isoconversion lines in Figure 5.21 found from these lines give an average activation energy of 161 ± 3 kJ/mol.

Despite the reduced scatter in the data, Figure 5.22 shows that there is still a trend between increasing conversion and decreasing activation energy. It is thought that this is attributable to the ramp effects but with a smaller absolute value compared to that in air due to the lower temperatures investigated (and thus less oxidation and shorter ramp times). Using Equation (5.10) and the method outlined above, an activation energy of 155 kJ/mol was determined from Figure 5.23. This value is significantly different from the value reported for boron in air (42 kJ/mol). This discrepancy will be discussed in more detail below.

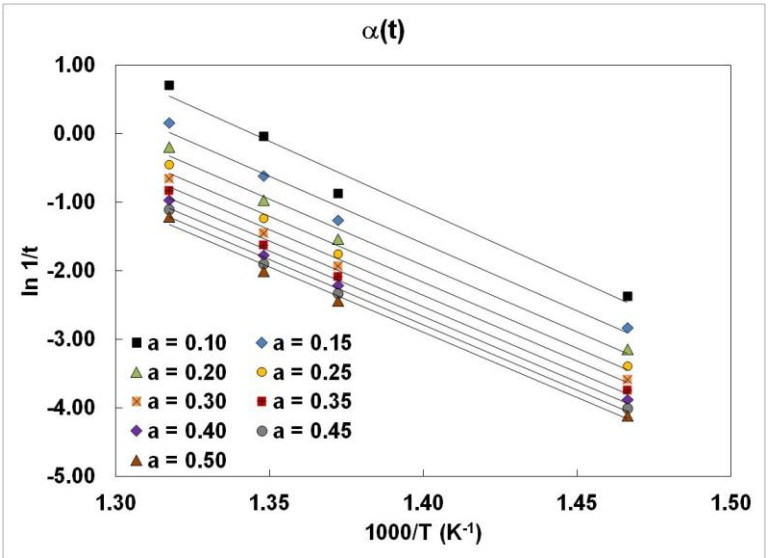

Figure 5.21. Isoconversion plot for boron in oxygen.

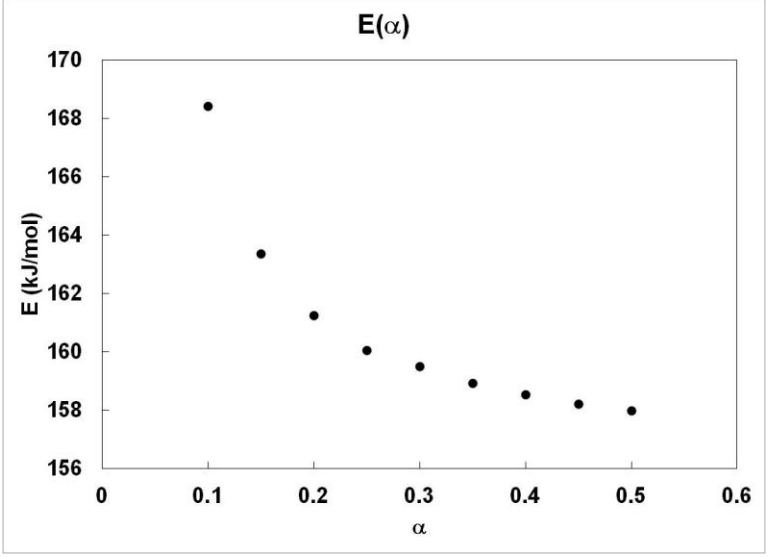

Figure 5.22. Activation energy as a function of conversion for boron in oxygen.

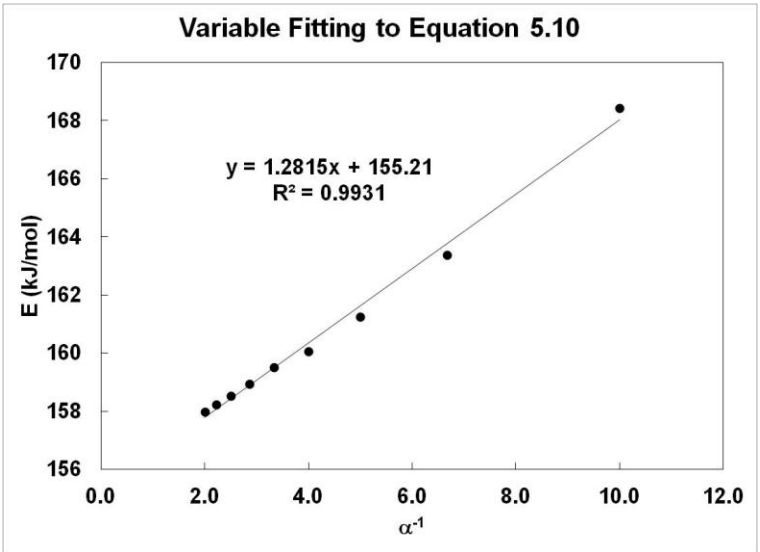

Figure 5.23. Determination of activation energy of boron through extrapolation

The $\alpha(t)$ for aluminum is shown in Figure 5.24. These curves are similar to those in air but with increased conversion at similar temperatures. This shift to higher conversions suggests that diffusion of oxygen through Al_2O_3 limited aluminum oxidation and that increasing the partial pressure of oxygen (and thereby increasing the diffusional flux through the oxide layer) allowed for increased reaction at a given temperature. The ceiling just below α=0.6 reflects a critical thickness of Al_2O_3 through which oxygen could not readily diffuse to the particle core. It is believed that a higher temperature would allow for a polymorphic transformation of the oxide layer to occur, allowing the rest of the particle to oxidize, as suggested in Chapter 3.

The isoconversion plot is shown in Figure 5.25 and the activation energy as a function of conversion in Figure 5.26. The activation energy tended to decrease with increasing conversion, but an interesting trend was observed. The activation energy appeared to remain constant up to a conversion of 0.25, at which point it began to

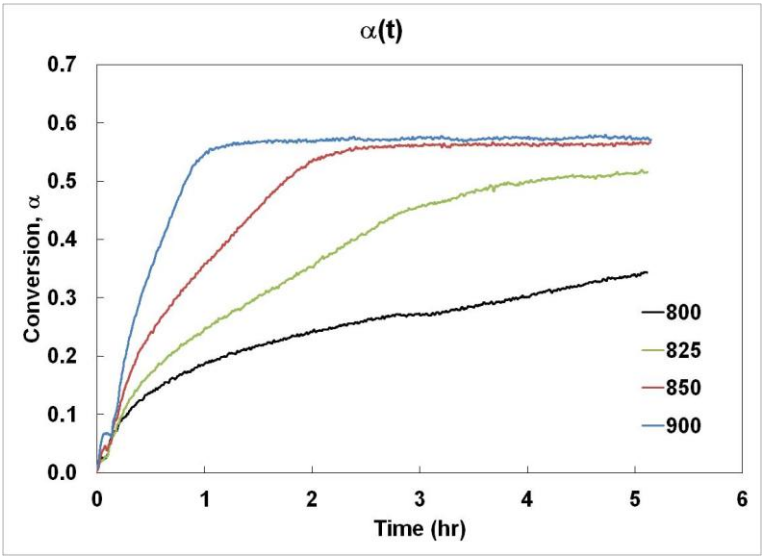

Figure 5.24. Conversion as a function of time for aluminum in oxygen.

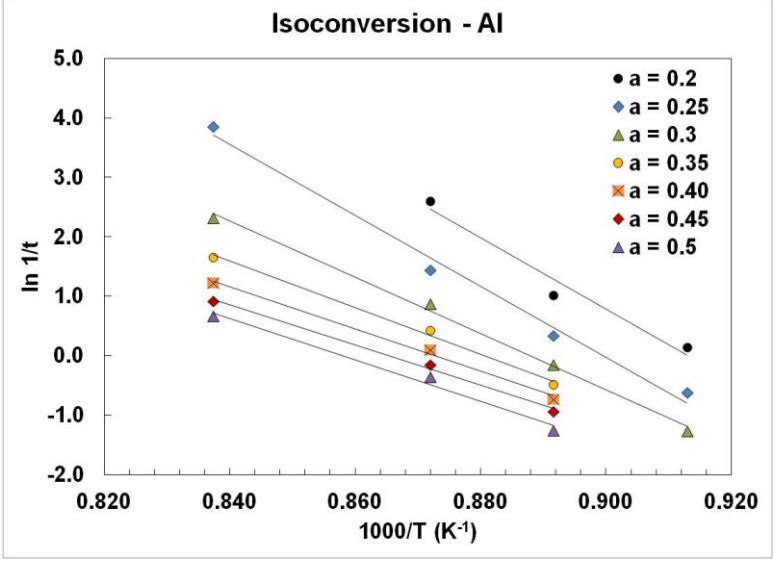

Figure 5.25. Isoconversion plot for aluminum in oxygen.

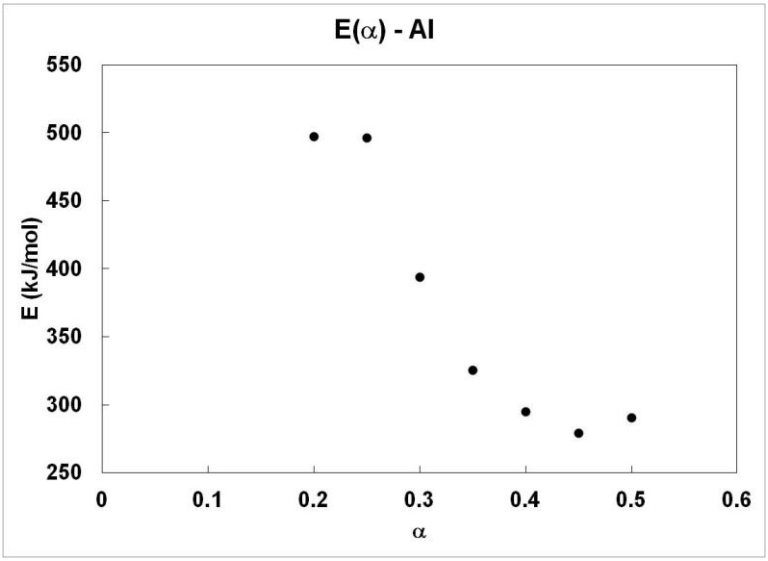

Figure 5.26. Activation energy as a function of conversion for aluminum in oxygen.

decrease with inverse proportionality to conversion, as it did in air. Although the decrease in activation energy in air was attributed to effects of the ramp, these data indicate that it is possible that there are, in fact, two competing processes contributing to the overall behavior. The first process was associated with oxidation of the surface of aluminum particles, giving a constant activation energy of 497 kJ/mol, while the second was controlled by diffusion through the oxide layer and approached 250 kJ/mol. The competition of these two processes at low conversions resulted in the decreasing trend in Figure 5.26 up to α=0.45. Above this point the oxide layer approached its average critical thickness (judging from Figure 5.24) and the activation energy appeared to increase.

Isothermal oxidation data for Al + 2B in oxygen were collected as well. The α(t) and isoconversion plots are given in Figure 5.27 and Figure 5.28. Figure 5.29 shows how the activation energy decreased almost linearly with conversion, similarly to AlB_2 in air. The low conversion points (α<0.35) seemed to be affected by the ramp, but the activation energy continued to decrease up to α=0.5. This behavior confirms that the borate

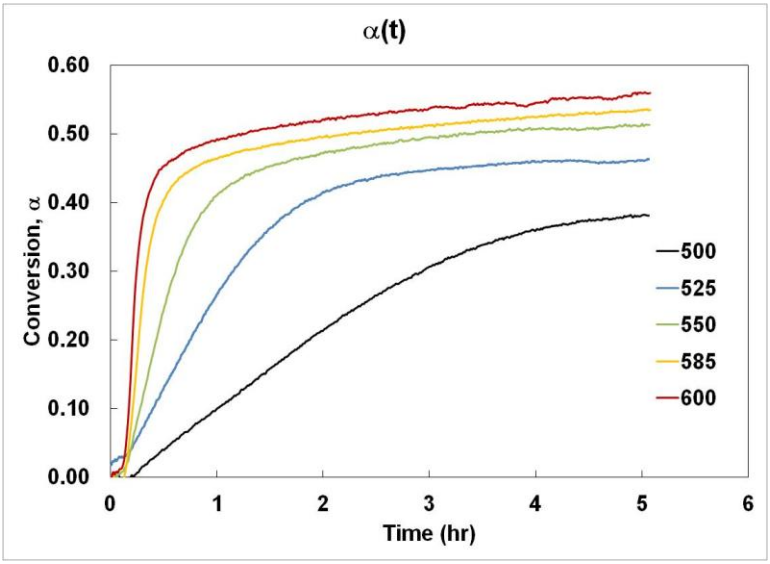

Figure 5.27. Conversion as a function of time for Al + 2B.

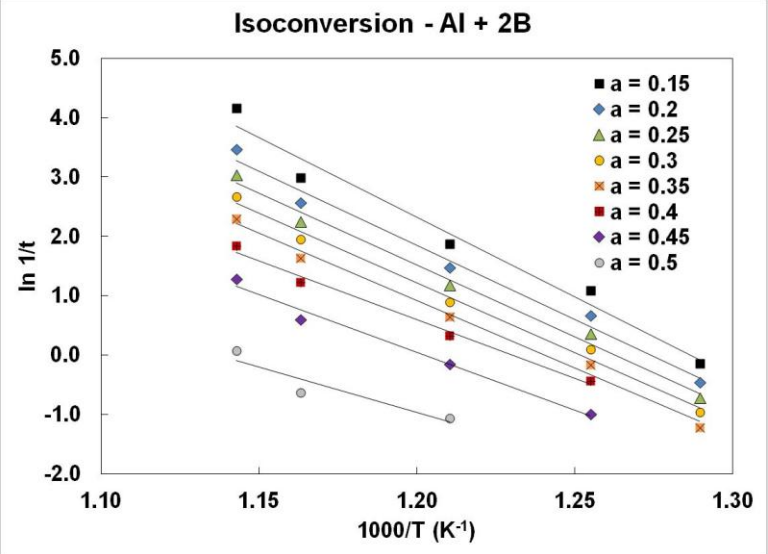

Figure 5.28. Isoconversion plot for Al + 2B.

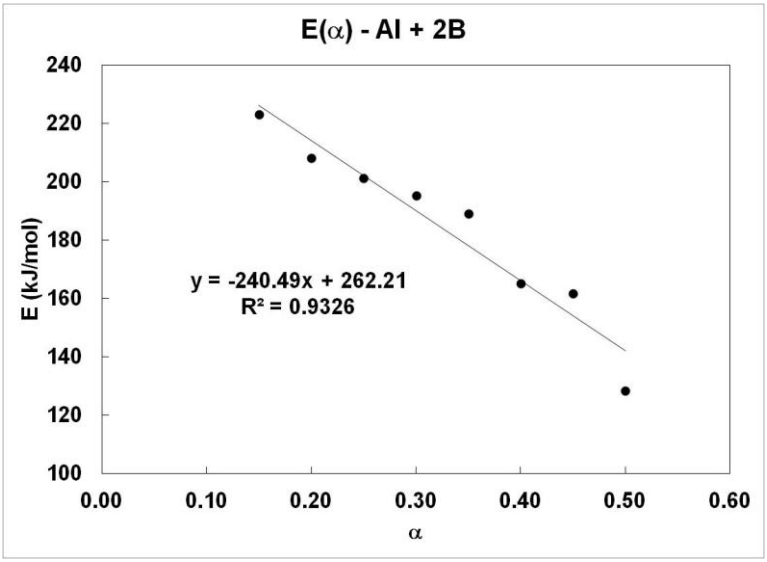

Figure 5.29. Activation energy as a function of conversion for Al + 2B.

formation mechanism is acting to reduce the activation energy as a function of conversion in Al + 2B. While this is promising for the energetic applications of Al + 2B, it prevented the calculation of an activation energy for this material. As a point of comparison to the other materials, it can be noted that the initial oxidation most likely had an activation energy greater than 180 kJ/mol.

The $\alpha(t)$ curves for AlB_2 in oxygen were somewhat similar to those in air but with higher conversions at slightly lower temperatures. The $\alpha(t)$ plot can be seen in Figure 5.30 and the isoconversion plot in Figure 5.31. Just as in air the line at a conversion of 0.15, and to some extent 0.2, are skewed because of the ramp. After this, the slopes level off and remain fairly well behaved. From the $E(\alpha)$ graph in Figure 5.32, the activation energy appeared to remain relatively constant up to α=0.5. Discarding the E_α at α=0.15 because the ramp effects were still significant, an average activation energy of 413 ± 20 kJ/mol was calculated. While there was scatter in the data, there did not appear to be a trend of decreasing activation energy with increasing conversion. This is the desired

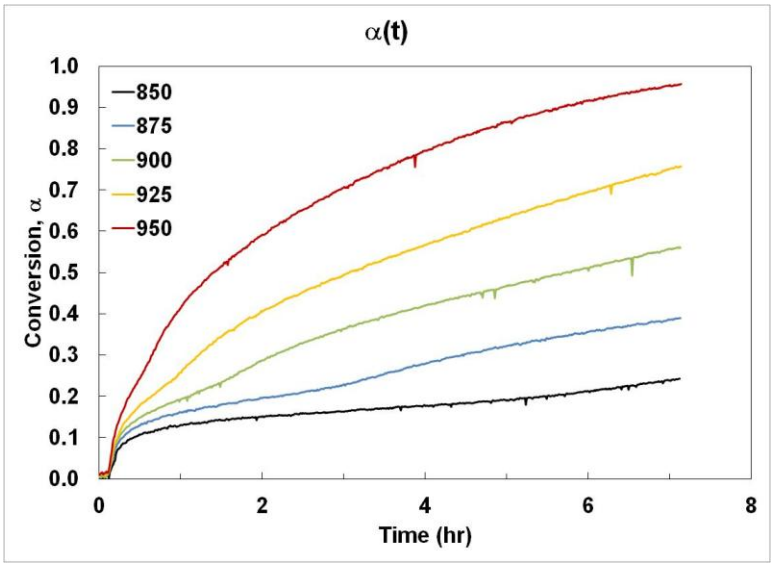

Figure 5.30. Conversion as a function of time for AlB_2 in oxygen.

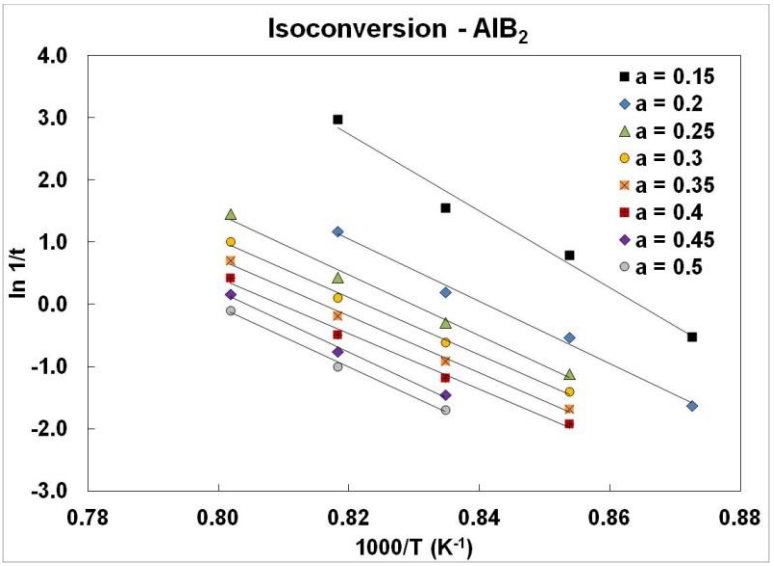

Figure 5.31. Isoconversion plot for AlB_2 in oxygen.

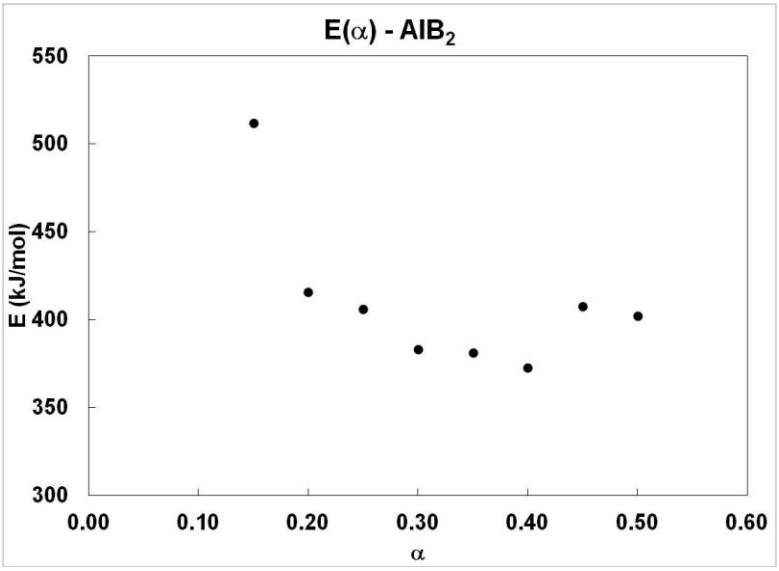

Figure 5.32. Activation energy as a function of conversion for AlB_2 in oxygen.

condition for determining the activation energy of a single process occurring over a large conversion range. Unfortunately, it is not clear if this behavior reflects the true activation energy for this process (rendering the analysis in air incorrect), if the mechanisms in air were different than those in oxygen (allowing both calculations to be correct but incomparable) or if there were other processes affecting the oxidation of AlB_2 in oxygen which gave the appearance of an invariant activation energy.

5.2 Discussion

Activation energies for aluminum and boron were found so that the accuracy of the model free method, when used for AlB_2, could be established. The values (or trends) calculated in this thesis are reported in Table 5.1. There are a number of activation energies reported in the literature for these materials as well. Values reported for the activation energy of oxidation of boron range from 34 kJ/mol to 205 kJ/mol.[4-9] The

Table 5.1

Activation Energy Summary

Material	Conversion Range, Air	E_{Air} (kJ/mol)	Conversion Range, O_2	E_{O_2} (kJ/mol)
B	0.15-0.40	42	0.10-0.50	155
Al	0.15-0.30	266	0.20-0.25, 0.30-0.50	497, ~250
Al+2B	0.20-0.65	~70	0.15-0.50	$-241\alpha+262$
AlB_2	0.15-0.50	$-778\alpha+576$	0.15-0.50	413 ± 20

experimental setups and analytical methods for these experiments vary greatly, but a nearly identical process to the one described in this thesis for the oxidation of boron in O_2 was used by Jain et al.[9] They tested two different samples of boron and found activation energies of 122 ± 7 kJ/mol for an electrodeposited boron of 96% purity and 4.2 m^2/g surface area and 205 ± 9 kJ/mol for a commercial boron powder (Aldrich Chemical Company, Inc., USA, 99% purity with a surface area of 3.8 m^2/g). These results validate the activation energy of 155 kJ/mol that was found for boron in oxygen. They also show that chemical purity, surface area and other factors can have a significant effect on the activation energy.

Talley[10] reported an activation energy of 50 kJ/mol for a boron powder of unknown composition or surface area oxidized in air. This is comparable to the 42 kJ/mol calculated in this thesis. Unfortunately the wide range of testing methods and various boron powders used in the literature result in a wide range of activation energies. Nevertheless, it is reasonable to assume that the values calculated for boron using the model free method are accurate. If this is true, and both activation energies for boron are reasonable, the analysis must be adjusted to mathematically account for the changing pressure of oxygen. Equation (5.3) can be more accurately rewritten as[17]

$$\frac{d\alpha}{dt} = k(T) f_1(\alpha) f_2(p_{O_2}) \quad (5.\ 12)$$

where $f_2(Po_2)$ is a function describing how conversion changes with changing Po_2. This function is generally experimentally determined from a series of isoconversional curves at different oxygen pressures, but such a study was not conducted for this thesis. It would be of interest to determine the $f_2(Po_2)$ for all the materials investigated in future work. Such a function would account for the increased oxygen gradient across an oxide layer, increased diffusion flux, morphology changes resulting from particle heating and other related phenomena. Suffice it to say that the conversion function can change dramatically depending on f_2 and this is the likely cause of the large difference in activation energies between air and oxygen.

The activation energy for aluminum oxidation has also been described in the literature. Values for the activation energy have been found to vary greatly between samples of different particle sizes[11] and even for nominally flat samples.[12] Nano aluminum, on the order of 10 nm, was found to have an activation energy as low as 24.6 kJ/mol, but that value increased to 56.9 kJ/mol for particles 50-100 nm and 174.6 kJ/mol for 100-150 nm aluminum[11]. Bulk samples of aluminum have been measured to have an activation energy of 189 kJ/mol.[12]

There have been a wide range of papers published on the phase transformation behavior of aluminum as it oxidizes.[2, 14 -15] Nanoparticles with a small enough diameter are controlled largely through surface reactions and have different oxidation behavior than larger particles. As the average diameter approaches 100 nm, particle behavior becomes similar to micron sized particles. The oxidation of aluminum is controlled by a

series of phase transformations[13] that start with the conversion of an amorphous oxide layer to γ-Al_2O_3 crystallites, followed by melting of the aluminum core, and finally the transformation of γ-Al_2O_3 to α-Al_2O_3 (and associated volume change). All these processes can occur in the low conversion range for micron sized particles and reported activation energies may account for some, or all, of these.

Aluminum with a particle size very similar to that investigated here (3-4.5 μm) was found to have activation energies between 291 ± 95 and 345 ± 54 in a linear heating rate study.[16] It was expected that the aluminum in this study would have an activation energy close to 300 kJ/mol based on the literature, and the calculated values of 266 kJ/mol in air and >250 kJ/mol in oxygen are comparable to the expectation. The lack of sufficient data for the oxidation of aluminum in air may have led to an underestimation of the activation energy, but it is sufficiently close to literature values to lend credibility to values calculated for Al+2B and AlB_2.

The activation energy of Al + 2B in air was not constant between conversions of 0.20-0.65, but approached a minimum around 70 kJ/mol before increasing at higher conversions. This activation energy is less than what would be expected if the two powders were oxidizing independently, reinforcing the significance of the borate formation mechanism. In oxygen, the activation energy decreased linearly with increasing conversion. It had an initial value that was above 180 kJ/mol.

AlB_2 had an activation energy that decreased linearly with time in air and approached a constant value in oxygen. The initial activation energy in air was greater than 250 kJ/mol, while the average value in oxygen was 413 ± 20 kJ/mol. These values

were the highest of the four powders in each atmosphere, reflecting the significant temperature dependence of the oxidation of AlB_2.

Activation energies in air and O_2 were not comparable. Different temperature ranges were used in the two cases because the extents of reaction (and oxidation occurring on the ramp) were much different in the two environments. The main reason for the discrepancy between the two atmospheres is probably due to effects captured in Equation (5.5), where the conversion is dependent on the partial pressure of O_2. As discussed above, the f_2 function can incorporate a number of factors that change as the system is exposed to different pressures of oxygen. This can be well understood for boron, where the diffusion of oxygen through B_2O_3 is a limiting factor in the oxidation process. A higher Po_2 increased the concentration gradient across the B_2O_3 and therefore the driving force for diffusion, speeding up the reaction and allowing it to proceed to higher conversions at a given temperature. Aluminum had a similar activation energy in both atmospheres. The pressure of oxygen has less of an effect on oxygen diffusivity in Al_2O_3 compared to B_2O_3,[2] which explains why the effect is much more exaggerated in the boron-oxygen system.

Despite the lack of correlation between oxidation in air and oxygen, this study produced a number of significant results. The activation energy for AlB_2 in air and oxygen has been reported for the first time. In both cases it was generally higher than that of aluminum, boron, or Al + 2B, which corresponded to higher initiation temperatures and increased oxidation at higher temperatures. This reflects the insensitivity of AlB_2, and suggests that it is a safer powder to handle. While comparing activation energies for materials of similar initiation temperatures is one way to evaluate static oxidation tests,

the activation energy may or may not correlate to its actual performance in an energetic system. The oxidation behavior of all four powders was shown to have a dependence on the partial pressure of oxygen, a result that is directly applicable to heterogeneous combustion systems like ramjet motors, where particles are injected into a hot, gaseous oxidizing environment. Finally, the effect of the borate formation mechanism on Al + 2B and AlB_2 was observed and quantified in the isothermal case.

5.3 References

1. P. Simon, "Isoconversional Methods, Fundimentals, Meaning and Application," *J. Therm. Anal. Calorim.* **76** 123-132 (2004)

2. T. A. Mikhalvo, M. Schoenitz, X. Zhu, and L. Driezin "Effect of Polymorphic Phase Transitions in Al_2O_3 Film on Oxidation Kinetics of Aluminum Powders," *Combust and Flame* **140**[4] 310-318 (2005)

3. H. Eyring "The Activated Complex and the Absolute Rate of Chemical Reactions," *Chem. Rev* **17[**1], 65–77, 1935

4. N. D Kostuchenko, J. I. Vovchuk and S. A. Kiro "Oxidation of Boron in Air," *Combustion of Boron-Based Solid Propellants and Solid Fuels* 205-210

5. V. G. Shevchuk, D. I. Polischuk, A. N. Solotko, J. I. Vovchuk and V. B. Osipov, "Experimental Defining Oxygen Diffusive Coefficient in the Liquid Boron Oxide," *Physics of Aerodispersive Systems,* **10**, 69 (1974)

6. D. Z. Safaneev, L. J. Kashporov and Y. M. Grigoryev, "Heat Liberation Kinetics in Boron-Oxygen Interaction," *Combustion, Explosion and Shockwaves* **2**, 210-214, (1981)

7. M. K. King, "Boron Ignition and Combustion in Air Augmented Rocket Afterburners," *Combustion Science and Technology* **4**, 155-164, (1972)

8. A. I. Girgoryev and D. I. Polishchuk, "Determination of the Coefficient of the Oxygen Diffusion in Boron Anyhdride and its Dependence on Temperature," *Physics of Aerodispersive Systems* **8**, 73 (1973)

9. A. Jain, K. Josepha, S. Anthonysamya and G. S. Guptab, "Kinetics of Oxidation of Boron Powder," *Thermochimica Acta* **514** 67–73, (2011)

10. C. P. Talley, Aero Space Eng. **18[**6] 37–41 (1959)

11. K. Park, D. Lee, A. Rai, D. Mukherjee and M. R. Zachariah, "Size-Resolved Kinetic Measurements of Aluminum Nanoparticle Oxidation with SingleParticle Mass Spectrometry," *J. Phys. Chem. B* **109**, 7290-7299 (2005)

12. J. A. Aumann, C. E., Skofronick, G. L., Martin, *J. Vac. Sci. Technol. B* **13[**3], 1178 (1995)

13. N. Eisenreich, H. Fietzek, M. del Mar Juez-Lorenzo, V. Kolarik, A. Koleczko, and V. Weiser "On the Mechanism of Low Temperature Oxidation for Aluminum Particles down to the Nano-Scale," *Propellants, Explosives, Pyrotechnics* **29**[3] 137-145 (2004)

14. Y.-S. Kwon, A. A. Gromov, A. P. Ilyin, E. M. Popenko, and G.-H. Rim, "The Mechanism of Combustion of Superfine Aluminum Powders," *Combust. and Flame* **133** 385-391 (2003)

15. A. Hahma, A. Gany and K. Palovuori, "Combustion of Activated Aluminum," *Combustion and Flame* **145** 464–480 (2006)

16. M. Schoenitz, B. Patel, O. Agboh and E. L. Dreizin, "Oxidation of Aluminum Powders at High Heating Rates," *Thermochimica Acta* **507–508** 115–12, (2010)

17. H. Y. Sohn and S. Emami, "Kinetics of Dehydrogenation of the Mg-Ti-H Hydrogen Storage System," *Int. J. Hydrogen Energy*, **36** 8344-8350 (2011)

6. MOISTURE SENSITIVITY

AlB_2 was hypothesized to have lower sensitivity to water than conventional metal fuel additives due to the formation of more favorable aluminum and boron chemical bonds. AlB_2 was compared to boron, aluminum, and Al + 2B. Aluminum has a known sensitivity to hydration and requires passivation to prevent hydrolysis. Removal of free aluminum from AlB_2 by an acid wash was expected to improve resistance to degradation. An electroless tin coating was applied to AlB_2 in order to limit oxidation. Silane coatings were applied to make the materials hydrophobic, even though these coatings are permeable to water vapor. Muller et al.[1] suggested that amines offer better protection from moisture absorption for nanoscaled TiN than organic polymers containing oxygen, so a commercially available amine coating was also investigated. The purpose of this study was to find ways to protect AlB_2, if not already moisture resistant, under ordinary storage conditions.

6.1 Experimental Procedures

Samples of AlB_2 powder were treated with six different surface modifications. These included silane, fluorosilane, amine, and tin coatings, as well as an acid treatment to remove the free aluminum. The different surface treatments were given a code, as shown in Table 6.1. The silane treatments were made by making a solution of 95 vol. % methanol-5 vol. % distilled water, adjusting the pH to 4.5-5.5 with acetic acid, adding 35

Table 6.1

AlB_2 Surface Treatments

Treatment	Code	Approach
Silane	S	n-octadecyltrimethoxysilane[a]
Fluorosilane	FS	Tridecafluoro-1,1,2,2-tetrahydrooctyl triethoxysilane[b]
Amine	A	Octadecylamine[c]
Silane (Shin-Etsu)	SE	3,3,3 Trifluoropropyl trimethoxysilane[d]
Tin Coating	Sn	Electroless Sn solution[e]
HCl Wash	HCl	HCl washed, water/acetone rinsed. and dried at 110°C

a. Gelest SI06645.
b. Gelest SI TB175.0
c. Aldrich 305391.
d. Shin Etsu KBM-7103
e. Liquid Tin (MG Chemicals No. 421).

grams of AlB_2 powder to 100 cc of solution while stirring, and adding 2 grams of the silane solution while stirring. The powders were stirred for 30 minutes at 500 rpm, filtered, washed with methanol, washed with acetone, and dried at 110°C for 15 minutes. The amine solution was made by adding 2.15 grams of octadecylamine (Aldrich 305391) to 500 cc of hexane and heating to get into solution. The AlB_2 powder (35 grams) was stirred for two hours and then filtered, rinsed with hexane, and dried at 110°C for 15 minutes.

An electroless tin was applied to 35 grams of AlB_2 powder by adding the powder, while stirring, to 475 ml of the tin solution. The powder was then washed with water, acetone, and dried at 110°C for 15 minutes.

The acid wash was accomplished by adding 50 grams of AlB_2 powder to 700 ml of water and slowly adding dilute HCl to the powder until the reaction stopped. The solution was filtered, rinsed with water and acetone, and dried at 110°C overnight. The powder stuck to the filter paper. The powder was pulverized in a mortar and pestle and

screened -325 mesh to remove the filter paper. However, some of the filter paper remained in this powder.

Salt solutions were made for different relative humidities.[2] A relative humidity chamber at ≈10% was made by adding KOH (Alfa Aesar 13451) to deionized water to form a saturated solution in the bottom of a bell jar. Relative humidity chambers at 75% and 90% were prepared using NaCl (Sigma Aldrich S9886) and KNO_3 (Spectrum P1345), respectively. The bell jars were equilibrated at temperature inside convection ovens (Yamato DKN 400). Powders were weighed (Shimadzu AUW 2200) before starting the tests and at periodic intervals during the test. X-ray diffraction and scanning electron microscopy were used to characterize powders.

Tests at 100 % relative humidity were made inside a constant temperature water bath (Polyscience model 2L) by placing approximately one gram of powder in a test tube filled with 15 cc of deionized water and heating at 80°C for 135 hours. The powders were dried for 24 hours, crushed, and x-rayed.

6.2 Results and Discussion

Figure 6.1 through Figure 6.4 show results from the first set of tests which did not include B, Al, or Al-B mixtures. These tests, conducted over the course of a month show that octadecylamine and silane (n-octadecyltrimethoxysilane[a]) coatings provided significant protection compared to the uncoated control powder, even at high humidity levels. It is very clear, however, that storage of powders in low-temperature, low-humidity environments will allow AlB_2 to avoid oxidation.

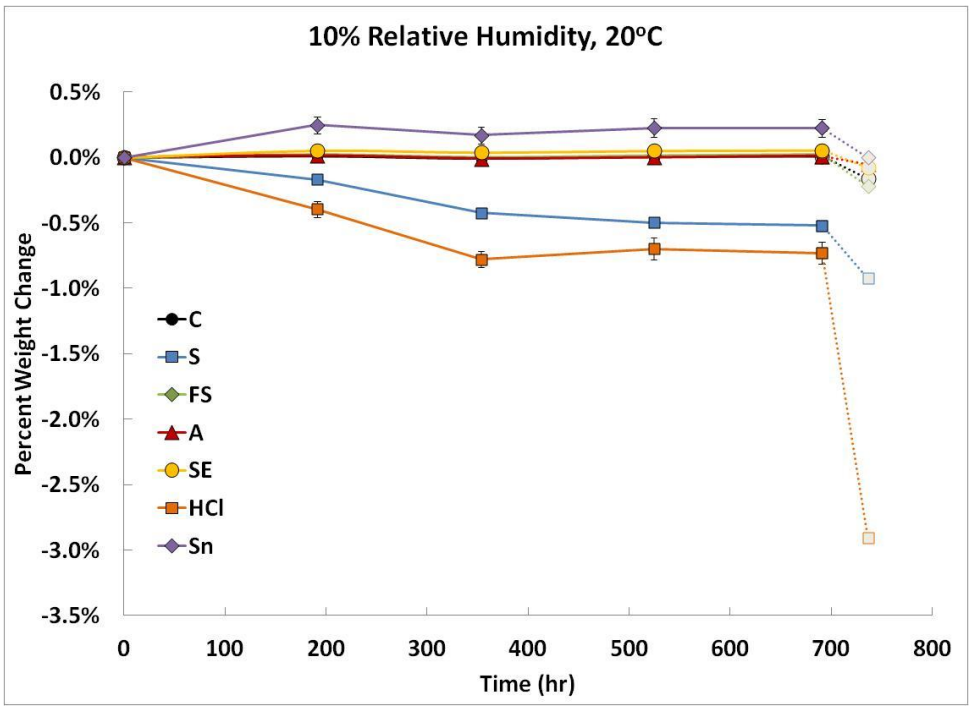

Figure 6.1. Weight change of AlB_2 (C) and treated samples in 10% relative humidity environment at room temperature. Last data point shows mass after drying at 110°C overnight.

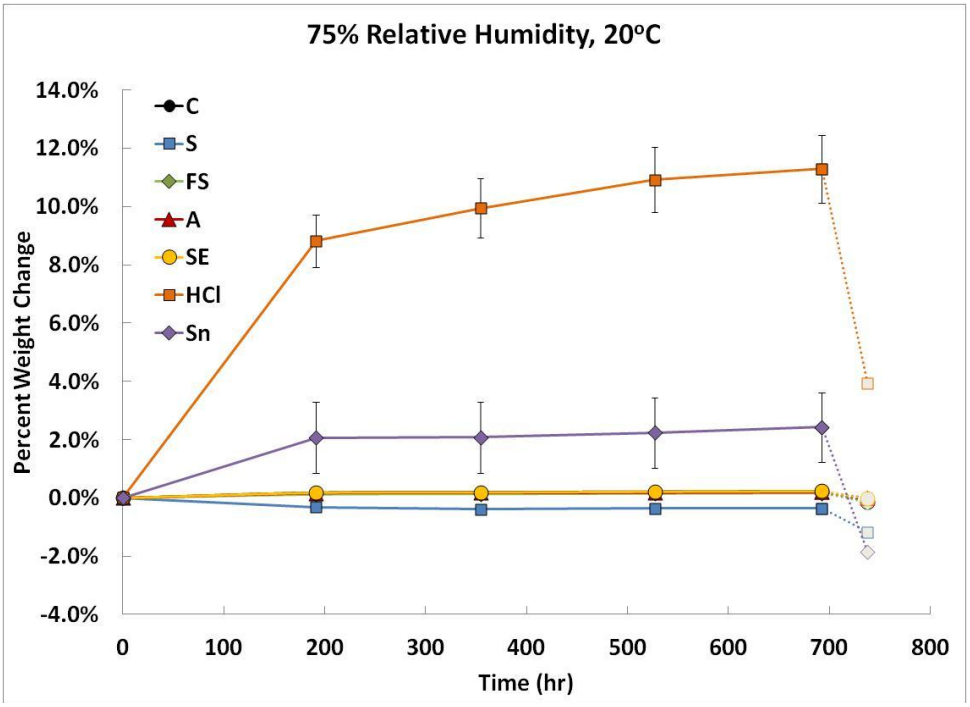

Figure 6.2. Weight change of AlB_2 samples in 75% relative humidity environment at room temperature. The larger standard deviations in the HCl and Sn samples are due to powder that was lost during weighing.

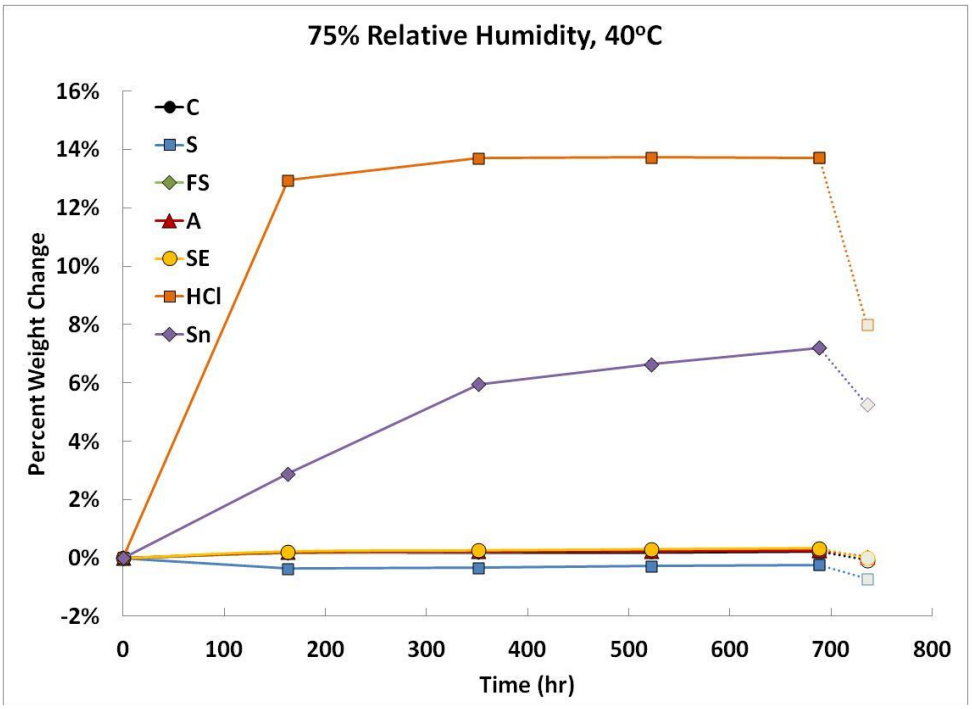

Figure 6.3. Weight change of AlB_2 samples in 75% relative humidity environment at 40°C.

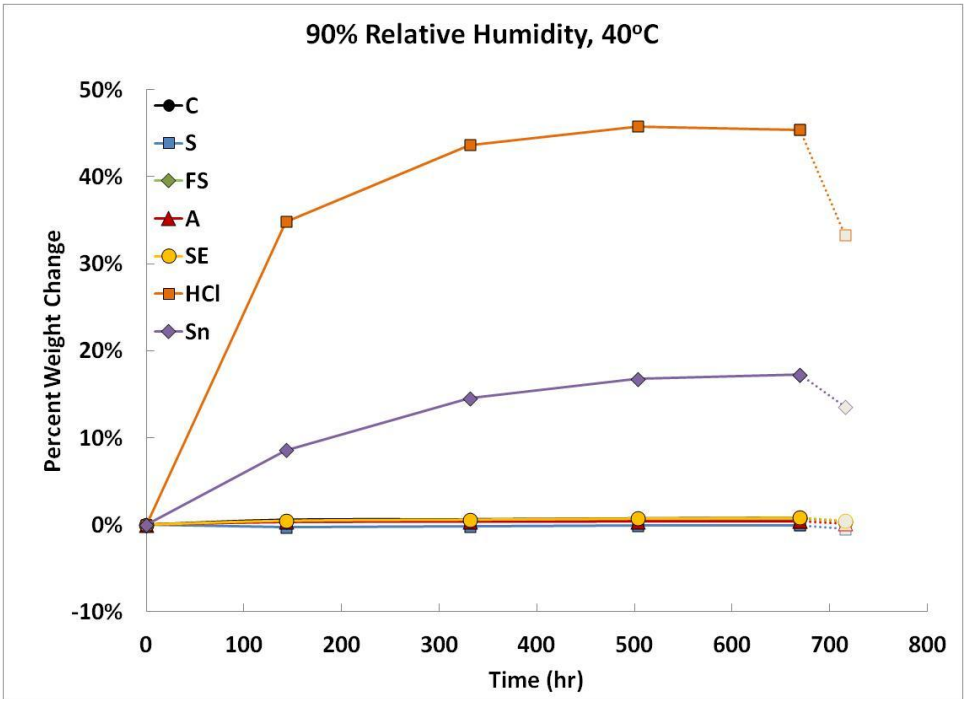

Figure 6.4. Weight change of AlB_2 samples in 90% relative humidity environment at 40°C.

Two of the treatments (HCl wash and Sn coating) were much worse than the control. While XRD showed that tin was present after the electroless deposition, SEM images (Figure 6.5) showed that the Sn did not coat the particles evenly, but was poorly distributed and agglomerated. These results do not preclude that a well-deposited (uniform and dense) electroless coating could provide protection. The rapid oxidation of the HCl washed powder was surprising and may be the result of chlorine remaining after the treatment, as evidenced by EDS. The removal of Al by an HCl wash is tedious and resulted in poor yields, so further testing concentrated on the silane or amine-coated materials.

Based on Figure 6.6 through Figure 6.12 it appeared that the n-octadecyltrimethoxysilane (S), due to its low moisture pick-up, or the octadecylamine (A), due to its low slope after initial exposure to moisture, were the most promising coatings. SEM evaluation could not detect the coatings, in accord with expectation that the coatings were very thin. It should be noted that an X-ray scan of the control sample after exposure to 90% relative humidity for 4 weeks at 40°C showed that the material was unchanged (see Figure 6.4). This suggests that simply storing the powder in closed, well-packaged containers will result in adequate lifetimes for AlB_2 powder.

Accelerated tests for the top candidate materials in comparison to B, Al, and Al-B mixtures are shown in Figure 6.13 and Figure 6.14. All powders were dried at 110°C for 24 hours prior to taking initial weights. The weight gain for Al is consistent with $Al(OH)_3$ formation, which was confirmed by X-ray diffraction. The AlB_2 powder was much more resistant to degradation than fine aluminum powder, in accord with expectation. At 60°C and 75 % relative humidity, the silane (S) coating provided the best

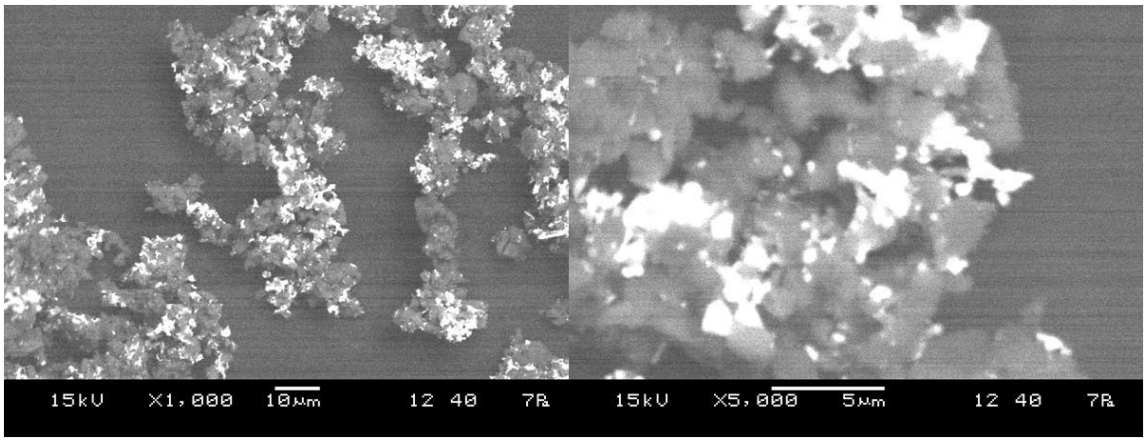

Figure 6.5. SEM image of electroless tin coated AlB_2 powder. Light regions are tin, which was clearly not covering the entire AlB_2 surface.

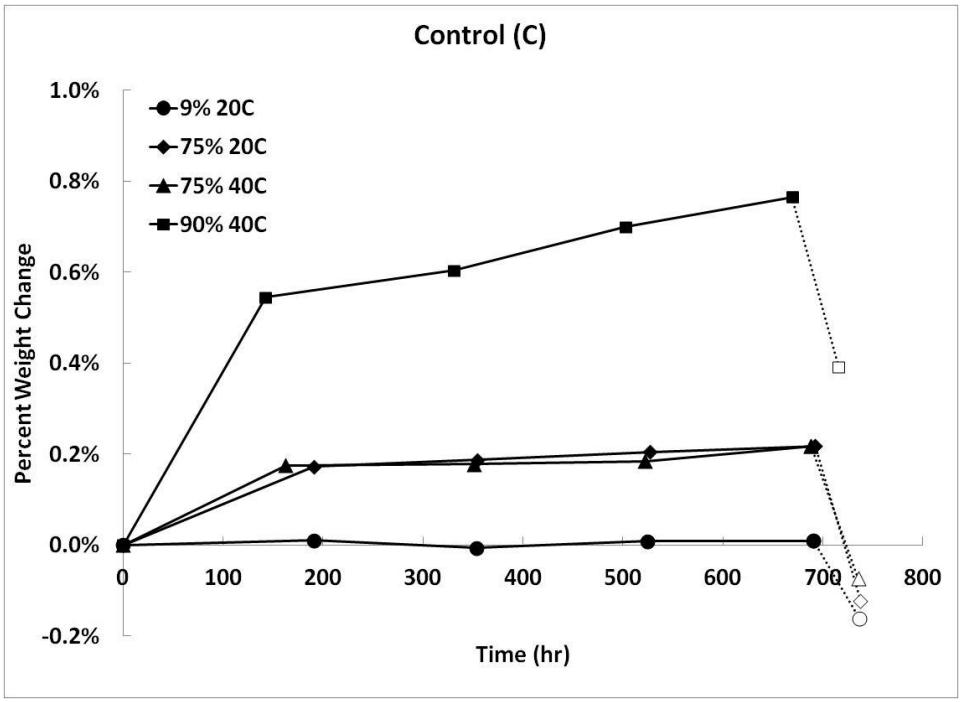

Figure 6.6.Summary of data for the control sample (C). Weight gain in this sample does not appear to be temperature dependent at 75% relative humidity.

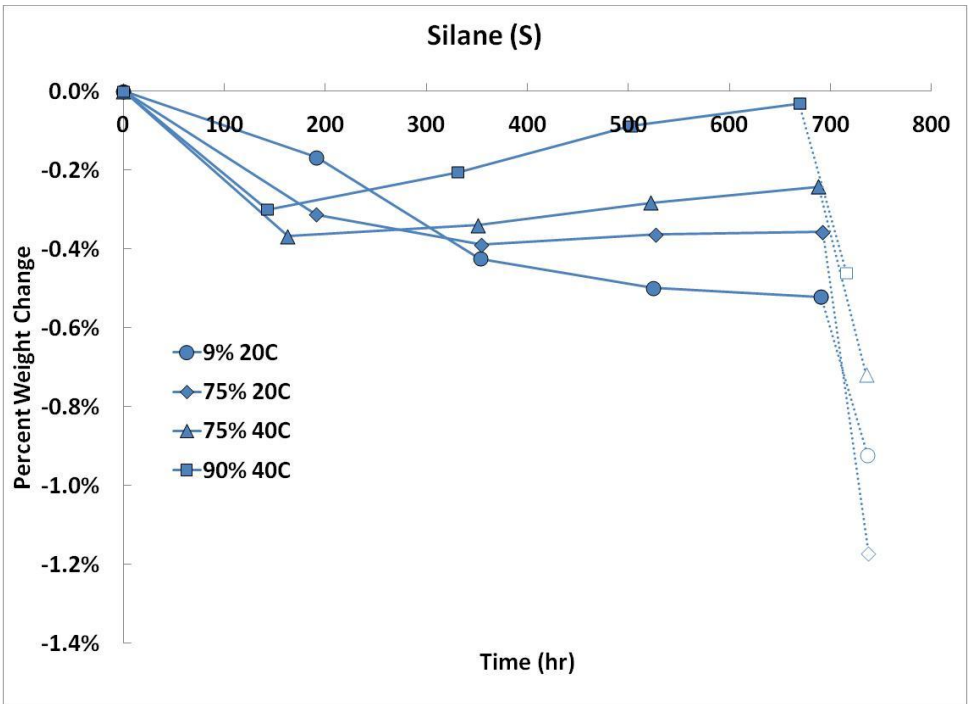

Figure 6.7. Summary of data for the silane coated sample (S). Samples under all conditions lost weight initially, suggesting that there was still moisture associated with powder initially.

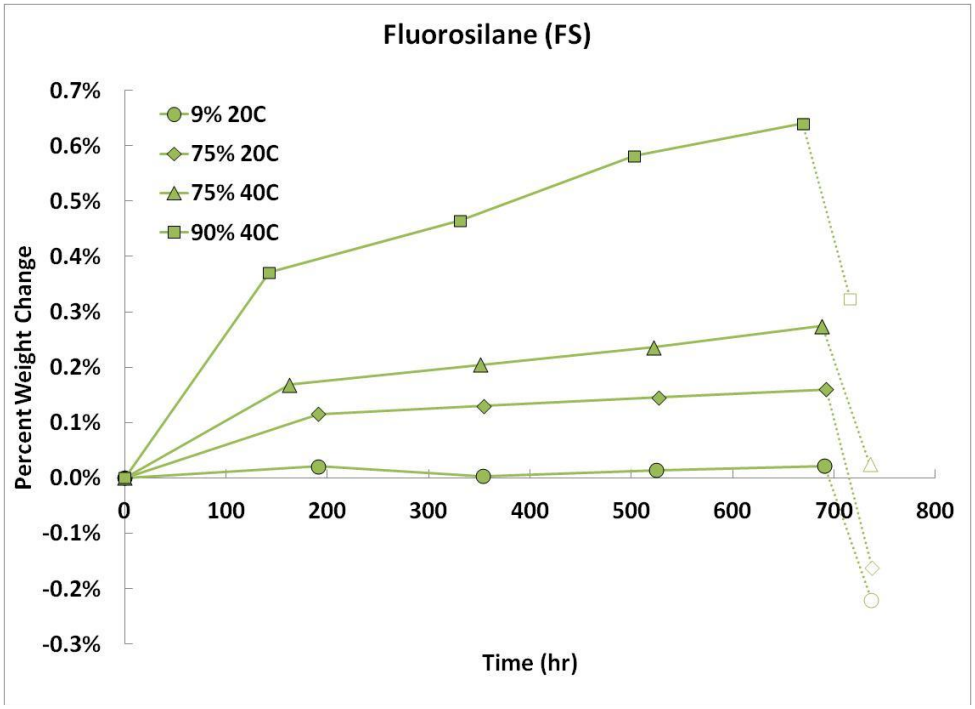

Figure 6.8. Summary of data for the fluorosilane coated sample (FS). This sample was similar to the control sample, but with a slight temperature dependence for weight gain at 75% relative humidity.

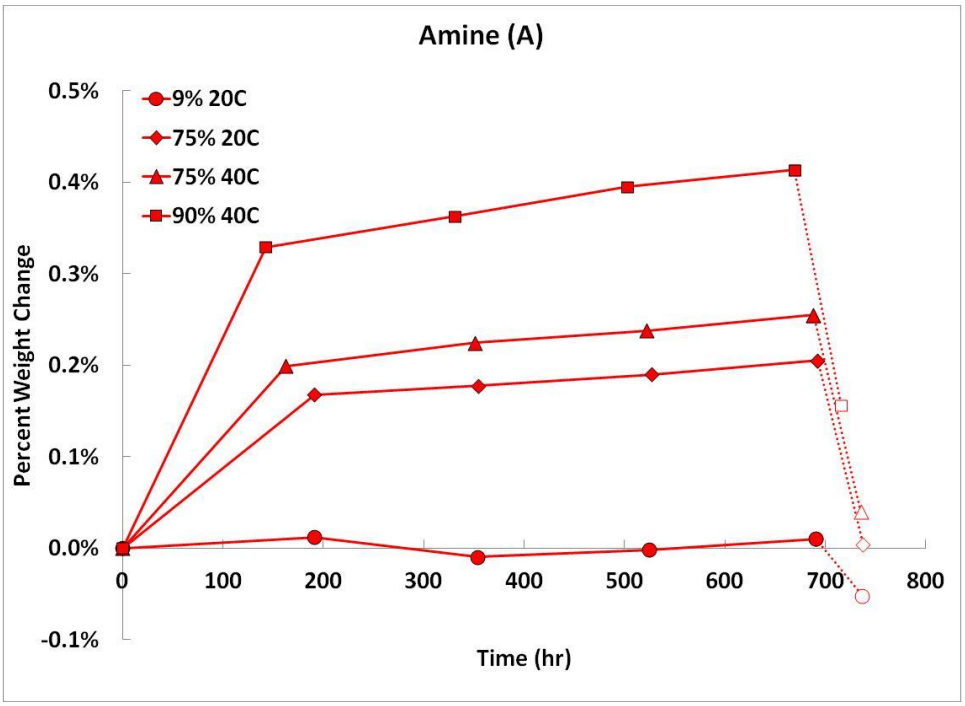

Figure 6.9. Summary of data for the amine coated sample (A). This sample had the lowest weight gain (besides the silane coated sample that lost weight) under all conditions.

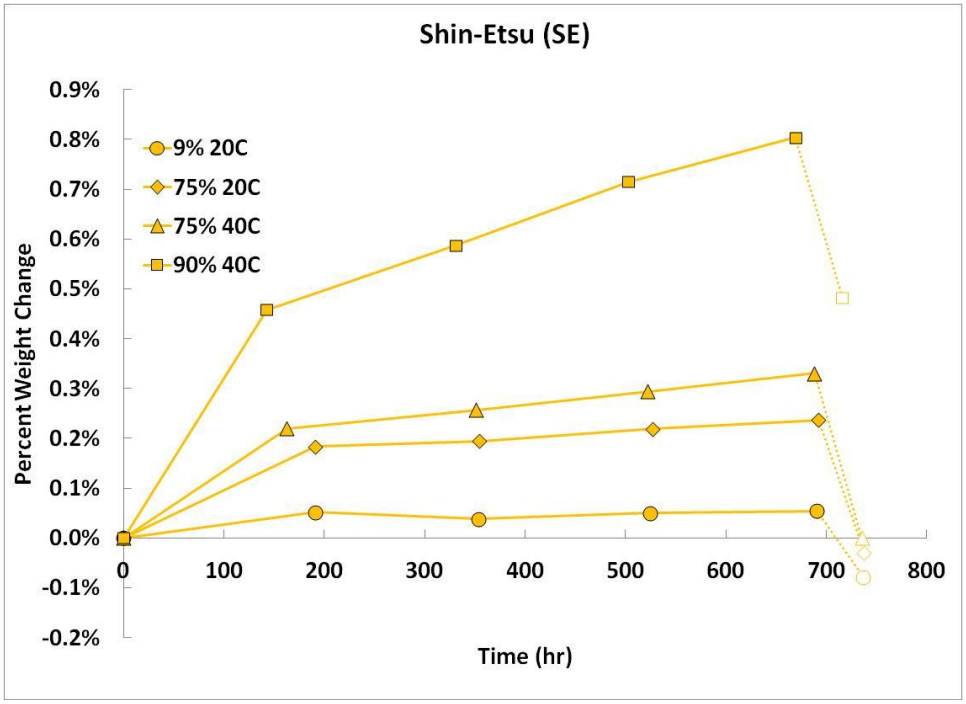

Figure 6.10. Summary of data for the Shin-Etsu silane coated sample (SE). This sample behaved similarly to the fluorosilane coated sample, but gained slightly more weight under all conditions.

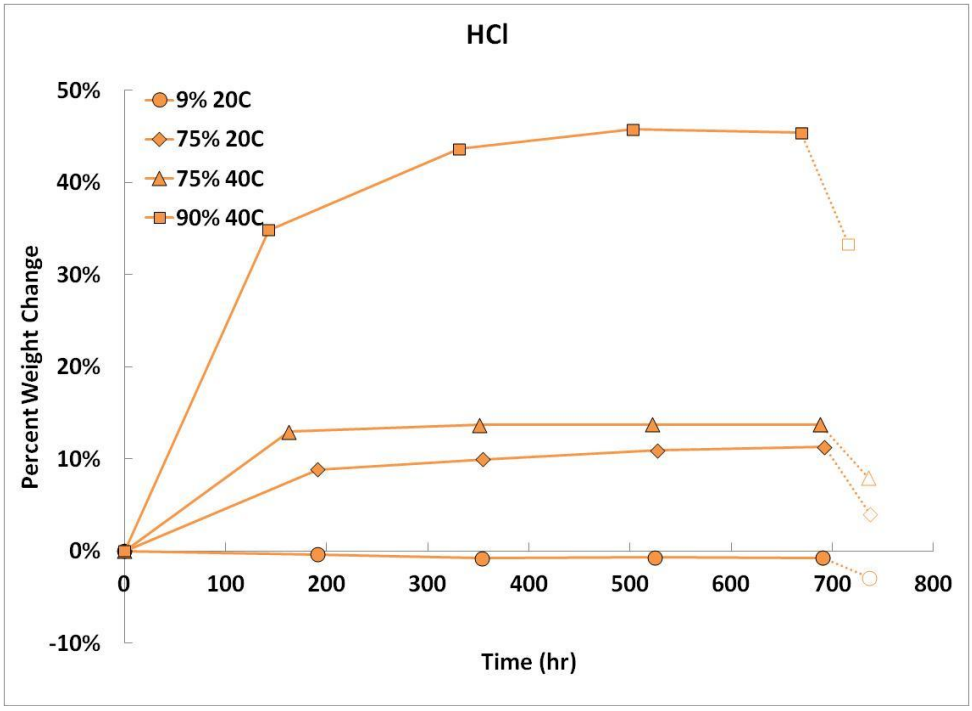

Figure 6.11. Summary of data for the HCl washed sample (HCl). This sample gained the most weight of any sample under all conditions. Though XRD showed the presence of some cellulose from the filter paper used to wash this sample in acid, the weight upon drying suggests that the weight gain was due to more than absorption by cellulose.

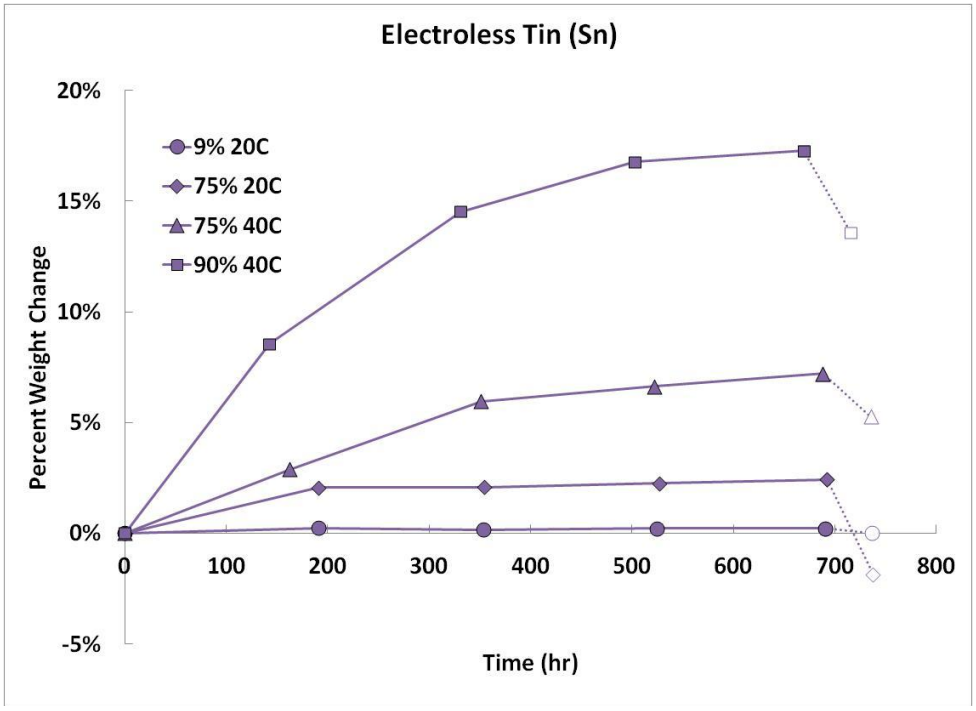

Figure 6.12. Summary of data for the electroless tin treated sample (Sn).

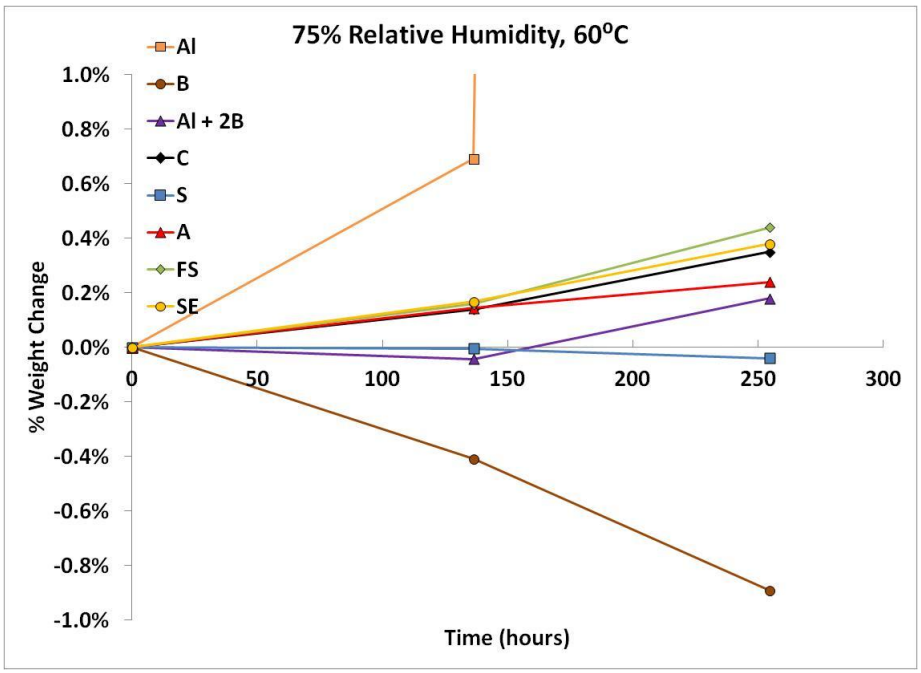

Figure 6.13. Summary of testing of the top performing coatings (S, A, FS, SE) and the starting powders for AlB_2 (Al, B, Al + 2B) versus the control (C). Aluminum (orange) reached 66% mass gain, over two orders of magnitude more than any other.

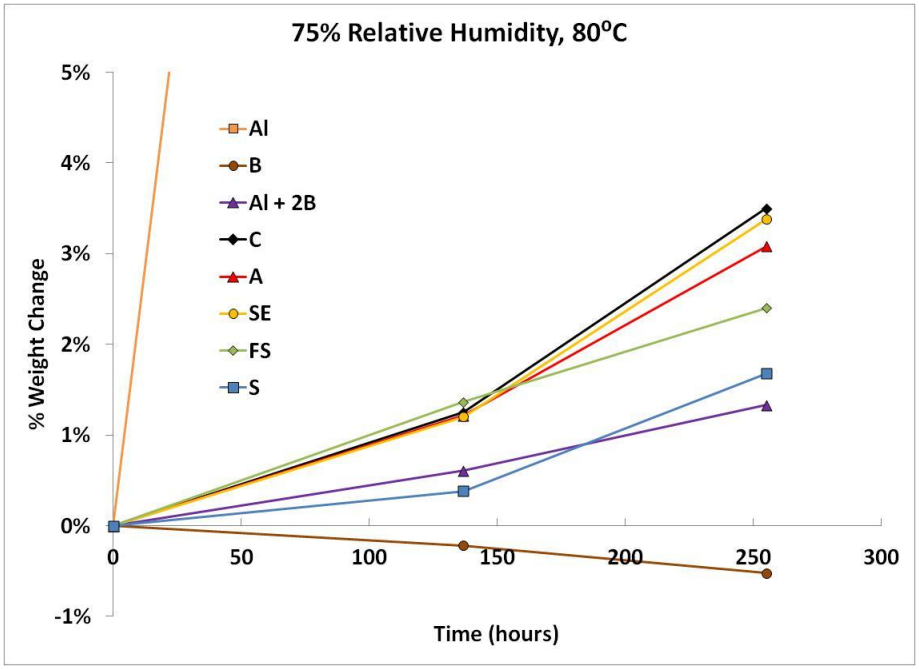

Figure 6.14. Summary of testing at 75% relative humidity and 80°C. Aluminum (orange) reached 71% weight gain. Boron continues to lose weight due to the formation of highly volatile boric acid.

protection with the amine (A) coating a distant second. The boron lost weight, presumably due to the formation of boric acid, which is soluble in water and has a high vapor pressure. What was surprising, however, was the excellent performance of the Al + 2B powder, which did not follow Vegard's law (rule of mixtures) with regard to aluminum oxidation. It is suspected that the milling step provided additional passivation of Al, indicating that Al/B mixtures are insensitive to moisture degradation and should continue to be compared to their boride counterparts.

Increased temperature accelerated the aluminum hydration and caused all coatings to show weight gain (Figure 6.14). It is very apparent that none of these coatings were impervious to moisture absorption, which was activated by temperature. Short-term exposure to boiling water caused no problem for the aluminum boride powder, but longer (135 hour) exposure to in water at 80°C caused severe degradation for all materials. The Al powder turned white due to hydroxide formation and gained 162% of its initial mass. The control powder agglomerated, turned gray, was primarily amorphous (bottom scan in Figure 6.15), and gained 130% of its initial mass. The silane (S) coated powder also turned gray, did not coarsen, and still showed some crystallinity but gained 109% of its initial mass. Thus it is apparent that high humidity combined with high temperature is detrimental to silane-coated powders. The fluorosilane fared slightly better, gaining 73% of its initial mass.

One of the main advantages of forming the borides is seen by examining the Al+2B powder, which looked identical in color after the same exposure treatment. However, XRD (Figure 6.16) clearly showed that the Al hydrolyzed to $Al(OH)_3$, which is not apparent in the AlB_2 samples. The weight gain for this material was 79 %, but clearly

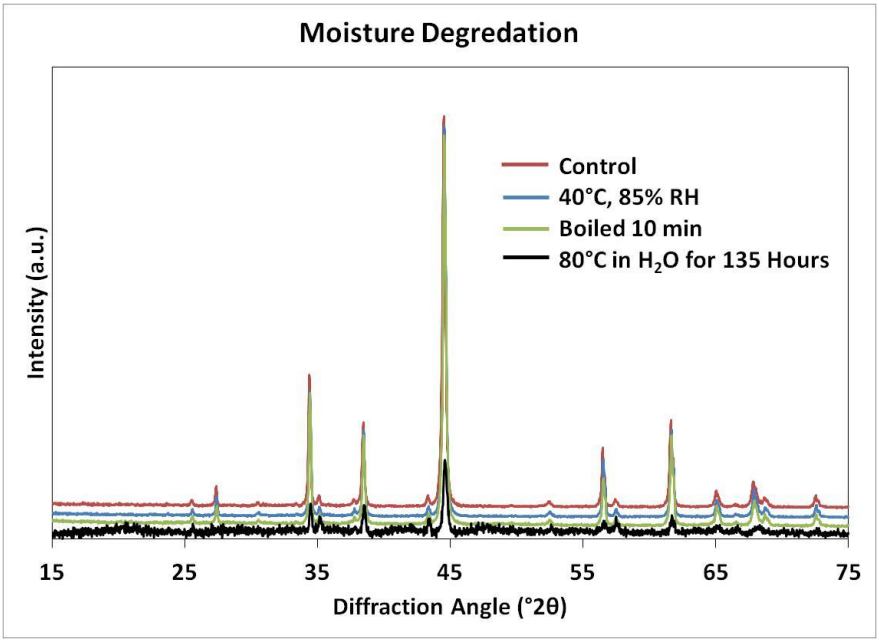

Figure 6.15. X-ray diffraction scans of control powder (red) exposed to water at 40°C (blue), boiled in water for 10 minutes (green), and held at 80°C in water for 135 hours. Only long-term exposure to water significantly changed the XRD pattern.

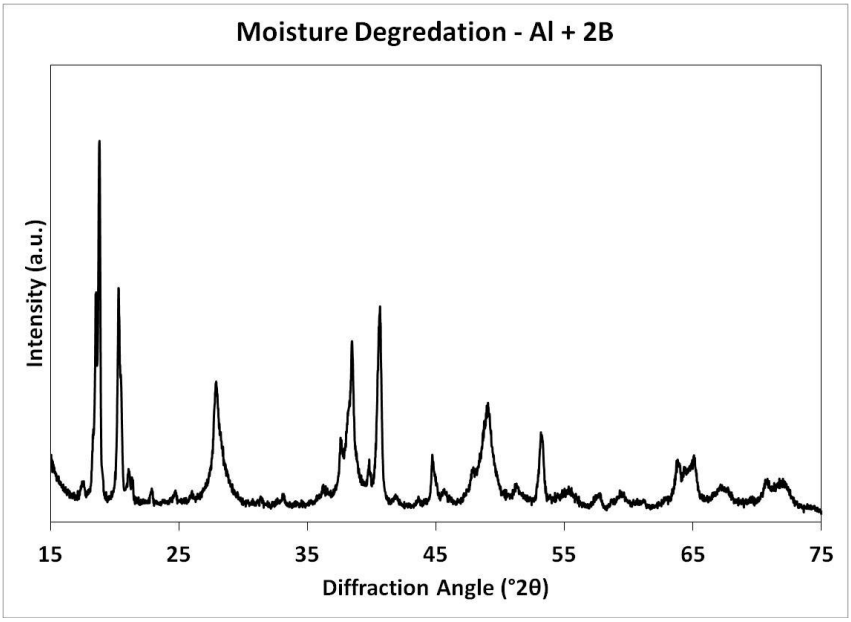

Figure 6.16. XRD pattern of Al+2B after exposure to water at 80°C for 135 hours. Aluminum hydroxide (Bayerite and Nordstradite) was prevalent in the material as the Al was attacked. The boron did not show up due to its low atomic number, but it was still present.

was aided by some dissolution of boron as boric acid.

The amine and Shin-Etsu fluorosilane both gained 112 %. None of the coatings protected the AlB_2 powder under these aggressive conditions. An interesting question is whether the powders would have been protected better by a polymeric coating, which more closely duplicates the condition when powders are mixed in energetic formulations. A hydrophobic polymer would likely give much better protection than any of the coatings investigated. Fortunately, storage conditions are easily controlled. By sealing in vacuum-packed bags under an Ar cover gas these powders can be stored for years with little degradation in quality.

6.3 Conclusions

Fine aluminum is susceptible to oxidation, forming $Al(OH)_3$ in moist environments. Boron is only affected by the formation of boric acid, which is water soluble. Surprisingly Al + 2B showed good stability at moderate temperature and relative humidity (eg, 60°C in 75% relative humidity). The formation of AlB_2 gave improved stability over Al + 2B mixtures, as expected. It is very likely that there is no issue with storing AlB_2 powders for long periods of time if stored in a low-humidity condition. Once energetic formulations are prepared, it is believed that the binder will protect them from exposure to moisture making short-term storage of these mixtures possible.

An n-octadecyltrimethoxysilane provided excellent protection at temperatures up to 60°C under high humidity conditions. It was slightly better than the fluorosilanes and amine coatings investigated. Even at higher temperatures, under moderate humidity conditions, the silane provided significant protection. The weight gain, for example, at

80°C and 75 % relative humidity for a silane-coated powder was about one-third that of the control powder.

None of the powder was able to withstand exposure to water for an extended period of time (135 hours) at 80°C even though short (15 minute) exposure to boiling water did not cause significant problems. The way the silane coatings were prepared, although hydrophobic, still allowed degradation of the powders when submerged in hot water. Studies using thin hydrophobic polymeric coatings should be conducted.

6.4 References

1. R. Muller, M. Knapp, K. Heckmann, M. von Ruthendorf, and G. Boden, "Protecting Nanoscaled Non-Oxidic Particles from Oxygen Uptake by Coating with Nitrogen-Containing Surfactants," *Langmuir*, **20** 2598-2606 (2004)

2. L. Greenspan, "Humidity Fixed Points of Binary Saturated Aqueous Solutions," *J. Res. NBS-A, Phys. Chem.*, **81A**[1] 89-96 (1977)

7. SUMMARY AND CONCLUSIONS

Boron, aluminum, magnesium, silicon, and carbon are energetic elements with potential applications in a wide variety of combustion and detonation systems. Aluminum is the most commonly used energetic fuel additive because of its high enthalpy of combustion, rapid reaction kinetics, and relatively low cost. Thermodynamic calculations for the oxidation of aluminum confirmed its high potential on a volumetric and gravimetric basis. Thermal gravimetric analyses and differential thermal analyses supported its kinetic benefits by showing that the oxidation of aluminum proceeded to completion through a sequence of rapid exotherms. Boron has one of the highest enthalpies of combustion of any element, but the oxidation of boron was reported to be kinetically limited by a growing layer of liquid B_2O_3 on the boron particle surface. Thermal gravimetric analysis showed that the high surface area boron investigated was not slowed down by B_2O_3 for the first half of its oxidation due to the high surface area of the powder. Particle size analysis and BET surface area measurements gave the median particle size as 200 nm, with a surface area of ~11 m^2/g. This allowed much of the boron to oxidize before the oxide layer became too thick. Once the boron reached a conversion around 0.5, B_2O_3 began to limit the reaction by slowing diffusion. These results were in general agreement with the literature.

Magnesium is less commonly used as an energetic material because it is more reactive with air and water, has a lower enthalpy of combustion and is slightly more

expensive than aluminum. Thermal gravimetric analysis in air with a linear heating rate of 10°C/min indicated that magnesium only reached 77% of its theoretical oxidation limit because oxygen diffusivity in MgO is much smaller than for the other oxides in this study and the magnesium particle size was much larger than that of the other metals. The aluminum-magnesium alloy, with a particle size intermediate to aluminum and magnesium, reached unity conversion (like aluminum) over a small temperature range (like magnesium). This behavior demonstrated why aluminum-magnesium alloys are also common in energetic formulations. Boron carbide had nearly identical oxidation behavior to boron, suggesting that it oxidized by the same mechanism of B_2O_3 formation. Silicon did not oxidize readily due to the formation of passivating SiO_2.

While metallic fuels are most commonly used in energetic applications, they are sensitive to accidental discharge. It was hypothesized that the sensitivity of these powders could be reduced by forming compounds, and that compounds of metals and boron would be both insensitive and energetically promising. Thermodynamic analysis of the boride compounds showed that they have enthalpies of combustion equal to or greater than the elemental fuels on a mass or volume basis. The boride compounds AlB_2, MgB_2, $Al_{0.5}Mg_{0.5}B_2$, AlB_{12}, $AlMgB_{14}$ and SiB_6 were synthesized from mixtures of the elemental powders, with special emphasis on making high purity AlB_2. Because boron is an expensive raw material, boron carbide (B_4C) was also investigated as a substitute for boron in the synthesis of AlB_2. The mixture (B4C + 2Al) was reacted under the same conditions as AlB_2 and produced Al_3BC and AlB_2 as the major products.

All of the reacted compounds had minor impurities, including oxides and unreacted material. The reaction between aluminum and boron was significantly

incomplete, so methods to improve the extent of reaction of aluminum and boron and decrease impurities were used. It was found that moderate compaction was necessary to reduce diffusion distances and promote particle interactions. Increasing the reaction temperature increased the extent of reaction between the two powders up to a maximum around 85% at 900°C. At that point, no further reaction was observed as the temperature was increased to the decomposition temperature of ~975°C. It was speculated from EDS maps that incomplete wetting of boron (or AlB_2) by aluminum at the reaction temperature was limiting the extent of reaction. Remilling the reacted powder and reacting again reduced the amount of excess aluminum and boron, confirming that segregation of aluminum and boron was limiting the reaction. However, increasing the hold time at the reaction temperature did not have an effect on the extent of reaction. A phase pure material was never synthesized, but higher purity than one of the few commercially available AlB_2 powders was attained.

The low temperature oxidation behavior of all materials was investigated by thermal gravimetric analysis. It was confirmed that the boride compounds were less sensitive to oxidation at temperatures below 500°C. Physical mixtures were generally no less sensitive than their constituent powders. While the addition of metals to boron did not significantly change its sensitivity, metals (aluminum, magnesium and aluminum-magnesium) helped increase the extent of oxidation that boron achieved at high temperatures. Silicon severely reduced the extent of reaction of boron and is considered a poor energetic additive. It has not been established whether this high temperature oxidation behavior in flowing air corresponds to increased performance in energetic formulations, but many literature sources describe increased performance of boron

through the addition of metals. A mechanism for this increase in performance was proposed for the Mg-B and Al-B systems, originating from the formation of metal borates ($2Al_2O_3 \cdot B_2O_3$ or $3MgO \cdot B_2O_3$) that convert liquid B_2O_3 into a solid oxide compound.

The compounds AlB_{12}, $AlMgB_{14}$, and SiB_6 did not reach high conversions and were considered poor energetic additives. Oxidized silicon and boron are known to form borosilicate phases, which acted like B_2O_3 in limiting diffusion and made SiB_6 as poor a material as silicon. The cause of reduced conversion in AlB_{12}, $AlMgB_{14}$, is hypothesized to be due to the higher boron content limiting the effectiveness of the borate formation mechanism and perhaps icosahedral bonding reducing oxidation kinetics. Al_3BC and AlB_2 did not reach high conversions in the temperature range investigated, but unlike the AlB_{12}, $AlMgB_{14}$, and SiB_6, it did not significantly slow down at higher temperatures. Due to the high conversion of the B_4C + 2Al powder mixture and the formation of AlB_2 in the reacted compound, further investigation of this powder is warranted.

Isothermal oxidation studies of aluminum, boron, Al + 2B and AlB_2 in air and oxygen complemented the linear heating rate data and allowed for the calculation of activation energies. Similar values to those in the literature were found for aluminum and boron, confirming the validity of the isoconversional method approach and the experimental procedures. The activation energies for Al + 2B and AlB_2 were not constant over the conversion ranges investigated, with the possible exception of AlB_2 in oxygen. An average activation energy of 413 ± 20 kJ/mol was calculated for this material. The other studies showed decreasing activation energies as a function of conversion, suggesting that the borate formation mechanism was acting to reduce the temperature dependence of oxidation. AlB_2 reached the highest conversions with no significant

slowing of oxidation. Alternate methods of analysis of the isothermal curves and in-depth linear heating rate experiments are of interest to augment these activation energies.

The moisture sensitivity of aluminum, boron, Al + 2B and AlB_2 was compared by placing samples in elevated temperature and humidity environments and recording weight change. Aluminum readily formed $Al(OH)_3$ in moist environments, while AlB_2 was much more resistant to high relative humidity and high temperature. Aluminum and AlB_2 gained weight upon oxidation but boron lost weight due to the formation of water soluble boric acid. The tradeoff between weight gain and weight loss in Al + 2B did not follow a rule of mixtures relationship, but instead tracked the behavior of AlB_2 and was much less sensitive to moisture than expected. Boron, Al + 2B and AlB_2 can be stored for long periods of time in cool, moisture free environments with little degradation of the powder.

After characterization was conducted, the powders were sent to ARDEC for energetic testing. Detonation calorimetry was performed on Al + 2B and AlB_2 in energetic formulations. Thermodynamic models of the reaction estimated that AlB_2 reacted completely, while Al + 2B only achieved approximately 70% reaction. It is unclear whether this increase in extent of reaction was related to the borate formation mechanism observed in ‘static’ oxidation or another process because analysis of the reaction products was not conducted. Nonetheless, this is a promising result that warrants follow up work. $AlMgB_{14}$ was tested by cylinder expansion, a proprietary detonation test conducted at ARDEC. Results of this test showed that $AlMgB_{14}$ was poor energetic material compared to less expensive and more abundant additives. Again, it is unclear

whether this test corresponded to phenomena observed during characterization, but this result would have been anticipated if TGA correlates with energetic performance.

Insensitive energetic metal boride powders have been synthesized, characterized, and tested. Metal diboride compounds that are less sensitive to low temperature oxidation and moisture than aluminum and have favorable oxidation characteristics have been demonstrated. More cost effective synthesis routes, including the use of boron carbide have been investigated and shown to have potential. Preliminary energetic testing suggested that AlB_2 is a promising energetic candidate. Further testing of AlB_2 should be conducted in order to confirm its performance in situ. Testing of MgB_2 and $Al_{0.5}Mg_{0.5}B_2$ is also warranted in light of the similar TGA results and oxidation mechanisms. Investigations into the energetic characteristics of Al_3BC should be carried out. This thesis produced many promising results that require future efforts in synthesis, characterization and testing of these boride compounds. Through future work, with this thesis as a starting point, the possibility of low cost, insensitive, high performance energetic materials can be realized.

APPENDIX A

PARTICLE SIZE HISTOGRAMS

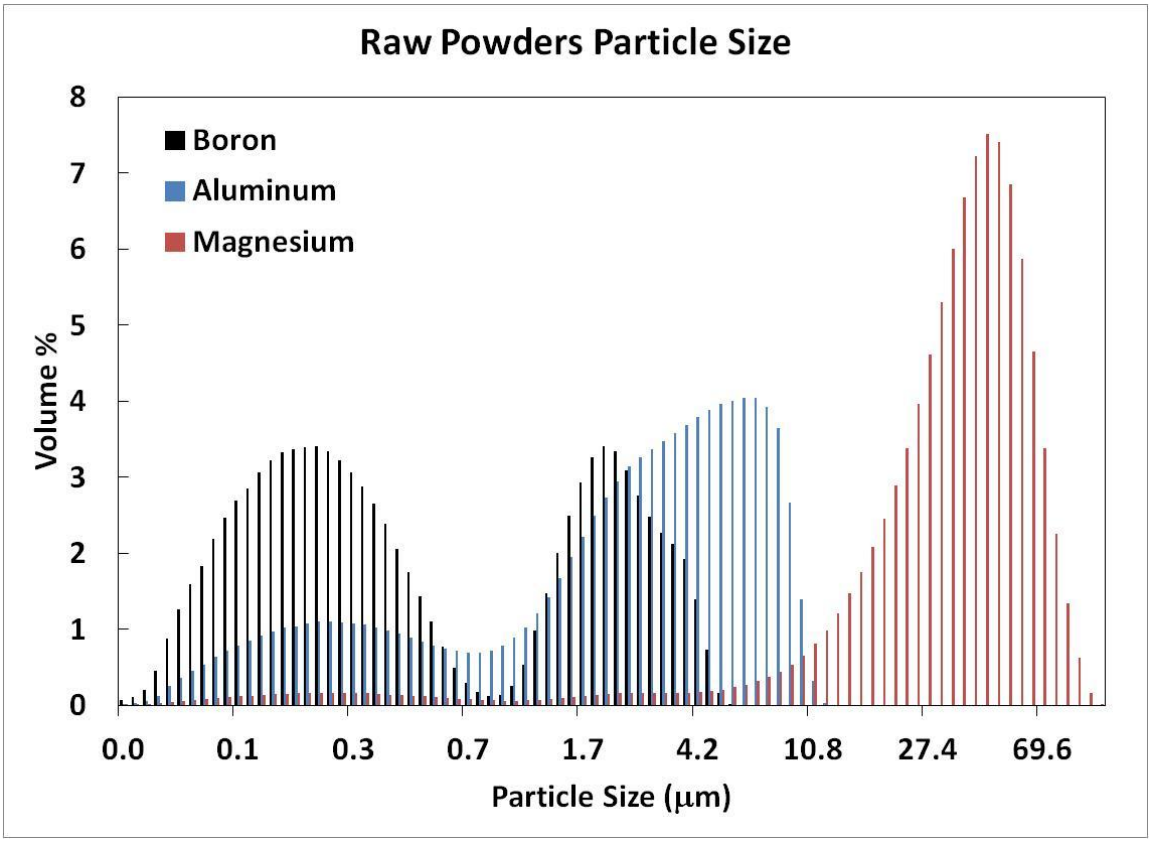

Figure A-1. Particle size histogram for boron, aluminum and magnesium.

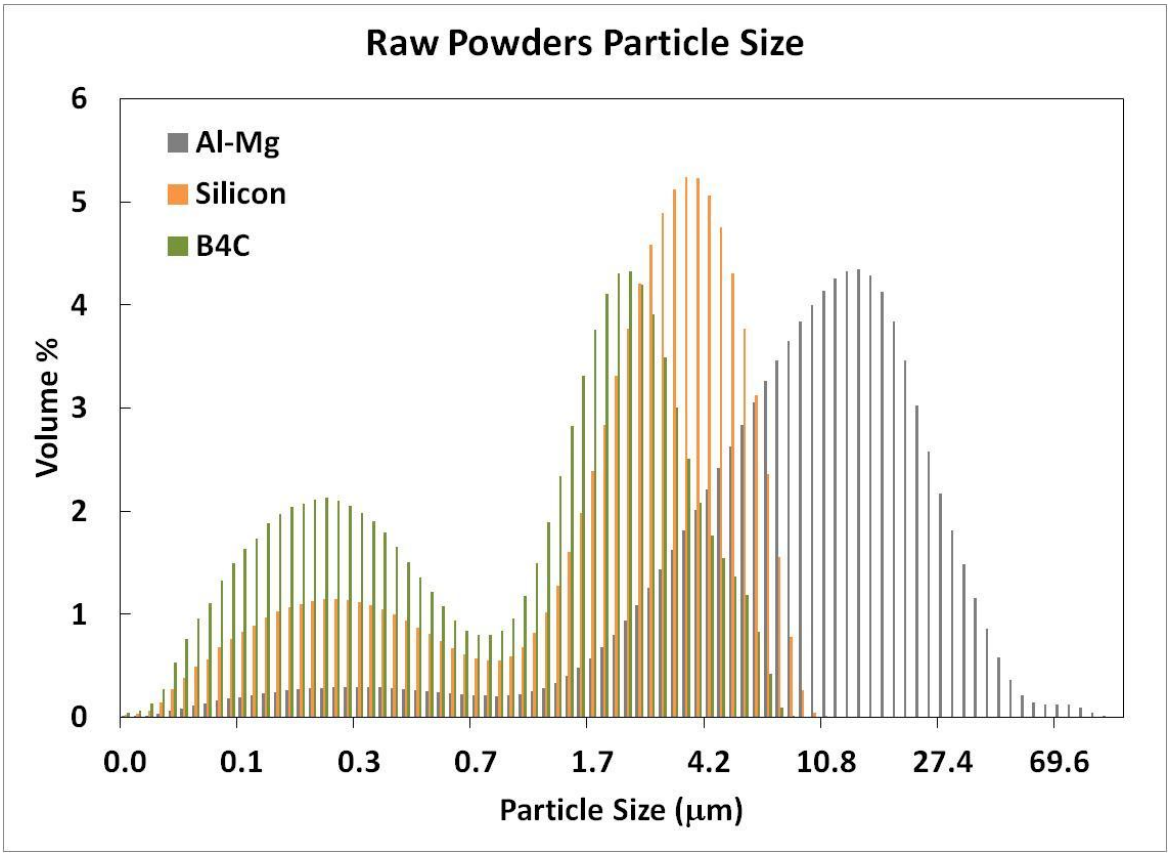

Figure A-2. Particle size histogram for Al-Mg, silicon and B_4C.

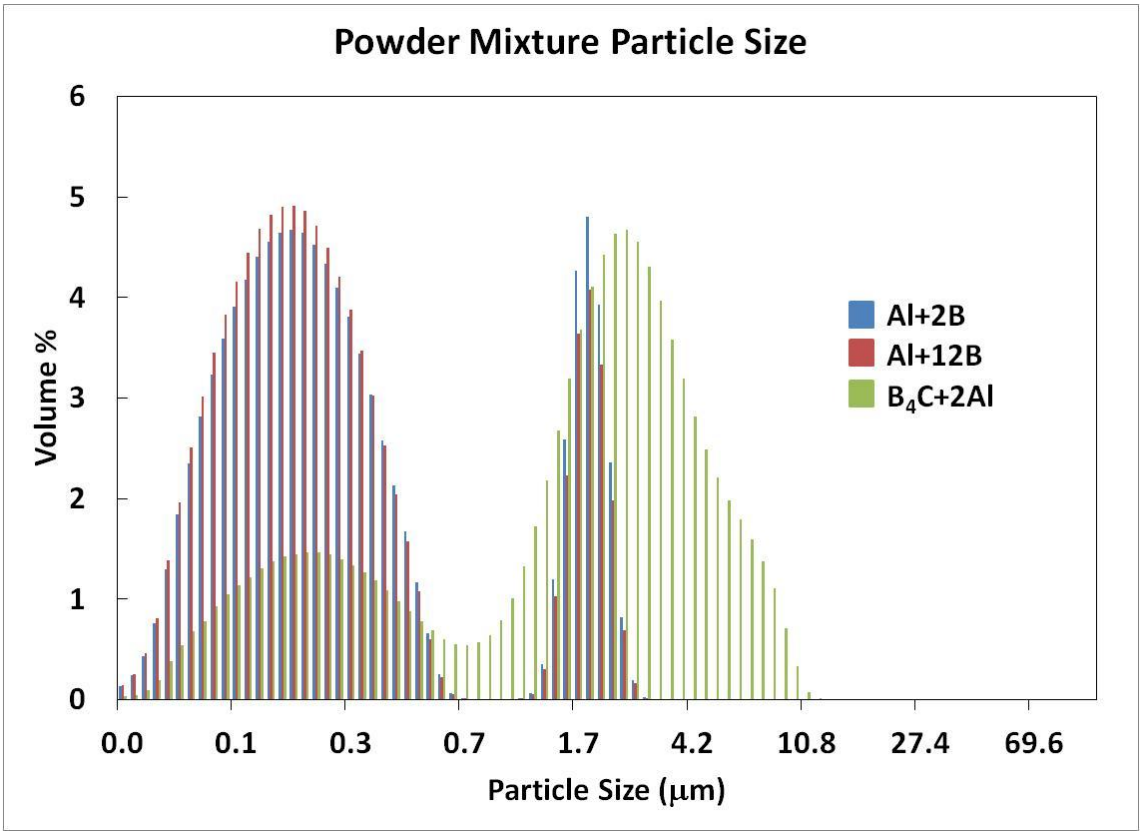

Figure A-3. Particle size histogram for Al + 2B, Al + 12B and B_4C + 2Al.

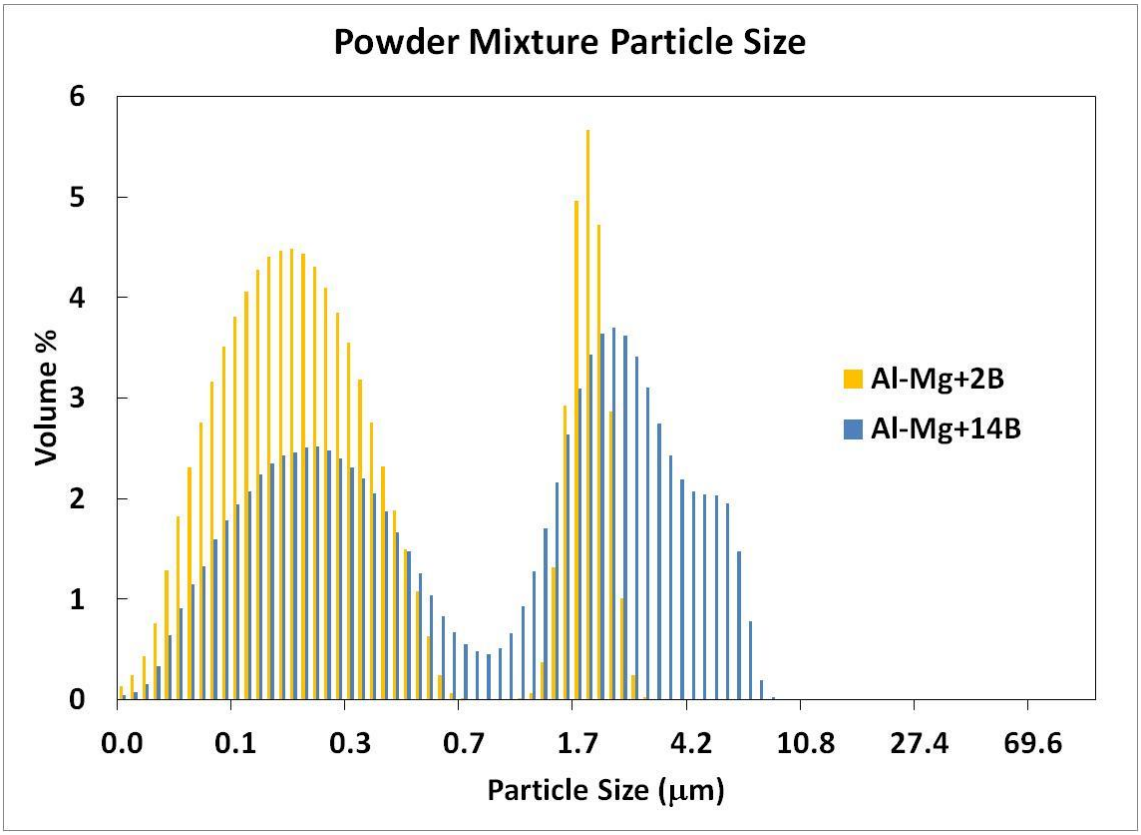

Figure A-4. Particle size histogram for Al-Mg + 2B and Al-Mg + 14B.

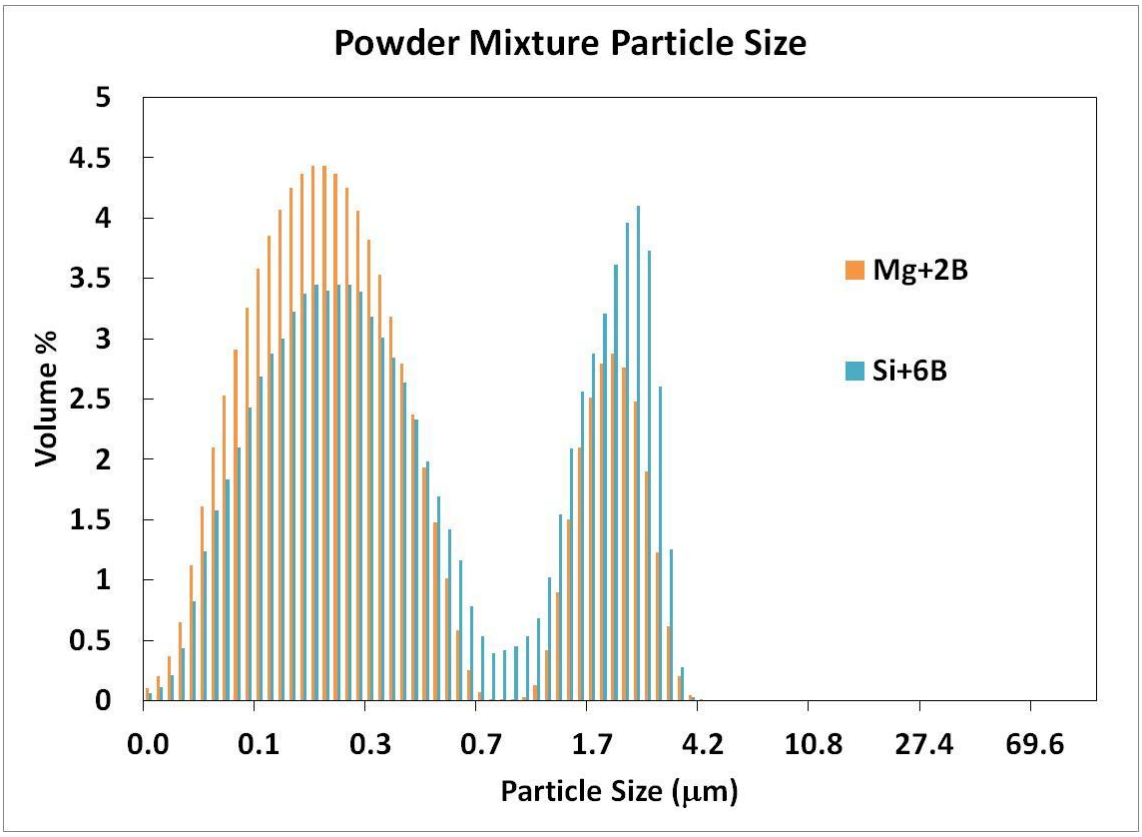

Figure A-5. Particle size histogram for Mg + 2B and Si + 6B

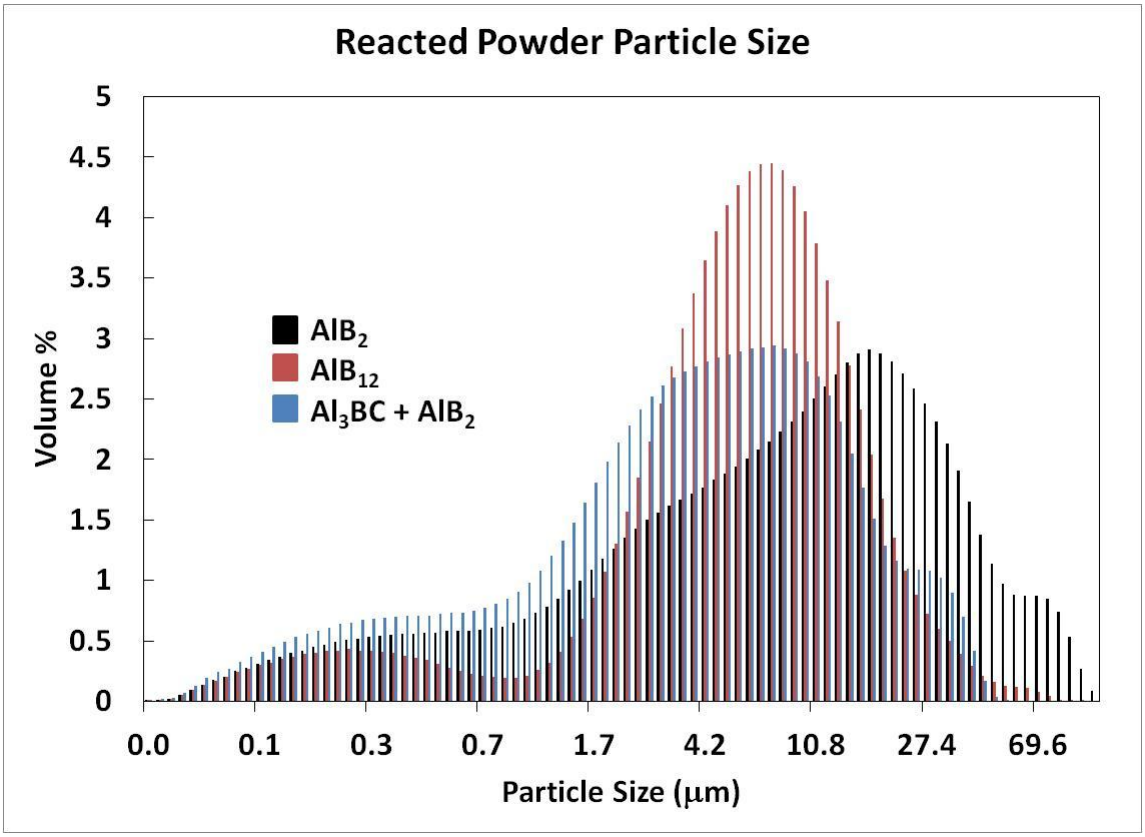

Figure A-6. Particle size historgram for AlB_2, AlB_{12} and Al_3BC + AlB_2.

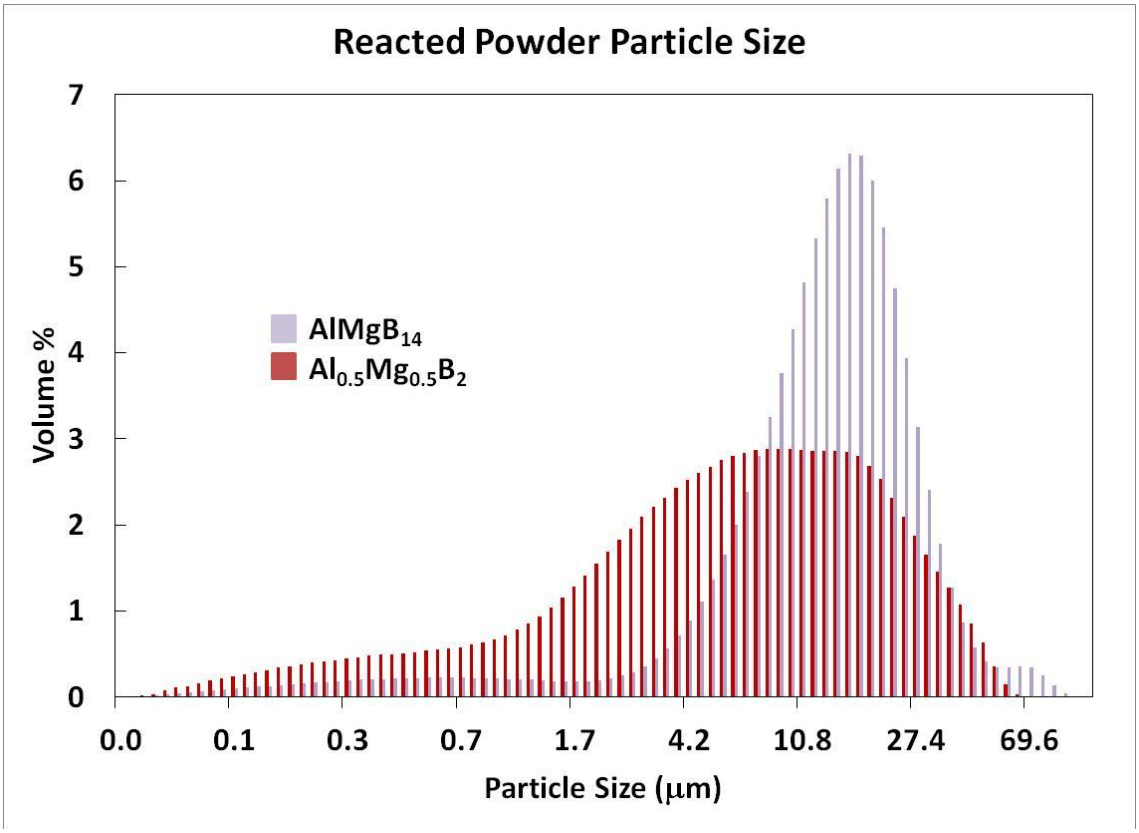

Figrue A-7. Particle size histogram for $AlMgB_{14}$ and $Al_{0.5}Mg_{0.5}B_2$.

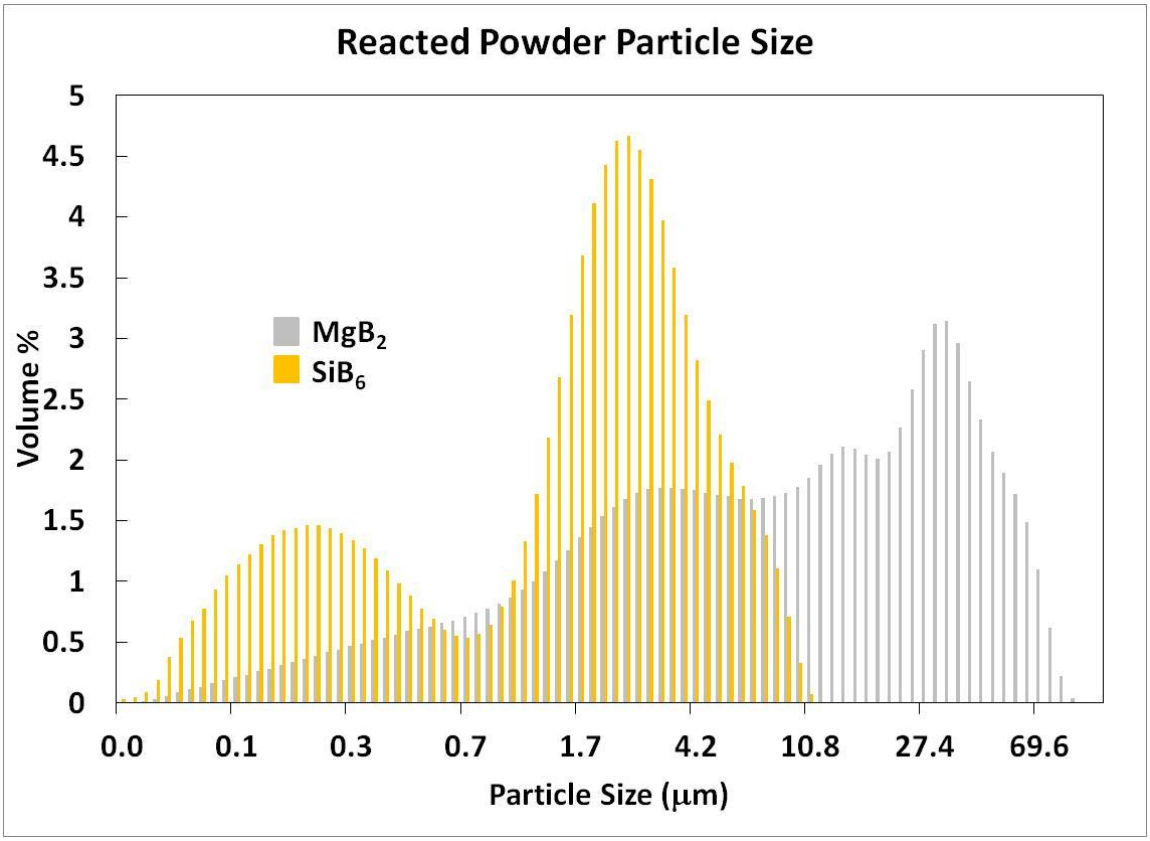

Figure A-8. Particle size histogram for MgB_2 and SiB_6.

APPENDIX B

MICROSTRUCTURE, MECHANICAL PROPERTIES AND PERFORMANCE OF MAGNESIUM ALUMINUM BORIDE ($MgAlB_{14}$)

M. L. Whittaker, R. A. Cutler, J. La Salvia, J. Campbell

Ceramic Engineering and Science Proceedings
Volume 31, Chapter 7, 239-250 (2010)

MICROSTRUCTURE, MECHANICAL PROPERTIES, AND PERFORMANCE OF MAGNESIUM ALUMINUM BORIDE ($MgAlB_{14}$)

Michael L. Whittaker and Raymond A. Cutler
Ceramatec, Inc.
2425 South 900 West
Salt Lake City, Utah, 84119

James Campbell and Jerry La Salvia
Army Research Laboratory
Aberdeen, Maryland 21005

ABSTRACT

$Mg_{0.78}Al_{0.75}B_{14}$, which is herein referred to as $MgAlB_{14}$, is a boride which has been studied in the laboratory but has not been tested ballistically previously due to the difficulty in making large components. This orthorhombic material consists of B_{12} icosahedra and is reported to have high hardness like the rhombohedral B_4C in which similar covalent bonding occurs. The density of $MgAlB_{14}$ (≈2.64 g/cc) is closer to B_4C (2.52 g/cc) than SiC (3.21 g/cc). While B_4C is preferred at lower threats, the ballistic performance of SiC is much better at higher threat levels. Hot pressed B_4C, $MgAlB_{14}$, and SiC were compared in the present work. The single-edged pre-cracked beam (SEPB) fracture toughness of $MgAlB_{14}$ was 3.4±0.4 MPa√m, which was intermediate between B_4C (2.2±0.5 MPa√m) and SiC-N (4.7±0.1 MPa√m). The fracture mode of magnesium aluminum boride was mostly transgranular, like B_4C, as opposed to the mainly intergranular fracture mode of SiC-N. The flexural strength of $MgAlB_{14}$ (390±37 MPa with a Weibull modulus of 11.7) was similar to B_4C (387±8.8 MPa with a Weibull modulus of 8.8), but much lower than that of SiC-N (558±50 MPa with a Weibull modulus of 14.5). The Vickers hardness values (at a one kilogram load) of all three materials (B_4C=26.0±2.0 GPa, SiC-N=22.5±0.8 GPa, and $MgAlB_{14}$=22.1±0.8 GPa) were much higher than that of the bullet (14.7 GPa) used for ballistic testing. The Young's modulus of $MgAlB_{14}$, which contained 4 wt. % $MgAl_2O_4$ as an impurity phase, was 397±1 GPa, which is lower than the other two materials (437±3 GPa for SiC-N and 436±2 GPa for B_4C). The V_{50} ballistic performance of $MgAlB_{14}$ was approximately 250 m/s lower than SiC-N at the same areal density indicating that the material does not have promise for use at moderate or heavy threats.

INTRODUCTION

While there is much debate on what makes good armor it is universally agreed that low areal density (lightweight), high hardness (at least as hard as the projectile), and low cost (ceramic armor is expensive and is only used in limited applications) are important. The armor material of choice against steel-cored bullets is boron carbide (B_4C) due to its low areal density, while silicon carbide (SiC) is used against WC-cored bullets. While SiC (3.21 g/cc) has a higher density than B_4C (2.52 g/cc) it performs better at higher threats. Al_2O_3 (3.98 g/cc) is used due to its low cost and pressureless sintered materials are preferable to hot pressed materials when armoring tanks, due to the high volume of material that must be produced. Hardened steel is currently used to armor vehicles due to the cost of ceramic armor. In spite of the widespread use of steel, the ceramic armor market is substantial and fluctuates greatly based on need. It is difficult to find mechanical properties that correlate with ballistic performance, but ceramic

materials that perform well all have low porosity, high elastic modulus, and relatively high hardness.[1] Hardness and fracture toughness, however, do not correlate with the ballistic performance of SiC armor.[1-3]

A wide variety of borides exist with a spectra of interesting electrical, mechanical, thermal, and physical properties.[4] Matkovich and Economy identified $MgAlB_{14}$ as an orthorhombic structure (space group Imam) made up of B_{12} icosahedra with partial occupancy of Mg atoms, giving a theoretical density of 2.75 g/cc.[5] Further crystallography showed that about one quarter of the Al and Mg sites are vacant in the orthorhombic structure, leading to the formula $Mg_{0.78}Al_{0.75}B_{14}$, which results in a theoretical density of 2.59 g/cc.[6] The orthorhombic unit cell (a=5.844 Å, b=10.218 Å, and c=8.017 Å) has four molecules per unit cell as shown in Figure 1 resulting in a theoretical density of 2.64 g/cc.[7] The formula $MgAlB_{14}$ is used here for simplicity. Letsoala and Lowther have recently reviewed the structure of a variety of borides in an attempt to explain their properties.[7] They suggest that the average charge density between B atoms partially explains the high hardness of these materials. The B atoms lying outside the icosahedra donate part of their charge, which enhances the strength of the B-B bonds. Hardness for $MgAlB_{14}$ covers a range of values[7] partly due to the difficulty in measuring hardness and the different loads used. Single crystals have hardness in the range of 24-25 GPa.[8] High pressure densification of polycrystalline material resulted in 30-46 GPa hardness.[9] The hardness of aluminum magnesium boride is certainly in the range that would make acceptable armor.

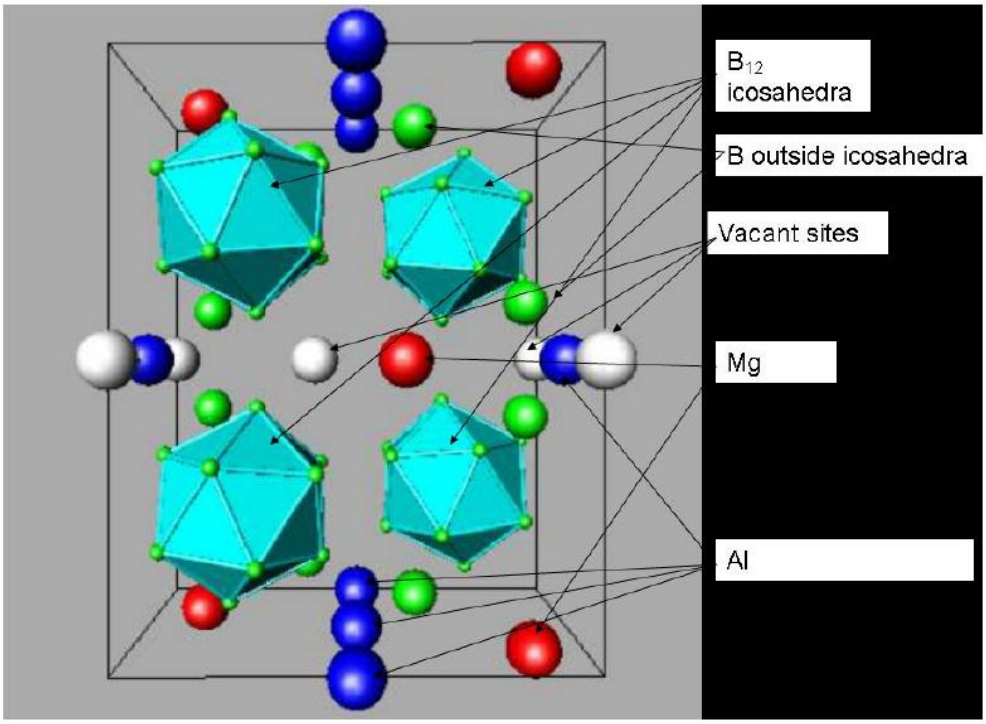

Figure 1. Structure of $Mg_{0.78}Al_{0.75}B_{14}$, where four B_{12} icosahedra occupy the orthorhombic unit cell at positions of (0,0,0), (0,0.5,0.5), (0.5,0,0) and (0.5,0.5,0.5), with the remaining eight B atoms located outside the icosahedra bonding. The Mg and Al atoms, which have four-fold coordination, are located at (0.25,0.359,0) and (0.25,0.75,0.25), respectively.[5-7,10]

Lee and Harmon[10] predicted high (470-509 GPa) Young's modulus, E, for $MgAlB_{14}$. Muthu, et al.[11] used high temperature X-ray diffraction to calculate a bulk modulus, K, between 196 and 264 GPa. The bulk and elastic moduli are related by $E=3K(1-2\nu)$, where ν is Poisson's ratio. Taking a value of 0.1 for Poisson's ratio, gives a calculated Young's modulus in the range of 470 to 633 GPa. It is apparent that the material will have a high modulus and is of interest as a ballistic material.

There are no data for the ballistic performance of $MgAlB_{14}$, due to the fact that it has been difficult to produce. Single crystal growth or high-pressure densification of Mg, Al, and B has been the normal method for making the material. Bodkin[12] showed that dense $MgAlB_{14}$ could be produced by heating $MgAlB_{14}$ powder to 1600ºC for one hour under 75 MPa pressure. The incorporation of Al and Mg in the unit cell lowers the densification temperature of $MgAlB_{14}$ by 600ºC compared to B_4C, which is typically processed at 2200ºC. New Tech Ceramics (Boone, IA), has recently been able to produce small tiles (50 mm x 450 mm x 5 mm) of $MgAlB_{14}$ by a proprietary process. Characterization of the material at Ceramatec resulted in properties as shown in Table 1. The fracture toughness and strength of $MgAlB_{14}$ are comparable to those of SiC-N but the elastic modulus is slightly lower than that of both SiC-N or solid state SiC when measured by the same technique.[1] The hardness is similar to that of SiC-N and lower than B_4C. Figure 1 shows a fracture surface of the material indicating that it fractures primarily transgranular, similar to B_4C and solid state SiC, but different than SiC-N. As Ceramatec is aware, there is no good method for predicting ballistic performance other than getting actual data.[1-3] SiC is the ceramic armor of choice for moderate to heavy threats due to the likely amorphitization of B_4C at high pressures. While mechanical properties look good for $MgAlB_{14}$, the question is whether it is at least comparable with hot pressed B_4C at the same areal density. Due to its lower processing temperature it has the potential to be a material of interest to the Army if the cost of processing the material were similar to boron carbide. This work was undertaken in order to ballistically test $MgAlB_{14}$ tiles in comparison with SiC and B_4C.

EXPERIMENTAL PROCEDURES

The three materials for this study were purchased by the Army Research Laboratory and provided to Ceramatec for characterization. The B_4C and SiC-N were hot pressed materials purchased from BAE Systems (Vista, CA) and are given the code of B and N, respectively. The $MgAlB_{14}$, given the code M in this paper, was purchased from New Tech Ceramics (Boone, IA) and no processing details are available. The thickness of the materials supplied were 11.4 mm (material B), 15.5 mm (material M), or 25.4 mm (material N). The billets were sliced and then ground with a 180 grit diamond wheel to make 3 mm x 4 mm x 45 mm bars as specified by ASTM C-1421-99. Density was measured by water displacement. Fracture toughness was measured using the single-edge precracked beam (SEPB) technique[13] as described previously[14]

Table I
Properties of New Tech $MgAlB_{14}$ Measured at Ceramatec

Density (g/cc)	SEPB Toughness (MPa-$m^{1/2}$)	Elastic Modulus (GPa)	Flexural Strength (MPa)	HV1 (GPa)
2.64	4.2±0.3	396±3	516±76	23.6±0.5

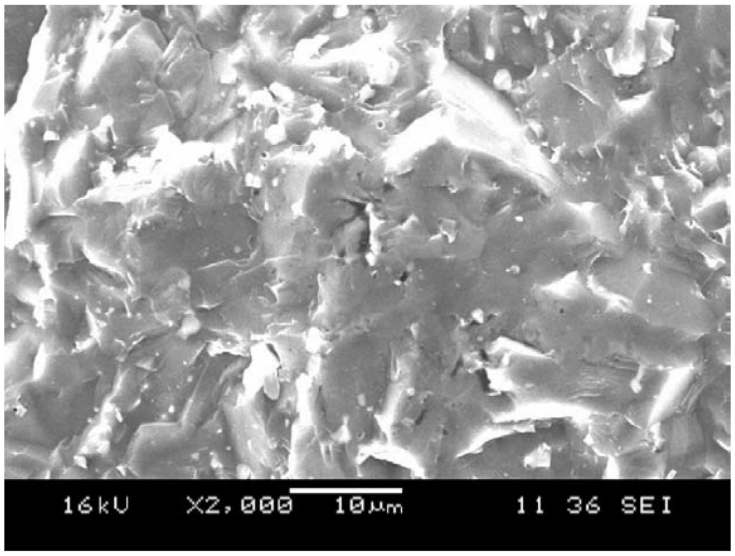

Figure 2. Fracture surface of New Tech's $MgAlB_{14}$ showing mainly transgranular fracture. See properties of this material in Table I.

except that black printer ink was used to mark the crack location. All crack planes were parallel to the hot pressing direction. Each data point is the mean of 5 bars tested, with error bars representing two standard deviations.

A microhardness machine (Leco model LM-100) was used to obtain Vickers and Knoop hardness data on polished SEPB bars. Data were taken at a load of 9.8 N. Each data point represents the mean of ten measurements, with error bars representing two standard deviations. Rietveld analysis[15,16] was used to quantify phases or polytypes present in the materials with X-ray diffraction patterns collected from 20-80° 2Θ, with a step size of 0.02°/step and a counting time of 4 sec/step.

Polished samples were etched to reveal their grain boundaries. Material M was etched in a modified Murakami solution[17] at 80°C for 60 seconds. Materials B and N were thermally etched at 1550°C in flowing Ar for one hour. Grain size was determined by the line-intercept method, where the multiplication constant was 1.5 (equiaxed grains).[18] Approximately 500 grains were measured for each composition in order to get a mean grain size. The aspect ratios of the three most acicular grains in each of 5 micrographs were used to estimate a comparative aspect ratio.

The fracture mode was determined from polished, precracked SEPB bars. The precracked bars were subsequently etched as described above to get a quantitative estimate of the fracture mode by viewing the crack path over a distance of 150-650 µm, depending on grain size.

Flexural strength was measured on 25 bars (3 mm x 4 mm x 45 mm) using a 40 mm support span and a 20 mm loading span, with the crosshead speed at 0.5 mm/min. A two-parameter Weibull analysis was used to calculate the characteristic strength. Young's modulus was measured in flexure using strain gages.

Ballistic testing was performed at ARL on 100 mm x 100 mm tiles using steel to surround the targets and composite backing and cover plates. The M (thickness of 15.5 mm) and

N (thickness of 12.8 mm) materials were tested using the same technique at the same areal density. The V_{50}, in theory, is the velocity of the bullet at which the probability of the projectile penetrating through the composite backing plate is 50%. Due to the limited number of targets tested, this value was taken as the mean of the two highest velocity tests at which the bullet did not fully penetrate the composite backing and the two lowest velocity tests at which the bullet fully penetrated the backing.

RESULTS AND DISCUSSION

Materials Characterization

Table II gives density, SiC polytypes, mean grain size, aspect ratio, Young's modulus, as well as other phases identified by XRD for the three materials described in Table I. The N material was similar to what has been reported previously for this material, consisting primarily of the 6H polytype, with minimal porosity and high Young's modulus.[1] The B material had lower density than would be expected for a hot pressed material and consisted of a variety of boron carbide phases, as evidenced by the asymmetric peaks (see Figure 3(a)). While free carbon is used as a sintering aid, resulting in the graphite found in the microstructure, the aluminum oxynitride and hexagonal boron nitride phases were unexpected. No Rietveld fitting was attempted for Material B. The low Young's modulus measured is indicative of the porosity in the material and the additional phases present. Material M consisted of 95.6 wt. % $Mg_{0.78}Al_{0.75}B_{14}$, 3.9 wt. % $MgAl_2O_4$, and 0.5 wt. % Al (see Figure 3(b)). No FeB or W_2B_5 were present, as had been reported by other researchers.[9,12] The lattice parameters for the $Mg_{0.78}Al_{0.75}B_{14}$ phase were a=5.8491±0.0003 Å, b=10.3171±0.0006 Å, and c=8.1175±0.0004 Å resulting in a theoretical density of 2.58 g/cc for the $Mg_{0.78}Al_{0.75}B_{14}$ phase, similar to the value reported by Higashi and Ito.[6] Using the Rietveld fit, the theoretical density of the M material was calculated to be 2.61 g/cc, which is lower than the measured value. The theoretical density of material M is therefore unknown, but there is little porosity in the material (see Figure 4). The modulus is similar to that measured at Ceramatec previously (see Table 1) and is lower than what was predicted for this material. The presence of the spinel and aluminum phases lowers the modulus, which is similar to some solid-state sintered silicon carbides. These pressureless sintered SiC materials perform reasonably well ballistically against moderate threats. The modulus of the B material was similar to N, likely due to the porosity and secondary phases in the B material.

The N material is the finest-grained of the three materials, all of which are primarily equiaxed (see Figure 5). The N material fractures mostly intergranularly, which is apparent on both fracture surfaces (see Figure 6) and with hardness indentations on polished surfaces, as shown in Figure 7. The M material has a grain size which is smaller than the boron carbide. The $MgAl_2O_4$ phase, which likely forms due to the oxygen adsorbed on the starting materials,[12] is

Table II
Characterization of Materials

Designation	Density (g/cc)	SiC Polytypes 4H	6H	15R	Other Phases or Polytypes	Grain Size (μm)	Aspect Ratio	E (GPa)
B	2.47±0.02	Not aplicable			Al_3O_3N, BN, C	9.8±0.7	2.8±0.1	436±2
M	2.62±0.01	Not aplicable			$MgAl_2O_4$, Al	4.3±0.4	2.4±0.2	397±1
N	3.22±0.01	2.1	92.3	4.1	2H=0.1, 3C=1.4	3.2±0.2	2.7±0.4	437±3

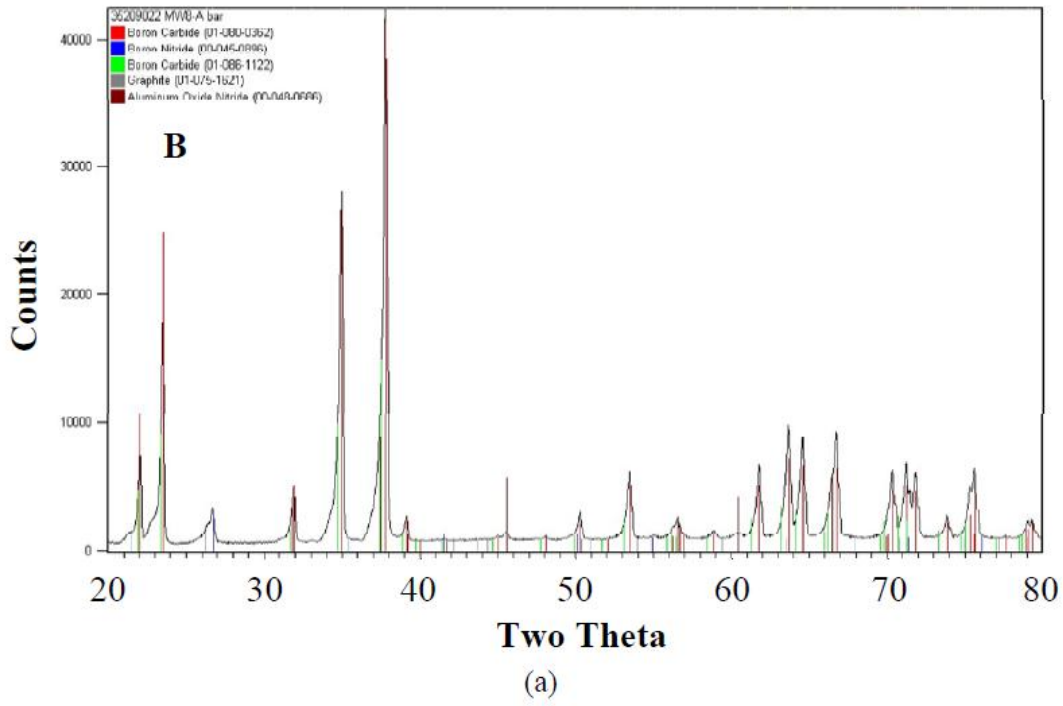

Figure 3. X-ray diffraction patterns for materials (a) B and (b) M. Rietveld fit shown for M.

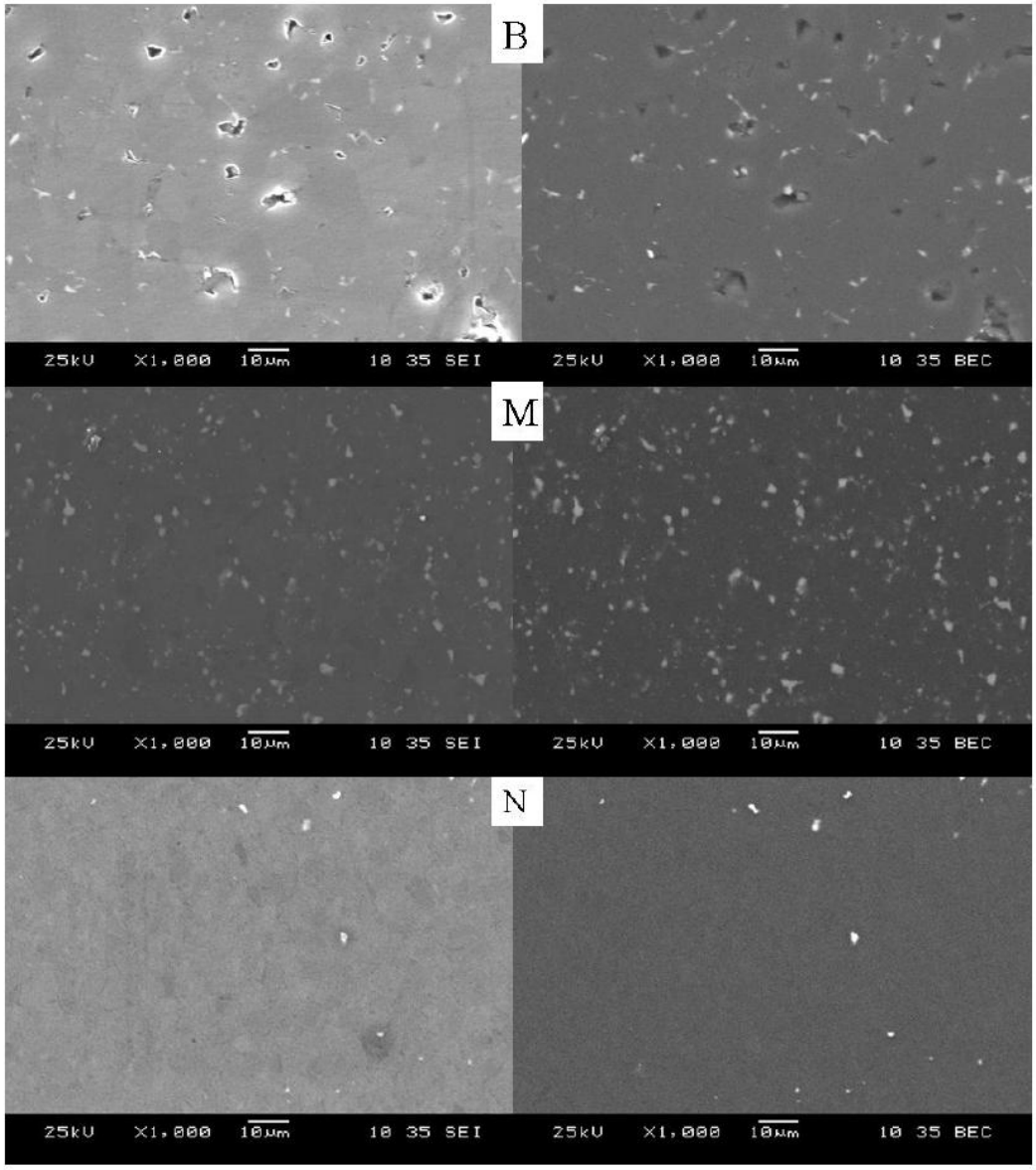

Figure 4. SEM images (secondary on left and backscattered on right) of polished surfaces. Markers are 10 µm.

located at triple points and grain boundaries, although transmission electron microscopy would be required in order to see if a continuous grain boundary phase exists. Material M appears microstructurally to be a ceramic that could perform well ballistically, as it has little porosity and only a small amount of secondary phase present in the material. The apparent porosity on the polished surface is not indicative of the porosity in the material. The B material looked the most porous of the three hot pressed materials, with porosity apparent on fracture surfaces (see Figure 5) and pullout on polished surfaces (see Figure 6).

Table III
Mechanical Property Comparison

Designation	Strength (MPa)			% Intergranular	Toughness	Hardness (GPa)	
	Mean	Char.[a]	m[b]	Fracture	(MPa-m$^{1/2}$)	HK1	HV1
B	387±64	411	8.8	8	2.2±0.5	19.7±1.0	26.0±2.0
M	390±38	407	11.7	6	3.4±0.4	18.8±0.4	22.1±0.8
N	558±50	579	14.5	72	4.7±0.1	19.5±0.5	22.5±0.8

a. Characteristic strength (63.2 % probability of failure).
b. Weibull modulus.

Table III gives mechanical properties for bars cut out of the 100 mm x 100 mm billets. The N material is similar to what has been reported previously.[1] The fracture toughness and strength of the M material were not has high as had been expected, based on the properties evaluated previously (see Table 1). This is the first time to the authors' knowledge that large $MgAlB_{14}$ plates have been prepared. The Weibull modulus (see Figure 8) was very acceptable for this material with strength similar to pressureless sintered SiC. The fracture toughness of material M is considerably higher than that of pressureless sintered silicon carbide, which is 2.5 MPa$\sqrt{m}$ when measured by this same technique. The M material was not as hard as the B material, but comparable in Vickers hardness to material N. The fracture toughness values of the materials are not highly correlated with the amount of intergranular fracture, as had been expected.

The reason for the difference in mechanical properties of $MgAlB_{14}$ for the small plates tested previously (see Table I) and the larger plates tested in this work (see Table III) is not related to density or phases present, as XRD patterns were similar for both materials. Further characterization of these materials would be necessary to explain their difference in toughness and strength.

Ballistic Testing

Only materials M and N were ballistically tested. The initial testing of material M was at the same velocity as the V_{50} of material N. The test velocity was successively dropped until partial values were obtained. The V_{50} of material M is not well quantified, but is approximately 250 m/s below that of material N. No characterization of ballistic debris or TEM work was

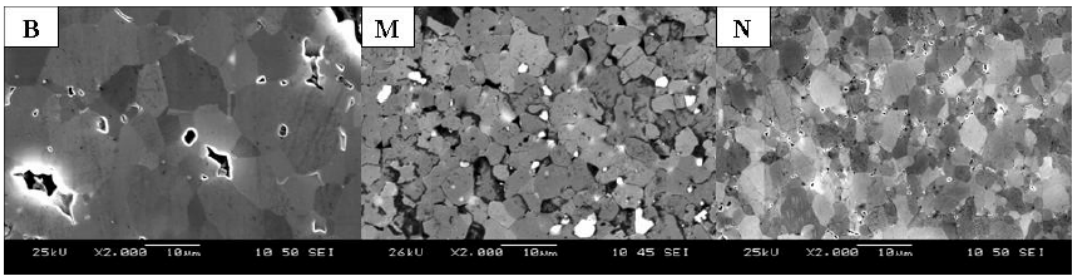

Figure 5. Polished and etched cross-sections. Markers are 10 µm.

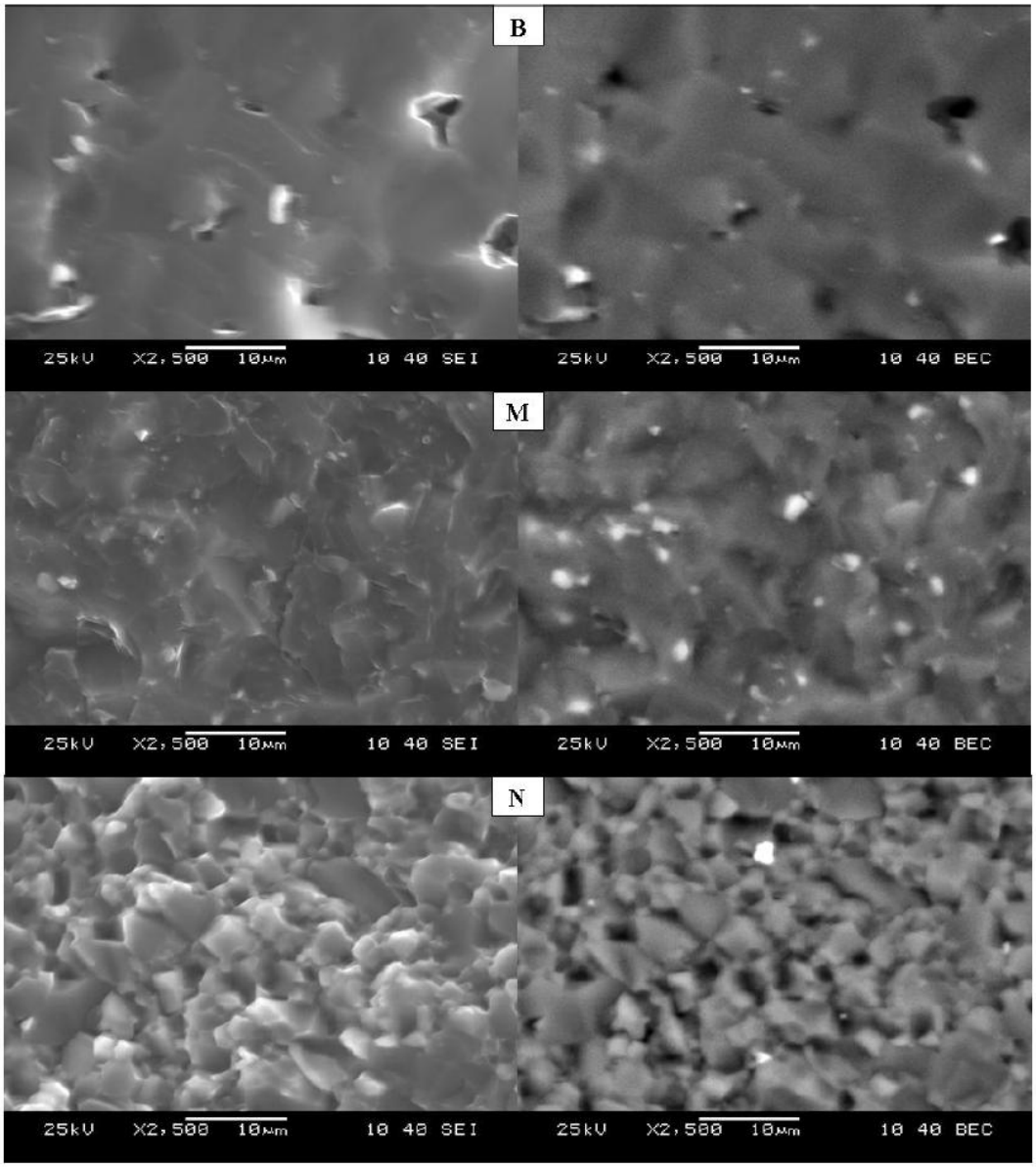

Figure 6. SEM images of the fracture surfaces of three materials. Secondary images on left and backscattered imaging on right. Markers are 10 µm. Note that B and M fracture primarily transgranularly while N fractures intergranularly. Light phase in backscattered imaging of M is the spinel phase.

performed so it is difficult to speculate on the reasons for the poor performance of this material. It is not entirely unexpected, however, as B_4C does not perform well when tested at moderate to heavy threats. If phase pure material M can be produced, it should be tested, since secondary

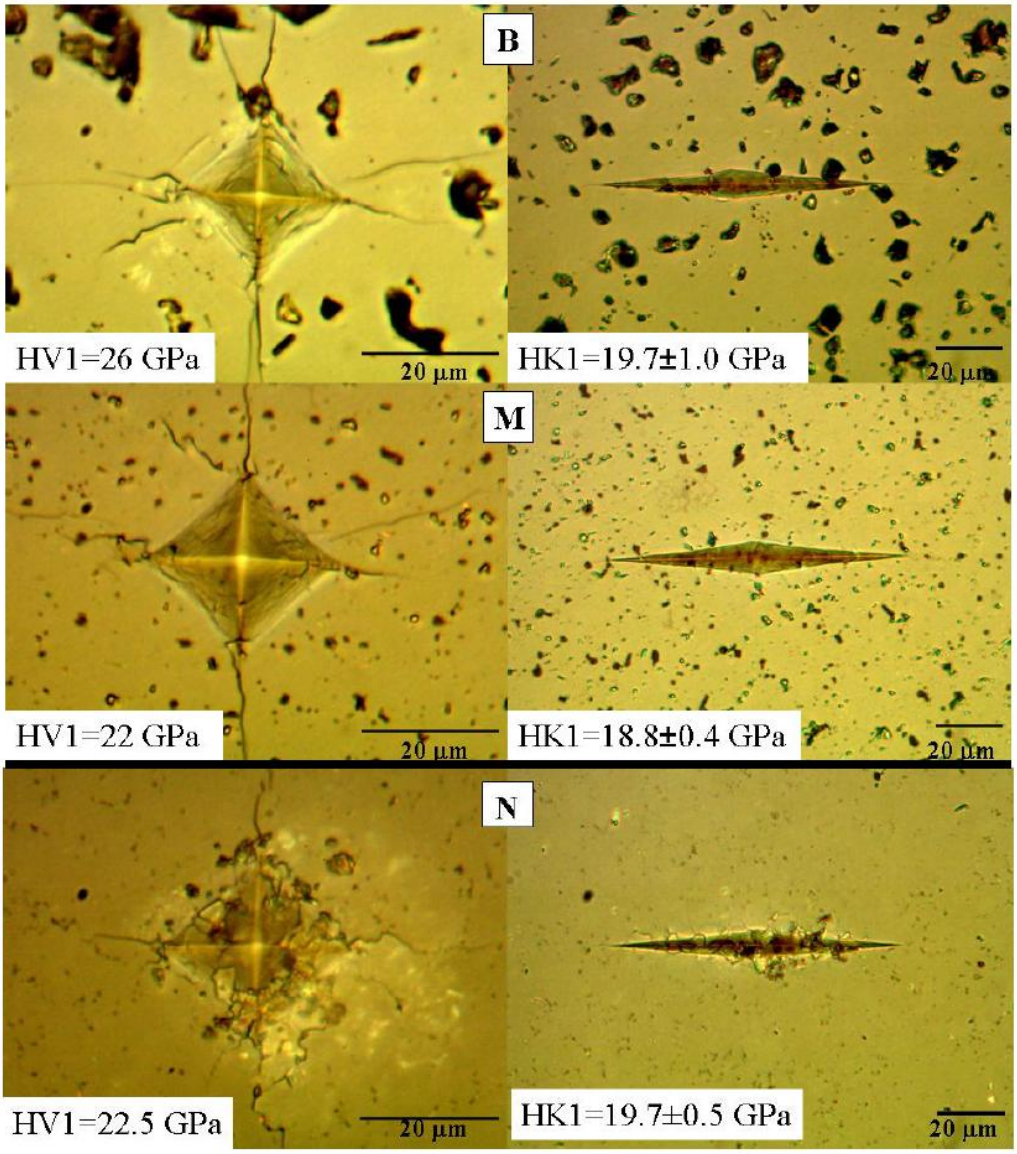

Figure 7. Hardness indents at one-kilogram loads. Markers are 20 µm. Intergranular fracture of N material is readily apparent on polished and indented surfaces.

phases can influence ballistic performance. It is apparent that $MgAlB_{14}$ performs not only much worse than SiC-N, but also is much worse than pressureless sintered SiC, which is within 10 % of the V_{50} value of SiC-N. Since cost is a big driver for ballistic materials, further efforts should not be directed at using this material in armor applications since B_4C is already a commodity material and $MgAlB_{14}$ armor can not be produced at similar cost.

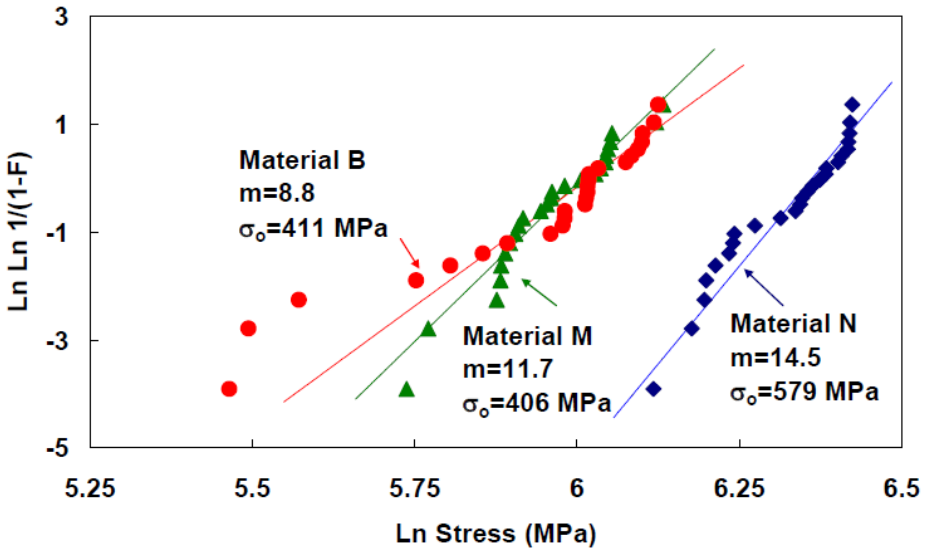

Figure 8. Weibull plots for the three materials tested.

CONCLUSIONS

The V_{50} performance of $MgAlB_{14}$ was approximately 250 m/s lower than that of SiC-N, a standard material used in ballistic tests, at the threat level investigated when identical areal densities were compared. The poor ballistic performance of $MgAlB_{14}$, coupled with its high cost, militates against its use as an armor material. While the mechanical properties of $MgAlB_{14}$ are similar to, or exceed those of pressureless sintered SiC, it performs much worse ballisitically at a moderate threat level. This demonstrates again the importance of performing ballistic tests in order to evaluate a material. The results of this work are not entirely surprising in light of the known poor performance of B_4C, which is also made by bonding B_{12} icosahedra.

ACKNOWLEDGEMENT

Appreciation is expressed to Sarbjit Kaur, Ben Isaac, and Lyle Miller for their help.

REFERENCES

[1] D. Ray, R. M. Flinders, A. Anderson, R. A. Cutler, J. Campbell, and J. W. Adams, "Effect of Microstructure and Mechanical Properties on the Ballistic Performance of SiC-Based Ceramics," *Ceram. Eng. Sci. Proc.*, **27**[7] 85-96, (2006).

[2]D. Ray, R. M. Flinders, A. Anderson, R. A. Cutler and W. Rafaniello, "Effect of Room-Temperature Hardness and Toughness on the Ballistic Performance of SiC-Based Ceramics," *Ceram. Eng. Sci. Proc.*, **26**[7], (2005).

[3]R. Marc Flinders, D. Ray, A. Anderson and R. A. Cutler, "High-Toughness Silicon Carbide as Armor," *J. Am. Ceram. Soc.* **88**[8], 2217-26 (2005).

[4]R. A. Cutler, "Engineering Properties of Borides," pp. 787-803 in Engineered Materials Handbook, Vol. 4: Ceramics and Glasses (ASM, Materials Park, PA 1991).

[5]V. I. Matkovich and J. Economy, "Structure of $MgAlB_{14}$ and a Brief Critique of Structural Relationships of Higher Borides," *Acta. Cryst.*, **B26** 616-21 (1970).

[6]I. Higashi and T. Ito, "Refinement of the Structure of $MgAlB_{14}$," *J. Less Common Metals*, **92**[2] 239-46 (1983).

[7]T. Letsoala and J. E. Lowther, "Systematic Trends in Boron Icosahedral Structured Materials," *Physica B*, **403** 2760-67 (2008).

[8]S. Okada, K. Kudou, T. Mori, T. Shishido, I. Higashi, N. Kamegashira, K. Nakajima, and T. Lundström, "Crystal Growth of Aluminum Magnesium Borides from Al-Mg-B Ternary System Solutions and Properties of the Crystals," *Mater. Sci. Forum*, **449-452**, 315-368 (2004).

[9]B. A. Cook, J. C. Harringa, and A. M. Russell, "Processing Studies and Selected Properties of Ultra-Hard $AlMgB_{14}$," *J. Adv. Mater.*, **36**[3] 56-63 (2004).

[10]Y. Lee and B. N. Harmon, "First Principles Calculation of Elastic Properties of $AlMgB_{14}$," *J. Alloys Compounds*, **338**[1-2] 242-247 (2002).

[11]D. V. S. Muthu, B. Chen, B. A. Cook, and M. B. Kruger, "Effects of Sample Preparation on the Mechanical Properties of $AlMgB_{14}$," High Pressure Res., 28[1] 63-68 (2008).

[12]R. Bodkin, "A Synthesis and Study of $AlMgB_{14}$," Ph.D. Dissertation, University of the Witwatersrand (Johannesburg, South Africa, 2006).

[13]ASTM C 1421-99, Standard Test Methods for Determination of Fracture Toughness of Advanced Ceramics at Ambient Temperature, pp. 641-672 in *1999 Annual Book of Standards* (ASTM, Philadelphia, PA 1999).

[14]D. Ray, M. Flinders, A. Anderson, and R. A. Cutler, "Hardness/Toughness Relationship for SiC Armor," *Ceram. Sci. and Eng. Proc.*, **24**, 401-10 (2003).

[15]H. M. Rietveld, "A Profile Refinement Method in Neutron and Magnetic Structures," *J. Appl. Crystallogr.*, **2**, 65-71 (1969).

[16]D. L. Bish and S. A. Howard, "Quantitative Phase Analysis Using the Rietveld Method," *J. Appl. Crystallogr.*, **21**, 86-91 (1988).

[17]D. H. Stutz, S. Prochazka and J. Lorenz, "Sintering and Microstructure Formation of b-Silicon Carbide," *J. Am. Ceram. Soc.*, **68**[9], 479-82 (1985).

[18]E. E. Underwood, *Quantitative Stereology*, (Addison-Wesley, Reading, MA. 1970).

APPENDIX C

BORIDE BASED MATERIALS FOR ENERGETIC APPLICATIONS

M. L. Whittaker, R. A. Cutler, P. E. Anderson

Materials Research Society Proceedings
Volume 1405, Y11 (2012)

Boride-Based Materials for Energetic Applications

Michael L. Whittaker,[1] Raymond A. Cutler,[2] and Paul E. Anderson[3]

[1] University of Utah, 122 S. Central Campus Drive, Salt Lake City UT, 84112
[2] Ceramatec, Inc., 2425 South 900 West, Salt Lake City, UT 84119
[3] Explosives Research and Development Branch, ARDEC, Picatinny Arsenal, NJ 07806

ABSTRACT

Metal borides (AlB_2, MgB_2, $Mg_{0.5}Al_{0.5}B_2$, AlB_{12}, SiB_6 and $MgAlB_{14}$) and boron carbide (B_4C) reacted with Al were compared to B, Mg, Al, Mg-Al and Si as potential energetic fuel additives. Stoichiometric physical mixtures of powders corresponding to unreacted boride compounds (Al+2B, Mg+2B, Mg-Al+2B, Al+12B, Si+6B, Mg-Al+14B, and B_4C+2Al) were also investigated in comparison to the compounds. Submicron boron was used, which resulted in very fine particle sizes for all materials studied. It was demonstrated that boride compounds were less sensitive to low-temperature oxidation in flowing air than physical mixtures or metallic fuels. Compounds with high mole fractions of boron were generally less sensitive, but their high temperature oxidation behavior showed no improvement over boron. Cylinder expansion testing of $MgAlB_{14}$ exposed its poor performance in an energetic mixture. However, aluminum and magnesium diborides (AlB_2, MgB_2 and $Mg_{0.5}Al_{0.5}B_2$) also had relatively low sensitivity and exhibited mechanisms to increase the rate of boron oxidation at high temperatures, showing promise as insensitive high-energy-density fuel additives. Detonation calorimetry of mixtures with AlB_2 or Al+2B suggested that the AlB_2 mixture released approximately 50% more heat per gram than Al +2B and underwent complete reaction. These results warrant further testing of the diboride compounds in energetic formulations. Due to the high cost of boron and acceptable performance of B_4C-Al mixtures, B_4C should also be investigated as a lower-cost alternative to boron.

INTRODUCTION

Boron has long been recognized as fuel for rocket boosters and other energetic applications where high energy density is required.[1,2] The heat of combustion for the oxidation of boron to boron oxide is highly exothermic on both a volumetric and gravimetric basis. The main problems with using boron have been obtaining complete combustion due to slow oxidation kinetics[1] and the high cost of the material. Metals like Al, Mg and Mg-Al have typically been used despite lower enthalpies of combustion and higher sensitivity to accidental discharge due to more favorable oxidation kinetics.

Mitani and Izumikawa[3] showed that the addition of micron sized Al to B increases its combustion efficiency in simple strand burner studies. Flower et al.[4] demonstrated a similar improvement in performance by bomb calorimetry for mechanically alloyed boron and Al powders. Hsia[2] measured ignition delay and burning time for 30-75 μm Al, Mg and Li borides in air using optical techniques and came to the conclusion that the metal borides are superior to B for use in rocket propulsion systems due to faster ignition and complete combustion.

Mixtures of metal powders and submicron boron have not been previously tested, nor have metal borides less than 10 μm. These materials have not been compared side by side in any

experimental setup. Problems associated with such fine powders include higher sensitivity and a higher concentration of inert oxide, but if boron can be made to combust completely the increase in energy density may compensate for higher oxide content. Due to the high cost of boron, alternative sources are desirable. Because B_4C is used in other industrial applications, it has the potential to be a less expensive source of boron. Recent studies by Sabatini et al.[5] showed that B_4C can work well in pyrolants. The objective of this work was to compare a variety of borides with similarly sized boron-metal mixtures for comparison in energetic mixtures.

EXPERIMENTAL PROCEDURE

Powder mixtures were made from amorphous B (H.C. Starck, 97% with 2% O and 0.8% Mg), spherical Al (Valimet H3, 99.9%), spherical Mg-Al alloy (Valimet Al-Mg alloy 55% Al-44% Mg with 0.4% Fe), Mg flake (Atlantic Equipment Engineers, 95%), atomized Si (Elkem Silgrain, 99%) and B_4C (UK Abrasives, 99%). Reacted compounds were synthesized at Ceramatec using proprietary processing.

Powder size was characterized by BET surface area and laser light scattering particle size analysis and particle morphology was investigated by scanning electron microscopy (SEM) and energy dispersive spectroscopy (EDS). Thermal gravimetric analysis (TGA) and differential thermal analysis (DTA) were used to characterize the response of the powders (50 mg samples) to oxidation in flowing air (~150cc/min). Detonation calorimetry was used to compare combustion behavior of AlB_2 and Al+2B mixtures. Cylinder expansion testing was conducted on $MgAlB_{14}$.[6] Impact, friction and shock sensitivity testing was performed on MgB_2 and AlB_2 powders by ATK.

RESULTS AND DISCUSSION

Table I gives surface area and particle size for the raw materials, mixtures, and borides. The average particle size was generally below 10 µm, although the agglomerated powders were above that size, as shown in Figure 1 for selected powders. The fine particle sizes contributed to rapid oxidation in air, with initiation between 500 and 950°C (see Table II). Increased initiation temperature is believed to be related to the sensitivity of the powder. In general, the powder mixtures were no less sensitive than the starting powders, but the reacted compounds didn't begin to oxidize until much higher temperatures.

TGA results for Al, B, Al+2B, and AlB2 are shown in Table 2. The high surface area boron exhibited faster initial oxidation kinetics than Al or AlB_2. At ≈50% conversion the oxidation of B was retarded by the formation of B_2O_3 and reached only 69% of its theoretical limit. This exemplifies the kinetic limitations of B oxidation at high temperatures. The oxidation of Al followed the general trend described in the literature[7] where polymorphic transformations in the Al_2O_3 shell gave rise to the step-like weight gain behavior. Despite the irregularity of the process, Al reached 100% of its theoretical limit. Al + 2B, with an approximately even weight distribution of Al and B, reached 85% of its theoretical weight gain, as expected. Surprisingly, AlB_2 reached 98% of its theoretical value despite having a much higher initiation temperature than its constituent powders. AlB_{12} and $MgAlB_{14}$, with high B contents, did not oxidize fully, although they showed the same benefits of increased insensitivity as AlB_2.

Table I. Powder Size and Surface Area

Material	Surface Area (m^2/g)	Particle Size (μm) d_{10}	d_{50}	d_{90}	Mean	Calculated Particle Size (μm)*
B	10.88	0.1	0.2	3.2	1.2	0.2
Al	1.39	0.2	2.9	7.8	3.4	1.6
Mg	0.82	11.8	38.2	66.5	38.6	3.9
Mg-Al	0.40	2.0	10.0	25.9	12.4	6.8
Si	3.56	0.2	2.7	5.9	2.7	0.7
B_4C	6.92	0.1	1.4	3.8	1.7	0.3
Al + 2B	6.23	0.2	2.3	6.5	2.8	0.4
Al + 12B	9.11	0.1	0.4	3.2	1.3	0.3
Mg + 2B	6.73	0.3	8.6	65.4	24.0	0.4
½ Mg-Al + 2B	5.85	0.1	1.6	5.1	2.0	0.4
Al-Mg + 14B	7.75	0.1	1.3	4.4	1.8	0.3
Si + 6B	9.10	0.1	0.4	2.6	0.9	0.3
B_4C + 2Al	4.30	0.2	2.0	5.4	2.4	0.6
AlB_2	1.64	0.5	8.4	28.8	11.9	1.2
AlB_{12}	1.38	1.3	6.4	17.5	8.6	1.8
MgB_2	4.78	0.7	9.2	46.0	17.4	0.5
$Mg_{0.5}Al_{0.5}B_2$	2.30	0.9	7.3	27.5	11.4	0.9
$Mg_{0.78}Al_{0.75}B_{14}$	0.55	4.8	14.7	28.2	16.0	4.1
SiB_6	0.71	3.2	14.9	38.4	20.8	3.9
AlB_2C + AlB_2	2.60	0.3	4.3	17.7	7.2	0.9

*The calculated average particle size assumed monosized spheres ($d=6/(SA\cdot\rho)$).

Oxidation in the Mg-B system was also promising. MgB_2 reached nearly the same extent of oxidation (90%) as the physical mixture (91%) and had a higher initiation temperature by more than 80°C. The ternary diboride $Mg_{0.5}Al_{0.5}B_2$ was similar to MgB_2, reaching 87% of its theoretical value, while the mixture Mg-Al + 2B achieved 92% of its theoretical value.

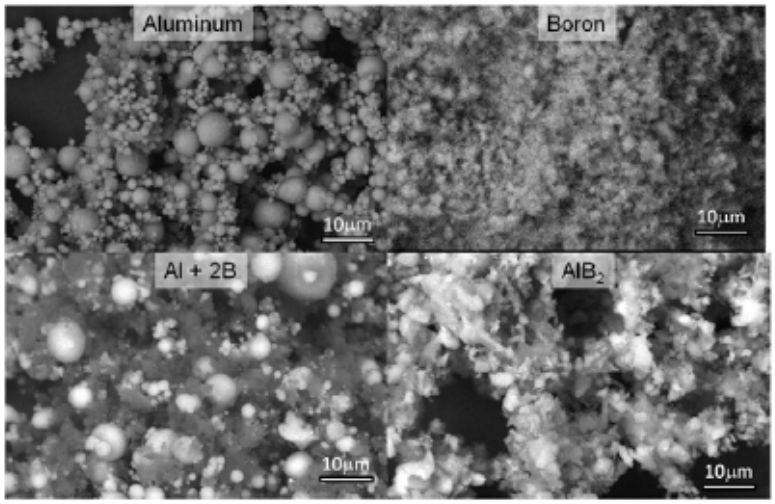

Figure 1. SEM backscattered images of selected powders. Markers are 10 μm.

Table II. Boride Powder Oxidation Characteristics

Material	Actual % Mass Change	Theoretical % Mass Change	% of Theoretical	Initiation Temp (°C)*	T_{50} (°C)**
B	152	222	69	563	906
Al	89	89	100	583	998
Mg	51	66	77	534	685
Mg-Al	78	78	100	527	735
Si	47	114	41	924	N/A
B_4C	100	152	65	522	825
Al + 2B	141	149	84	577	961
Al + 12B	147	199	71	543	968
Mg + 2B	126	139	91	597	802
½ Mg-Al+2B	122	146	92	596	848
Al-Mg + 14B	141	186	66	573	1088
Si + 6B	128	144	68	528	1225
$2Al + B_4C$	115	121	95	535	790
AlB_2	145	149	98	755	1074
AlB_{12}	146	199	72	746	1076
MgB_2	126	139	90	673	1107
$Mg_{0.5}Al_{0.5}B_2$	126	146	87	753	1051
$MgAlB_{14}$	135	186	64	890	1351
SiB_6	116	144	61	683	1464
AlB_2C+AlB_2	100	121	83	699	960

* Initiation temperature is reported as temperature at 5% mass gain.
** Temperature at which 50% of theoretical oxidation is reached

The lowest extents of reaction were seen in Si, Si + 6B and SiB_6. Si oxidizes to SiO_2, which is more viscous than B_2O_3 and presents an even greater barrier to diffusion. When the two oxides are present concurrently they form borosilicate glassy oxides, which only exacerbate the diffusional limitations caused by B_2O_3. These materials are obviously not promising candidates for further testing.

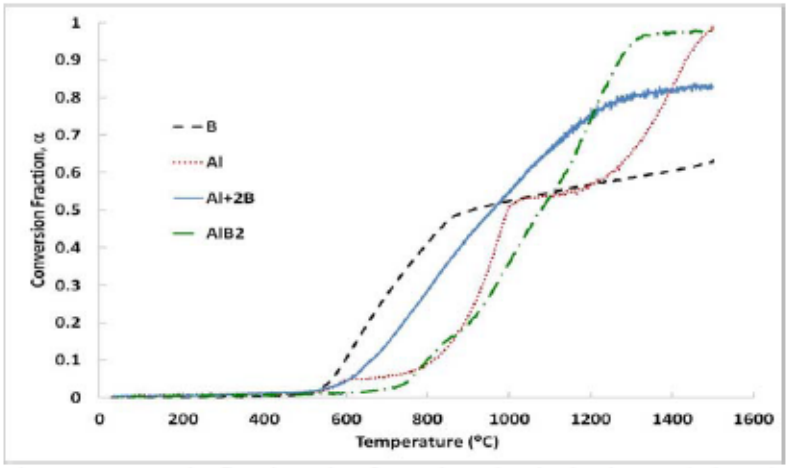

Figure 2. TGA in flowing air of B, Al, a physical mixture (Al+2B), and AlB_2.

Reaction products in the Al-B-O and Mg-B-O systems offered alternate mechanisms for oxidation that resulted in higher conversions. The main reaction products in these systems are $2Al_2O_3 \cdot B_2O_3$ ($Al_4B_2O_9$, see XRD pattern in Figure 3) and $3MgO \cdot B_2O_3$ ($Mg_3B_2O_6$), which produce solid, needle like structures on the surface of the oxidizing particle. These borates act to remove liquid B_2O_3 from the surface, exposing unoxidized material underneath and thereby increasing the rate of diffusion of oxidizer to the surface of the fuel particle. It can be seen from the stoichiometry of the borates that an Al:B or Mg:B molar ratio of 1:2 in the starting material (Al + 2B, Mg + 2B, Al-Mg + 2B, AlB_2, MgB_2 or $Mg_{0.5}Al_{0.5}B_2$) will allow for the removal of much of the B_2O_3 by Al_2O_3 or MgO through borate formation. Ratios of 1:7 and 1:12 (in Mg-Al + 14B, $MgAlB_{14}$, Al + 12B and AlB_2) do not provide significant decreases in B_2O_3 removal and because of the larger particle size of these materials they perform no better than boron.

When Al was intimately mixed with B_4C, results similar to those for Al + 2B were seen. Al greatly increased the extent of reaction for B_4C. Analysis of the reacted compound was more complicated. A 1:2 ratio of Al:B was maintained so that this system could be compared to AlB_2. The products of the reaction between Al and B_4C were Al_3BC, AlB_2 and unreacted Al and B_4C, which made determination of an oxidation mechanism more difficult. The reacted compound reached 83% of its theoretical value. Based on these results, and in light of the fact that B_4C is about 25% of the cost of boron, it is worthwhile to continue investigations into the use of B_4C as a precursor to boride compounds.

The similar extents of reaction for the diboride mixtures and compounds suggests that borate formation is not transport limited in the flowing air regime. This can be attributed to low glass transition temperature of B_2O_3, which is present as a liquid above 450°C. Subsequent tests have shown a similar situation in pure oxygen. However, in a rapid energetic event with many other components the borate formation mechanism may not provide a significant advantage if B_2O_3 is separated by more than a few nanometers from a metal oxide, as the time scale may not allow diffusion and reaction of the two oxides to occur. This gives boride compounds a distinct advantage over physical mixtures.

Detonation calorimetry was conducted on energetic mixtures containing either AlB_2 or Al + 2B to determine the effects of boride compound formation on heat release in an otherwise

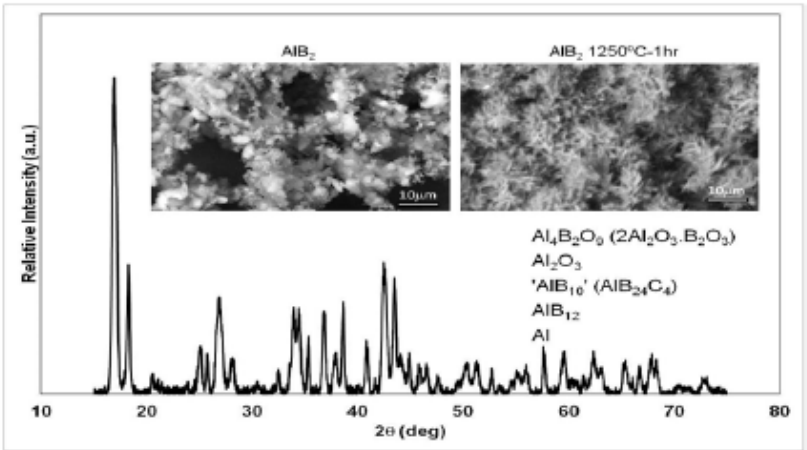

Figure 3. XRD pattern with SEM images inserted for AlB_2 oxidized in air at 1250°C for 1 hour showing needle-shaped $Al_4B_2O_9$ formation.

equivalent system. AlB_2 released about 50% more heat than Al + 2B in the proprietary energetic mixes evaluated. Cylinder expansion testing is the next step in assessing if the boride is an improvement over the metal boron mixture. Earlier cylinder expansion tests conducted on $MgAlB_{14}$ revealed that it did not perform as well as detonation models predicted. It is imperative that energetic testing, not 'static' oxidation testing, guide the development of new energetics.

Shock, impact and frication sensitivity data taken on AlB_2 and MgB_2 suggest that they are less sensitive than the conventional metal additives and are safe to handle. These borides are ready to be subjected to larger-scale testing.

CONCLUSIONS

At small particle sizes (200 nm) boron is more sensitive to low temperature oxidation in air than larger (3-40 μm) metallic fuels. At high temperatures, boron oxidation is retarded by the formation of B_2O_3, as expected, while Al and Al-Mg continue to oxidize to their theoretical limit by 1500°C.

The addition of Al, Mg and Al-Mg to B with high metal:boron ratios increases the extent of reaction of boron in flowing air. Using lower metal:boron ratios does not provide the same benefit. Silicon reduces the extent of reaction even further below that of boron due to the formation of viscous borosilicate glassy oxides. Forming boride compounds, however, decreases sensitivity to low temperature oxidation and increases the initiation temperature compared to intimate physical mixtures based on TGA testing.

Detonation calorimetry of AlB_2 and Al + 2B indicated that AlB_2 reacts completely in an energetic mixture while Al + 2B does not. AlB_2 had 50% higher heat output than Al + 2B in comparative testing. Cylinder expansion testing of these materials are needed since early testing of $MgAlB_{14}$ showed that it is not suitable for an energetic fuel additive.

While diboride materials appear promising, it is doubtful that 'static' oxidation in flowing air is any indicator of energetic performance since specific mixtures change the reaction products. Testing energetic mixtures of a wide variety of materials, such as those produced in this study, is therefore necessary to guide further development efforts. The addition of Al to B_4C to improve its oxidation characteristics is of specific interest due to the lower cost of B_4C compared to B.

REFERENCES

1. C. L. Yeh and K. K. Kuo, *Prog. Energy Comb. Sci.*, **22**[6] 511-41 (1996).
2. H. T.-S. Hsia, AFRTL-TR-71-80 (June 1971).
3. T. Mitani and M. Izumikawa, *J. Spacecraft* **28**[1] 79-84 (1991)
4. P.Q. Flower, P.A. Steward, L.R. Bates, A.J. Shakesheff, and P.W. Reip, Insensitive Munitions European Manufacturers Group (2006).
5. J. J. Sabatini, J. C. Poret, and R. N. Broad, *Angew. Chem. Int. Ed.*, **50** 4624-25 (2011).
6. M. L. Whittaker, R. A. Cutler, J. Campbell and J. LaSalvia, *Ceram. Eng. Sci. Proc.*, **31**[7] 239-250, (2010).
7. N. Eisenreich, H. Fietzek, M. d.M. Juez-Lorenzo, V. Kolarik, A. Koleczko, and V. Weiser, *Propellants Explos. Pyrotech.* **29**[3] (2004).